Studies of Earthquake Pounding Risk and of Above-Code Seismic Design

By

Moad Hassen Isteita

B.Sc., University of Omar Al-Mukhtar, Libya, 2002

M.Sc., University of Colorado, Boulder, USA, 2009

A thesis submitted to the

Faculty of the Graduate School of the

University of Colorado in partial fulfillment

of the requirement for the degree of

Doctor of Philosophy

Department of Civil, Environmental and Architectural Engineering

2019

This thesis entitled:
Studies of Earthquake Pounding Risk and of Above-Code Seismic Design
written by Moad Hassen Isteita
has been approved for the Department of Civil, Environmental and Architectural Engineering

____
Prof. Keith A. Porter

____
Prof. Ross Corotis

____
Prof. Bruce Ellingwood

____
Dr. Jim Harris

____
Dr. M. Amin Hariri-Ardebili

Date_______________

The final copy of this thesis has been examined by the signatories, and we find that both the content and the form meet acceptable presentation standards of scholarly work in the above mentioned discipline.

Isteita, Moad (Ph.D. Civil Engineering)

Studies of Earthquake Pounding Risk and of Above-Code Seismic Design

Thesis directed by Professor Keith A. Porter

This thesis tests three hypotheses: (1) Some US practice to determine the required separation distance to preclude pounding between neighboring buildings is overly conservative. (2) Pounding between buildings with aligned floors significantly contributes to collapse. (3) Above-code design of a common engineered commercial building type is cost effective in many though perhaps not all US locations, at least from a benefit-cost-analysis perspective.

The first part of this thesis reexamines the required minimum permissible space between two adjacent buildings to preclude earthquake pounding. This part of the thesis employs and compares three analytical approaches to estimate the minimum safe distance conditioned on the occurrence of risk-targeted maximum considered earthquake (MCE_R) shaking. 1) First, safe separation distance between buildings is estimated using elastic spectral displacement response of adjacent buildings at the top of the shorter building, accounting for mode shape and the height difference. 2) ASCE 7-16's equivalent lateral force procedure is also examined. 3) Finally, multiple linear elastic dynamic structural analyses of two adjacent buildings are performed, factoring drift estimates by ASCE 7-16's Cd/R to approximate nonlinear response. To examine diverse, though not exhaustive, conditions, this thesis examines 3 combinations of shearwall and steel moment frame buildings; 5 building heights between 2 and 26 stories; fundamental periods of vibration vary between 0.2 sec and 2.8 sec; and 4 locations with degrees of seismicity in roughly equal increments corresponding to short-period mapped spectral acceleration response S_{MS} from 0.8 to 3.0g.

Part 2 repeats much of the analysis of part 1, but with an additional structural analysis procedure (nonlinear dynamic analysis) but with a narrower set of building types. As with part 1, this part evaluates the required minimum permissible space between two adjacent buildings to preclude earthquake pounding. Unlike part 1, this part develops a set of conversion factors to relate the separation distances calculated by any of the simpler methods (elastic spectral displacement, equivalent lateral force, and multiple linear elastic dynamic structural analyses) to multiple nonlinear dynamic structural analyses method. This part examines 3 combinations of special reinforced concrete moment frame buildings, *SMF*, and ordinary reinforced concrete moment frame buildings, OMF (i.e. ductile and non-ductile reinforced concrete frame structures); 5 building heights between 2 and 20 stories for SMF; 4 building heights between 2 and 12 stories for OMF; two risk-targeted shaking levels (i.e. shaking of 2/3 MCE_R and MCE_R).

While parts 1 and 2 address the estimation of safe separation distance, part 3 examines what happens when two buildings are not safely separated but have aligned floors. It examines how pounding affects (and either reduces or does not reduce) the collapse capacity of adjacent buildings. Its focus is limited to post-2000 reinforced concrete moment frame buildings with aligned floors and various separation gaps. This methodology includes applying the framework of performance-based earthquake engineering to assess seismic safety concerns of pounding. In addition to the analytic study, part 3 includes a limited empirical validation, using a photo survey of California building collapses in the last 5 decades to search for evidence of the effect of pounding on collapse.

Part 4 examines a wholly different topic: is design of new buildings to exceed certain current seismic design criteria worth the added cost, in terms of reduction in the present value of future losses avoided? Does the answer vary by geographic location? This part employs standard benefit-cost analysis procedures, using a suite of buildings analyzed with FEMA P-58. The building suite is designed to reflect important variability within a building type using the Global Earthquake Model's (GEM) analytical methodology. The buildings represent a common engineered type: a single-story reinforced concrete shearwall building used for commercial purposes. The suite is designed so that its most seismically salient features vary similarly to actual buildings observed in a survey. Part 4 complements another study, not documented here, that addressed the same question but using a risk analysis procedure closely related to Hazus, entitled *Natural Hazard Mitigation Saves* (MMC 2017). The present study avoids the structural analytical simplifications of the Hazus methodology, albeit at the cost of a much narrower set of buildings and locations.

Each part includes a methodology, implements the methodology with a number of case studies, and presents results and conclusions. Parts 2 and 3 employ overlapping, though not identical, methods. They differ in the case study buildings so as to use available structural models.

Dedication

I dedicate this thesis to my parents, Hassen Isteita and Nafisa Rustum, who have been my source of inspiration and strength; to my lovely wife, Sara Alatrash, who have supported and loved me throughout; to my daughters, Nafisa, Maram, and Areen, the symbol of love; to my beloved brother, Swaihal, who continually provide his advice and encouragement; and to all my family and friends, who have been there for me throughout my doctorate program.

Acknowledgements

Foremost, I would like to sincerely thank my advisor, Professor Keith Porter, not only for his support, advising, and guidance through this research, but also for his patience, motivation, enthusiasm, and immense knowledge. So much of me is made of what I learned from him. I am very grateful for working under his supervision.

I would like to thank my thesis committee: Prof. Ross Corotis, Prof. Bruce Ellingwood, Dr. Jim Harris, Dr. M. Amin Hariri-Ardebili, and Prof. Petros Sideris for their encouragement, insightful comments, and valuable suggestions.

My sincere thanks also go to Prof. Curt Haselton and Prof. Abbie Liel for providing their structural models and modeling advice.

CONTENTS

Chapter

TABLES

Table

FIGURES

Figure

Chapter 1

1 Introduction

1.1 Motivation

This thesis examines two mostly independent topics: pounding and above-code design. First, consider the phenomenon in which two adjacent buildings pound into each other during earthquakes. Researchers have long examined earthquake-induced pounding between adjacent buildings because of the damage pounding has caused in past earthquakes. For example, a damage survey after the 1985 Mexico City earthquake asserted that “in 15 percent of all cases [pounding] led to collapse” (Rosenblueth and Meli 1986). Were those authors correct? What is a safe separation distance?

ASCE 41-13 (ASCE 2014) requires a separation distance on the order of 4% of the height of the shorter building, with the option of structural analysis of the building in question to justify a distance as little as 3% plus the displacement of the building in question. There is no mention of any pounding provisions changing in the update summary by “Summary of the updates to ASCE/SEI 41-17 - SEAOC” (2017). FEMA P-154 (ATC 2015) suggests that ASCE 41-13 is overly conservative. FEMA P-154, which provides a much quicker seismic assessment of existing buildings than does ASCE 41-13, uses a simpler estimate of safe separation distance based on spectral displacement, no structural analysis of either building, and concludes that the safe separation distance is at most 1.5% of height of the shorter building. ASCE 7-16 (ASCE 2016) requires the separation distance to be at least the square root of the sum of squares of the two buildings' maximum displacement, estimated either using an elastic structural analysis of both buildings, or an inelastic structural analysis of both buildings if one wants to reduce the separation distance. All of which beg several questions:

Is the simple FEMA P-154 spectral approach any good? How well does it estimate safe separation distance?

Is ASCE 41-13's 3% to 4% separation distance actually overly conservative?

Is ASCE 7-16's elastic structural analyses of both buildings worth the effort? Is its estimate any safer, more reliable, more accurate, than a simpler approach that does not require structural analyses of both buildings? Parts 1 and 2 of this thesis address these questions in slightly different ways for different combinations of buildings.

Now, in cases where the separation distance is insufficient to preclude neighboring buildings from pounding into each other, how does pounding change the probability of collapse for each building? FEMA P-154 estimates the increase in collapse probability if buildings are closer than the safe separation distance, but that increase is largely guesswork by the authors of FEMA P-154. Part 3 attempts to improve on that expert judgment with structural analysis.

Part 4 addresses a different issue. Earthquakes kill, injure, and traumatize people; damage property; cause homes and businesses to lose functionality; and cause numerous less-tangible losses to people, society, and the environment. These impacts are inevitable. We pay for them eventually. If we pay sooner rather than later, by making new buildings more resilient in the first place or by retrofitting existing buildings before an earthquake, does the investment pay for itself? How much extra resilience makes economic sense? A report entitled *Natural Hazard Mitigation Saves* (MMC 2017) makes the case that a simple approach to above-code design, using a factor to increase required strength and stiffness, results in lower long-term societal costs of ownership than life safety alone demands. That project for a practical reason used a Hazus-like methodology to estimate repair costs, life-safety impacts, and costs of loss of function with very simple building models. The simplicity of Hazus contrasts with second-generation performance-based earthquake engineering (PBEE) methods that characterize buildings with multi-degree-of-freedom structural models and numerous building components. The *Natural Hazard Mitigation Saves* project team (which includes the present author) wondered whether a PBEE-based method would yield similar or different results; hence the present study.

1.2 Objectives

The primary objective of this research is to test these hypotheses: (1) US practice to determine the required separation distance to preclude pounding between neighboring buildings is overly conservative. (2) Pounding between buildings with aligned floors significantly contributes to collapse. (3) It is cost effective to design a narrow category of common-looking commercial buildings to exceed IBC strength and stiffness requirements in many US locations, at least from a societal benefit-cost-analysis perspective. More specifically, the objectives of this study, and the contributions of this thesis, are as follows:

1. Examine the comparative accuracy of a set of increasingly demanding analytical approaches of estimating the minimum safe distance conditioned on the occurrence of risk-targeted maximum considered earthquake (MCE_R) shaking: elastic spectral displacement response, ASCE 7-16's equivalent lateral force procedure, multiple linear elastic dynamic structural analyses, and multiple nonlinear dynamic structural analyses of two adjacent buildings. I.e., estimate the degree to which one can be confident that pounding will not

actually occur, if one calculates the safe separation distance between the buildings by any of the three simpler approaches.

2. Develop a set of conversion factors to relate the separation distances calculated by any of the simpler methods (elastic spectral displacement, equivalent lateral force, and multiple linear elastic dynamic structural analyses) to multiple nonlinear dynamic structural analyses method, which is taken here to most closely approximate what happens in the real world.
3. Estimate the degree to which pounding aggravates collapse probability for reinforced concrete moment frame buildings whose floors align if buildings are closer than the safe separation distance.
4. Perform benefit-cost analysis of design of a common engineered commercial building type to exceed ASCE 7 minimum safety requirements for seismic loading using state-of-the-art, second-generation performance-based earthquake engineering as encoded in FEMA P-58 at geographic locations whose C_s values jointly span U.S. seismicity. Because FEMA P-58 operates only on individual buildings, not classes of buildings, use the Global Earthquake Model's analytical method to create a suite of particular buildings that jointly represent important sources of variability in the seismic performance within a building class. Answer the question, where and to what extent is it cost effective to design new buildings of one given class to exceed minimum life-safety requirements encoded in ASCE 7?
5. Cross-validate the answer to the previous question with of a societal risk analysis that produced by the simpler, Hazus-based, approach to estimating seismic vulnerability.

1.3 Organization and outline

This PhD dissertation is a based on a compilation of research articles. Some of its chapters have been submitted for publication as individual journal papers; other will be. Each chapter heading shows where the article is, or will be, submitted.

Chapter 2 examines three relatively simple approaches to estimate safe separation distance to avoid pounding at MCE_R shaking: (1) SRSS of 5% damped elastic spectral displacement response at the top of the shorter building; (2) ASCE 7-16's equivalent lateral force procedure; and (3) multiple linear elastic dynamic structural analyses, with drift results multiplied by C_d/R to approximate nonlinear response. The chapter exercises the approaches at four seismicity levels (S_{MS} from 0.8g to 3.0g), combinations of seismic two force-resisting systems (shearwall and steel moment frame), and a range of building heights (2 to 26 stories)and fundamental periods of vibration (0.2 sec to 2.8 sec). It offers a safe separation distance as a fraction of the height of the shorter building and as a function of S_{MS}, system combination, and analytical method.

The work of Chapter 2 is extended in **Chapter 3** by considering multiple nonlinear dynamic analysis, treating these new analyses as providing a better estimate of true safe separation distance compared with the other three approaches. That is, this chapter compares four analytical approaches:

1. Elastic spectral displacement
2. Equivalent lateral force
3. Multiple linear elastic dynamic structural analyses, and
4. Multiple nonlinear dynamic structural analyses.

This chapter examine 3 combinations of special reinforced concrete moment frame buildings—SMF—and ordinary reinforced concrete moment frame buildings, OMF (i.e. ductile and non-ductile reinforced concrete frame structures); 5 building heights between 2 and 20 stories for SMF; 4 building heights between 2 and 12 stories for OMF; two risk-targeted shaking levels (i.e. shaking of 2/3 MCE_R and MCE_R).

Finally, this chapter provides an estimate of the degree to which one can be confident that pounding will not actually occur, if one calculates the safe separation distance between the buildings by any of the three relatively simple approaches in MCE_R and 2/3 MCE_R shaking. It also proposes a set of conversion factors to relate the separation distances calculated by any of the simpler methods 1-3 above to method 4, which one might consider to best approximate what happens in the real world.

Chapter 4 presents and exercises a simple method to estimate the degree to which pounding aggravates collapse probability. This chapter assesses the effect of pounding on median collapse capacity by using the incremental dynamic analyses of 140 combinations of pairs of five adjacent post-2000 reinforced concrete moment frame buildings with aligned floors (20 permutations) and 7 separation gaps. The buildings included 2-, 4-, 8-, 12-, and 20-story models. Gap widths varied from near zero to effectively infinite (0.01 in, 1.0 in, 2.0 in, 5.0 in, 10.0 in, 35.0 in, 75.0 in, and 200 in). The analytical findings are compared with evidence of building collapse in reinforced concrete buildings in California in the last 50 years.

Chapter 5 focuses on estimating the benefit-cost ratio of above-code design of a common engineered commercial building type. In this chapter, benefit-cost analysis for above-code design is performed and presented for a single building type, height class, and occupancy: a special reinforced masonry shearwall (in ASCE 7-16 terms), 1 story, with flexible roof diaphragm, with a professional, technical, and business services occupancy such as an electric substation. The analysis is performed for several seismic regions and for several values of greater strength and stiffness (parameterized with the I_e value of ASCE 7). The framework of the Global Earthquake

Model's (GEM) analytical methodology (Porter et al. 2014) is implemented to parameterize and vary building configuration consistent with an observed joint probability distribution of size and shape. Then, the findings are compared with the findings of *Natural Hazard Mitigation Saves* (MMC 2017) in effort to cross-validate with Hazus-style approach to estimating seismic vulnerability.

Chapter 6 recaps the novelties of introduced here and summarizes the research findings. It also identifies some limitations of this research and future research needs.

Because this thesis comprises several standalone research papers, some introductory material and literature review are repeated across chapters. The author apologies for the redundancy. Also, chapter abstracts are included in the chapters, so if some readers decide to skip to a certain chapter that interests them, they find the abstract that summarizes the major aspects of the entire chapter.

Chapter 2

2 Safe Distance between Adjacent Buildings to Avoid Pounding in Earthquakes

This chapter is based on:

Isteita, M., and Porter, K. (2017). "Safe Distance between Adjacent Buildings to Avoid Pounding in Earthquakes." *16th World Conference on Earthquake*. [Published]

Abstract

We reexamine the required minimum permissible space between two adjacent buildings to preclude earthquake pounding damage. We examine several analytical approaches to estimate the minimum safe distance conditioned on the occurrence of risk-targeted maximum considered earthquake (MCE_R) shaking: 1) elastic spectral displacement response of the adjacent buildings at the top of the shorter building, accounting for mode shape and the height difference, 2) ASCE 7-16's equivalent lateral force procedure, and 3) multiple linear elastic dynamic structural analyses of the two adjacent buildings, factoring drift estimates by ASCE 7-16's C_d/R to approximate nonlinear response. We assume here that linear dynamic is the most accurate of the three and measure the safety of the others relative to it. Considering a suite of levels of MCE_R shaking and combinations of building heights and structural systems, both the more-approximate approaches appear to give modestly conservative estimates of safe separation distance. The spectral-response

approach would be safe with 66% probability and the equivalent lateral force approach with 90% probability, assuming that multiple linear elastic structural analyses give a fairly accurate estimate of the true distribution of building motion. In other work, we examine multiple nonlinear dynamic analysis and compare the first three with the fourth.

Keywords: seismic pounding; safe Structural Separation; adjacent buildings requirements

2.1 Introduction

Researchers have long examined earthquake-induced pounding between adjacent buildings because of the damage pounding has caused in past earthquakes. We reexamined safe separation distance because recent work on FEMA P-154 (ATC 2015) suggested US practice is overly conservative.

Pounding tends to occur in dense urban areas because of the small separation distances there. Several authors have performed surveys of pounding damage after earthquakes. Rosenblueth and Meli (1986) report on a damage survey after the 1985 Mexico City earthquake, performed by teams of engineering students, each team led by one or two experienced structural engineers. The teams performed mostly external (visual) inspection of 330 buildings that experienced severe damage or collapse, associated pounding with 40% of instances, and asserted that “in 15 percent of all cases [pounding] led to collapse.” The authors do not offer the teams’ basis for judgment, evidence, or any validation of the teams’ judgment is offered.

Kasai and Maison’s survey (1997) of pounding damage after the 1989 Loma Prieta earthquake found that about 500 buildings were affected by about 200 instances of pounding, mostly involving older multistory masonry buildings, many with virtually no separation, and predominantly involving minor architectural or structural damage, although the authors warned of the potential for more serious damage in future, closer or larger earthquakes. Cole et al. (2012)

performed a similar survey of a portion of downtown Christchurch after the 2011 earthquake, most of which had no separation distance. Three notable findings: some buildings suffered partial collapse in part because of pounding; unreinforced masonry buildings were disproportionately likely to experience pounding damage, compared with concrete, timber, and steel; and the authors are not sure that pounding contributed to the complete collapse of any buildings.

Jeng et al. (1992) used random-vibration theory to examine three approaches to estimate safe separation distance between single-degree-of-freedom systems subjected to white-noise excitation. (Actually, they examined MDOF systems, but only elastic response in the first mode, so essentially SDOF). They recommend a double-difference combination (DDC) rule for building separation over either the sum of maximum displacements or the square root of the sum of the squares (SRSS); the recommended approach is like SRSS reduced by an amount related to the product of the maximum displacements and a correlation coefficient that varies with damping ratio and building periods.

Filiatrault and Cervantes (1995), concerned that the separation distance prescribed by the 1990 National Building Code of Canada (1990) was overly conservative (the sum of the maximum deflections at the top of the shorter building), performed nonlinear dynamic structural analysis of 5 realistic concrete shearwall buildings designed for each of 3 Canadian cities whose design base shears were generally in proportion 1:2:3 for a given building height. They use the estimates of structural response to support a method to estimate safe separation distance that involves equivalent lateral force (pseudostatic linear analysis) to estimate first-mode maximum response at the height of the top of the shorter building, and application of Jeng et al.'s DDC approach.

Lopez Garcia (2004) provides a modified double difference combination (MDDC) approach similar to that of Jeng et al. but replacing the correlation coefficient with an empirical parameter that, he shows, provides consistent, modest conservatism and accounts for behavior of linear and nonlinear SDOF and MDOF systems. ASCE 7-16 (ASCE 2016) requires the separation distance to be at least the square root of the sum of squares of the two buildings' maximum response displacement by an equivalent lateral force approach that approximates inelastic response.

Our goal is to reexamine the required minimum permissible space between two adjacent buildings to preclude pounding, with some differences from prior studies. We employ 3 degrees of analysis up to linear dynamic structural analysis (later work will employ nonlinear dynamic analysis); 3 combinations of frame and shearwall buildings; 5 building heights between 2 and 26 stories; and 4 locations with degrees of seismicity in roughly equal increments corresponding to short-period mapped spectral acceleration response S_{MS} from 0.8 to 3.0g.

2.2 Research Methodology

The proposed procedure for this study can be summarized as follows:

2.2.1 Step 1: asset definition

To investigate both the effect of buildings seismic force-resisting systems and buildings fundamental periods of vibration on the minimum permissible space between two adjacent buildings, buildings with three combinations of seismic force-resisting systems (both wall, both frame, and mixed) and various fundamental periods of vibration are selected.

2.2.2 Step 2: hazard analysis and ground motions selection

To explore the effect of degree of seismicity on the safe distance between adjacent buildings, let us examine four locations with S_{MS} values (defined as in ASCE 7-16) between 0.8g and 3.0g. For each location, let us deaggregate the hazard to find the controlling source characteristics (modal magnitude M, distance R, and epsilon ε_0) associated with each location and its S_{MS}. Lastly, select suites of ground motions with approximately the same source characteristics and scale them to match the target S_{MS} for each location, attempting to limit the scaling factor (the constant that is multiplied by each acceleration to achieve the desired value of S_A(0.2 sec, 5%)) to 0.5 to 2.0, so as to keep the time histories realistic. For simplicity, we do not comply with the requirements of ASCE 7-16 Sec 16.2.3.2, which requires scaling motions so that "the average of the maximum-direction spectra from all ground motions generally matches or exceeds the target response spectrum" and "The average of the maximum-direction spectra from all the ground motions shall not fall below 90% of the target response spectrum for any period within the same period range."

2.2.3 Step 3: first approach, spectral displacement estimate of proximity

The minimum required safe distance according to this approach to avoid pounding can be estimated as the SRSS of the spectral displacement response of each pair of buildings, based solely on their estimated periods, heights, and the idealized design spectrum at the site of interest. This displacement spectrum is associated with the risk-targeted maximum considered earthquake (MCE_R), characterized by ASCE 7-16's S_{MS} and S_{M1} parameters, and translated to the roof of each building. Also, a triangular mode shape and the height of the shorter building for each building of the pair is considered as shown in Figure 2.1 and in accordance with Eq. ((2.1). The approach requires very modest effort, with the disadvantage that it does not account for any building characteristics other than height and estimated period. SRSS represents almost the simplest approach possible (absolute sum having been shown to be overly conservative and DDC or MDDC requiring somewhat more effort and complexity).

$$d^{(SD)} = \sqrt{\left(S_{d1} \cdot \frac{h_2}{h_1}\right)^2 + \left(S_{d2}\right)^2} \tag{2.1}$$

where $d^{(SD)}$ denotes the spectral displacement estimate of proximity, S_{d1} and S_{d2} denotes the spectral displacement response for the taller and shorter buildings, respectively, using the idealized design spectrum, and h_1 and h_2 are the heights of the taller and shorter buildings, respectively.

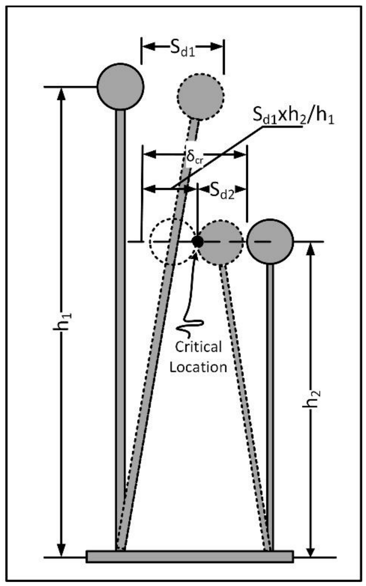

Figure 2.1 – Approach 1, the spectral estimate of proximity model

2.2.4 Step 4: second approach, equivalent lateral force

Our second approach is to follow the equivalent lateral force procedure (ELF) specified in section 12.8 of ASCE 7-16, omitting the 2/3 factor of ASCE 7-16 equations 11.4-3 and 11.4-4 so as to measure proximity at MCE_R shaking, rather than at 2/3 that value, i.e., according to Equation 2.2), which combines by SRSS the estimated maximum inelastic deformation of the two buildings at the top of the shorter building. Figure 2.2 illustrates the model. The second approach takes advantage of prior work to estimate the response modification factor R and the deflection amplification factor C_d—that is, it approximately accounts for lateral force resisting system—but it requires structural analysis of both buildings.

$$d^{(ELF)} = \sqrt{\delta_{M1}^2 + \delta_{M2}^2} \tag{2.2)}$$

$$\delta_M = \frac{\delta_{Max} C_d}{I_e} \tag{2.3}$$

where,

$d^{(ELF)}$ = equivalent lateral force estimate of proximity

δ_{MAX}= maximum elastic displacement at the critical location (the top of the shorter building) under loading $S_{MT} \cdot Ie/R$

S_{MT} = soil-amplified spectral acceleration response in the idealized design spectrum and the appropriate period under risk-targeted maximum considered earthquake shaking,

R = response modification factor in ASCE 7-10 table 12.2-1

C_d = deflection amplification factor from ASCE 7-10 table 12.2-1

I_e = importance factor from ASCE 7-16 section 11.5-1

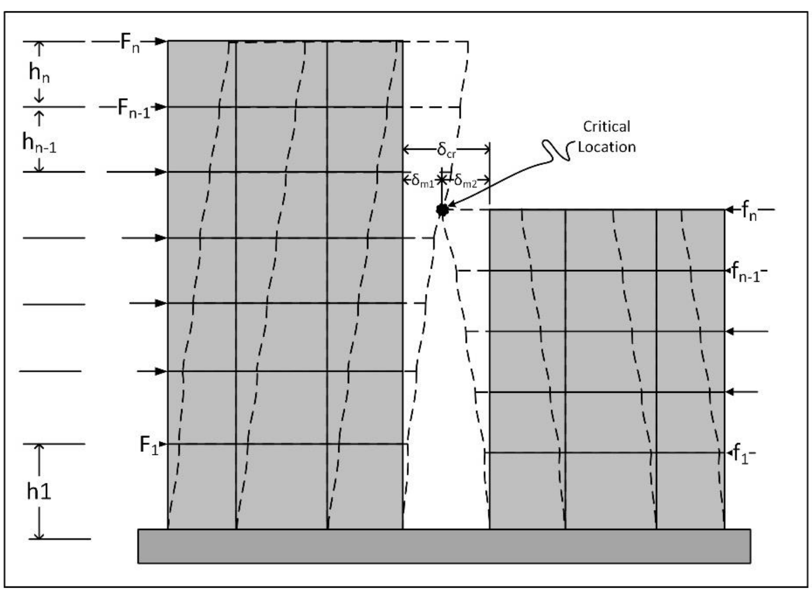

Figure 2.2 – Approach 2, equivalent lateral force estimate of proximity

2.2.5 Step 5: third approach, multiple linear dynamic analyses

In this approach, one estimates the minimum safe distance at the critical location by modeling, in structural analysis program such as SAP2000 (CSI 2017), in linear dynamic analysis the pair of buildings as if they were adjacent, connected by a flexible link at the top of the shorter building. One subjects the building pair to suites of ground motions as described in step 2, records the time-maximum shortening of the flexible link, and calculates its cumulative distribution function conditioned on building pair and location. To comply with the requirements of ASCE 7-16 Section 16.1, we multiplied drift by C_d/R, which takes on a value of 0.83 for special reinforced concrete shearwalls and 0.69 for steel special moment frames. In contrast to ASCE 7-16 however, we examine drifts at MCE_R shaking level rather than 2/3 of the MCE_R, because our initial motivation was to inform FEMA P-154, which screens buildings for collapse hazard at MCE_R shaking, not 2/3 MCE_R. Figure 2.3 illustrates the model assembly.

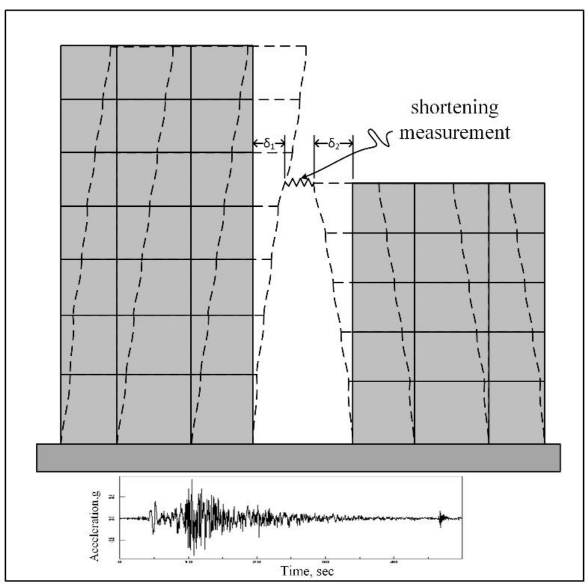

Figure 2.3 – The Linear Dynamic Estimate of Proximity

2.2.6 Step 6: iterate to characterize probabilistic structural response

One iterates steps 2 through 5 for each of many combinations of frame and shearwall buildings, several building heights, and several locations with degrees of seismicity in roughly equal increments corresponding to the range of S_{MS} values in the United States that correspond to ASCE 7-16 seismic design category D, i.e., $0.75g \leq S_{MS} \leq 3.0g$.

2.2.7 Step 7: comparisons

Finally, one examines how safe are approaches 1 and 2 versus 3? Assuming that approach-3 produces an approximately accurate probability distribution of the reduction in proximity of two buildings considering record-to-record variability and nonlinear response, with what probability would the actual reduction in distance between two buildings in a particular earthquake with MCE_R shaking be less than or equal to the safe distance calculated by either simpler approach? Idealizing the reduction in proximity under the 3rd approach with a lognormal cumulative distribution function, one can use Equation (2.4) to estimate the probability that a pair of buildings subjected to an earthquake with MCE_R shaking would experience a reduction in proximity less than or equal to the safe separation distance d calculated using an approximate approach (1 or 2):

$$p = \Phi\left(\frac{\ln(d/\theta)}{\beta}\right) \tag{2.4}$$

where Φ denotes the standard normal cumulative distribution function, d is either $d^{(SD)}$ or $d^{(ELF)}$, i.e., the safe separation distance calculated for a given building and geographic location by approach 1 or 2, θ is the median safe separation distance calculated for the same building and location using approach 3 (i.e., the median considering the various ground motion time histories), and β is the standard deviation of the natural logarithm of safe separation distance considering the various ground motion time histories. One can calculate p for each combination of building pair and location, and do so for approaches 1 and 2. (In later study will treat nonlinear dynamic analysis as the best estimate of true separation distance, and compare the first three with the fourth.)

2.3 Case studies

2.3.1 Asset definition

We investigated pounding within and between two seismic force-resisting systems: steel special moment frames and special reinforced concrete shear walls. To sample steel special moment frames, we used the 3-story, 9-story, and 20-story models provided to the SAC Steel project by Gupta and Krawinkler (1999), plus the 6- and 12-story steel-frame building models examples offered by BSSC to illustrate the 2009 NEHRP Provisions (FEMA 2012b). For the special reinforced concrete shear wall buildings, we idealized the lateral systems of five buildings (2-, 6-, 11-, 13, and 26 stories) as cantilever columns. Shearwall building plan dimensions and fundamental periods were estimated to match mean observations regressed from or offered by Goel and Chopra (1998). We estimated shearwall building dead loads based on the mass of a 6-in normal-weight concrete slab of the given plan dimensions factored up by 20% to account for shearwalls, columns, architectural finishes, and mechanical, electrical, and plumbing systems. We estimated realistic shearwall cross-section dimensions using the same source. Table 2.1 summarizes our 10 sample buildings: their fundamental period of vibration T, height H, and stories. Table 2.2 presents the combinations we examined: FF denotes adjacent steel-frame buildings; WW denotes two adjacent shearwall buildings, and WF denotes a shearwall next to a steel frame.

Table 2.1 – Sample buildings

Building ID	T, sec	H, ft	Stories	Building system
SMF-1	3.77	265.0	20	SMF

SMF-2	2.93	155.5	12	SMF
SMF-3	2.51	122.0	9	SMF
SMF-4	2.07	77.5	6	SMF
SMF-5	0.93	39.0	3	SMF
SW-1	1.8	258.1	26	SW
SW-2	1.0	134.3	13	SW
SW-3	0.9	119.4	11	SW
SW-4	0.5	62.1	6	SW
SW-5	0.2	22.4	2	SW
SMF: steel special moment frames structure SW : special reinforced concrete shear wall structure				

Table 2.2 – Building Combinations

Frame-frame			Wall-wall			Wall-frame		
Case #	Left	Right	Case #	Left	Right	Case #	Left	Right
FF-1	SMF-1	SMF-2	WW-1	SW-1	SW-2	WF-1	SW-1	SMF-1
FF-2	SMF-1	SMF-3	WW-2	SW-1	SW-3	WF-2	SW-1	SMF-3
FF-3	SMF-1	SMF-4	WW-3	SW-1	SW-4	WF-3	SW-1	SMF-5
FF-4	SMF-1	SMF-5	WW-4	SW-1	SW-5	WF-4	SW-2	SMF-4
FF-5	SMF-2	SMF-3	WW-5	SW-2	SW-3	WF-5	SW-3	SMF-1
FF-6	SMF-2	SMF-4	WW-6	SW-2	SW-4	WF-6	SW-3	SMF-2
FF-7	SMF-2	SMF-5	WW-7	SW-2	SW-5	WF-7	SW-3	SMF-3
FF-8	SMF-3	SMF-4	WW-8	SW-3	SW-4	WF-8	SW-5	SMF-1
FF-9	SMF-3	SMF-5	WW-9	SW-3	SW-5	WF-9	SW-5	SMF-2
FF-10	SMF-4	SMF-5	WW-10	SW-4	SW-5	WF-10	SW-5	SMF-3

2.3.2 Hazard analysis and ground motion selection

We explored the effect of seismicity by examining four locations: Sacramento CA (S_{MS} = 0.8g), eastern San Francisco (S_{MS} = 1.5g), western San Francisco (S_{MS} = 2.3g), and northwestern Tennessee (S_{MS} = 3.0g, which is near the highest value of S_{MS} in the United States). We estimated $Vs30$ using Wills and Clahan (2006) map for the California sites and Wald and Allen's (2007) map for the Tennessee site. We used the USGS's probabilistic seismic hazard deaggregation tool [http://geohazards.usgs.gov/deaggint/2008/] to estimate source characteristics (modal magnitude M, distance R, and epsilon ε_0) associated with S_{MS} at each location. We selected suites of 15 ground motions corresponding to the modal source characteristics and scaled them to match S_{MS} for each location. We selected records whose scaling factors were closest to 1.0 using the tools of the Pacific Earthquake Engineering Research (PEER) Center at http://ngawest2.berkeley.edu.

2.3.3 Results

Table 2.3 summarizes the statistics of safe distances under the three approaches. The column labeled "case group" indicates the building combinations: WW denotes all the cases with two adjacent shearwall buildings, WF denotes all the cases with a shearwall building adjacent to a moment frame, etc. S_{MS} denotes the hazard level in terms of risk-targeted site-soil adjusted, mapped 5%-damped short-period spectral acceleration response at the location of interest: 0.80 g indicates the Sacramento, California location, 1.5g indicates eastern San Francisco, 2.3g indicates western San Francisco, and 3.0g indicates northwestern Tennessee.

The subsequent columns give statistics of safe separation distance as a fraction of the height of the shorter building, averaging over all particular building combinations in the given case and hazard level: μ denotes average, δ denotes coefficient of variation, averaging over all the building combinations in the group. In the case of the 3rd approach, we averaged over all the ground motion time histories as well. The column labeled $\hat{\beta}_{RTR}$ measures record-to-record variability. To be precise, one calculates the natural logarithm of separation distance in each pair of buildings, S_{MS} value, and ground motion time history. There are 15 such distances per combination of building pair and S_{MS} value, one for ground motion time history. The standard deviation of those natural logarithms measures the record-to-record variability in separation distance. There are 10 such standard deviations for each case group and S_{MS} value, one for each of 10 building pairs. The record-to-record variability varies among the 10 cases; the value shown in the table is the average of those 10. The columns labeled $p^{(1)}$ and $p^{(2)}$ give the probability (averaging over all 10 cases in the group) that an actual earthquake with MCE_R shaking will produce a smaller reduction in separation distance than the value of d calculated by approach-1 or approach-2, respectively.

Table 2.3 – Summary statistics

Case group	S_{MS} (g)	1ST approach		2nd approach		3rd approach			$p^{(1)}$	$p^{(2)}$
		μ	δ	μ	δ	μ	δ	$\hat{\beta}_{RTR}$		
WW	0.80	0.004	0.14	0.006	0.34	0.003	0.56	0.38	0.79	0.98
WW	1.50	0.007	0.14	0.011	0.34	0.005	0.46	0.29	0.84	1.00
WW	2.30	0.012	0.16	0.019	0.37	0.010	0.51	0.33	0.74	0.97
WW	3.00	0.014	0.14	0.022	0.33	0.012	0.55	0.37	0.69	0.95
WF	0.80	0.009	0.30	0.012	0.27	0.008	0.48	0.34	0.64	0.90
WF	1.50	0.015	0.30	0.021	0.27	0.016	0.48	0.35	0.54	0.83
WF	2.30	0.026	0.30	0.036	0.27	0.027	0.52	0.40	0.57	0.82
WF	3.00	0.029	0.30	0.040	0.27	0.030	0.53	0.39	0.56	0.81
FF	0.80	0.013	0.13	0.019	0.31	0.011	0.43	0.31	0.68	0.93
FF	1.50	0.023	0.13	0.034	0.31	0.022	0.50	0.41	0.60	0.85

FF	2.30	0.040	0.13	0.060	0.31	0.037	0.52	0.46	0.62	0.85
FF	3.00	0.044	0.13	0.065	0.31	0.041	0.54	0.46	0.63	0.85

Some general observations of the summary statistics in Table 2.3:

- All three use linear elastic structural analysis, so average and median values tend to be proportional to S_{MS}. The third approach uses ground motions appropriate to the particular locations—Sacramento has different modal magnitude, distance, etc. than eastern San Francisco, so the ground motions for the two differ—but average and medians under the 3rd approach vary little from proportionality with S_{MS}.
- Wall-wall combinations have the smallest safe separation distances, wall-frame combinations have safe separation distances roughly twice that of wall-wall, and frame-frame roughly 3 times that of wall-wall.
- Average values for the 1st approach are slightly larger (within 20%) than those of the 3rd.
- Average values for the 2nd approach range from 1.5 to 2 times those of the 3rd.
- Variability in the 1st and 2nd approaches are much smaller than those of the 3rd, as measured by the coefficients of variation (δ). That observation should surprise nobody because only the 3rd approach reflects record-to-record variability.
- Record-to-record variability in safe separation distance ranges between 0.3 and 0.5, averaging 0.4.
- Approaches 1 and 2 both give modestly conservative estimates of safe separation distance. Approach 1 would produce a safe distance with an average 66% probability, approach 2, approximately 90%.

2.4 Conclusions

We examined three relatively simple approaches to estimate safe separation distance to avoid pounding at MCE_R shaking: (1) SRSS of 5% damped elastic spectral displacement response at the top of the shorter building; (2) ASCE 7-16's equivalent lateral force procedure; and (3) multiple linear elastic dynamic structural analyses, with drift results multiplied by C_d/R to approximate nonlinear response. We varied seismicity (four levels of S_{MS} from 0.8g to 3.0g), combinations of seismic force-resisting systems (shearwall and steel moment frame), building heights (2 to 26 stories), and fundamental periods of vibration (0.2 sec to 2.8 sec). We estimated safe separation distance as a fraction of the height of the shorter building and as a function of S_{MS}, system combination, and analytical method. Both the spectral displacement approach and the equivalent lateral force procedure appear to give modestly conservative estimates of safe separation distance. The former would be safe with 66% probability, the latter with 90% probability, assuming that the third approach (multiple linear elastic structural analyses with drifts factored by C_d/R to approximate nonlinear response) gives a fairly accurate estimate of the true distribution of building motion. In later work, we will examine multiple nonlinear dynamic analysis and compare the first three with the fourth.

Chapter 3

3 Safe distance to avoid pounding in earthquakes: 3 simpler ways and a state-of-the-art approach to calculate it

This chapter is based on:
Isteita, M., and Porter, K. (2019?). "Safe distance to avoid pounding in earthquakes: 3 simpler ways and a state-of-the-art approach to calculate it."

Abstract

We reevaluate the required safe separation distance between two adjacent buildings to avert pounding in earthquakes. We consider several alternative approaches: the FEMA P-154 spectral displacement approach, the ASCE 7 equivalent lateral force approach, multiple linear dynamic analyses, and multiple nonlinear dynamic analyses. Safe separation distance is evaluated at two shaking levels: 2/3 the risk-targeted maximum considered earthquake shaking (MCE_R) for use with ASCE 7, and at full MCE_R, for use with FEMA P-154. We exercise the competing approaches using a few specimens of reinforced concrete special moment-frame (SMF) and ordinary moment-frame (OMF) buildings. We assume that multiple nonlinear dynamic analyses most accurately estimate what actually happens in the real world and measure the safety of the other approaches relative to it. Considering the two shaking levels, two structural systems, and several combinations of building heights, spectral displacement as expressed in FEMA P-154 appears to be slightly

conservative at 2/3 MCE_R producing safe separation distance with 78% to 96% probability; however, at MCE_R, which it was intended for, is reasonably safe with 76% to 88% probability. One must multiply the estimate of spectral displacement approach by 0.8 for SMF cases and 0.6 for OMF cases to get the mean of the most accurate approach. In the other hand, the equivalent lateral force method as expressed in ASCE 7 and multiple linear dynamic analyses approach factored by C_d/R appear to be reasonably safe with 50% to 75% probability at both shaking levels with the exception where they appear to be unconservative for OMF cases at MCE_R shaking with 33% to 39% probability. The equivalent lateral force method from ASCE 7 provides a very good estimate of the mean of the most accurate approach, with conversion factors ranging between 0.9 to 1.2. Multiple linear dynamic analyses factored by C_d/R do a good job of estimating the median of the most accurate approach with a relatively small record-to-record variability.

Keywords: seismic pounding; safe Structural Separation; adjacent buildings requirements

3.1 Introduction

Researchers have long examined earthquake-induced pounding between adjacent buildings because of the damage pounding has caused in past earthquakes. We reexamined safe separation distance because recent work on FEMA P-154 (ATC 2015) suggests US practice encoded in ASCE 41-13 (ASCE 2014) is overly conservative. There is no mention of any pounding provisions changing in the update summary by “Summary of the updates to ASCE/SEI 41-17 - SEAOC” (2017). ASCE 41-13 requires a separation distance on the order of 4% of the height of the shorter building, with the option of structural analysis of the building in question to justify a distance as little as 3% plus the displacement of the building in question. By “safe separation distance,” we mean the smallest distance between the bases of two vertically prismatic buildings so that in an earthquake exhibiting some specified level of shaking, the two buildings will not touch. FEMA P-

154, which aims for greater speed than ASCE 41-13, uses a simpler estimate of safe separation distance based on spectral displacement, and no structural analysis of either building. ASCE 7-16 (ASCE 2016) requires the separation distance to be at least the square root of the sum of squares of the two buildings' maximum displacement, estimated either using an elastic structural analysis of both buildings, or an inelastic structural analysis of both buildings if one wants to reduce the separation distance. All of which beg several questions:

1. Is the simple FEMA P-154 spectral approach any good? How well does it estimate safe separation distance?
2. Is ASCE 41-13's 3% to 4% separation distance actually overly conservative?
3. Is ASCE 7-16's elastic structural analyses of both buildings worth the effort? Is its estimate any safer, more reliable, more accurate, than a simpler approach that does not require structural analyses of both buildings?

In this work, we attempt to answer these questions only for reinforced concrete special and ordinary moment-frame buildings, although the methodology can be used for other systems and pairs of different systems. Let us first review the relevant literature on pounding, then describe the analyses we performed to address these questions.

FEMA P-154 assumes that pounding increases the collapse probability if the buildings are separated less than the peak roof displacement of the shorter building, estimated using spectral displacement response. More precisely, FEMA P-154 assumes that buildings touch if they are separated by less than twice the spectral displacement of the shorter building, but that pounding significantly aggravates collapse if the buildings are less than half that distance apart.

Pounding tends to occur in dense urban areas because of the small separation distances there. Several authors have performed surveys of pounding damage after earthquakes. Rosenblueth and Meli (1986) report on a damage survey after the 1985 Mexico City earthquake, performed by teams of engineering students, each team led by one or two experienced structural engineers. The teams performed mostly external (visual) inspection of 330 buildings that experienced severe damage or collapse, associated pounding with 40% of instances, and asserted that “in 15 percent of all cases [pounding] led to collapse.” The authors do not offer the teams’ basis for judgment, evidence, or validation of the teams’ judgment.

Kasai and Maison (1997) survey of pounding damage after the 1989 Loma Prieta earthquake found that about 500 buildings were affected by about 200 instances of pounding, mostly involving older multistory masonry buildings, many with almost no separation, predominantly involving minor architectural or structural damage. The authors warned of the potential for more serious damage in future, closer or larger earthquakes. Cole et al. (2012) performed a similar survey of a portion of downtown Christchurch after the 2011 earthquake, most of which had no separation distance. Three notable findings: some buildings suffered partial collapse in part because of pounding; unreinforced masonry buildings were disproportionately likely to experience pounding damage, compared with concrete, timber, and steel; and the authors are not sure that pounding contributed to the complete collapse of any buildings.

Jeng et al. (1992) used random-vibration theory to examine three approaches to estimate safe separation distance between single-degree-of-freedom systems subjected to white-noise excitation. (Actually they examined MDOF systems, but only elastic response in the first mode, so essentially SDOF). They recommend a double-difference combination (DDC) rule for building separation over either the sum of maximum displacements or the square root of the sum of the squares (SRSS); the recommended approach is like SRSS reduced by an amount related to the product of the maximum displacements and a correlation coefficient that varies with damping ratio and building periods.

Filiatrault and Cervantes (1995) expressed concern that the separation distance prescribed by the 1990 National Building Code of Canada (1990) was overly conservative, based on the sum of the maximum deflections at the top of the shorter building. They performed nonlinear dynamic structural analysis of 5 realistic concrete shearwall buildings designed for each of 3 Canadian cities whose design base shears were generally in proportion 1:2:3 for a given building height. They use the estimates of structural response to support a method to estimate safe separation distance that involves equivalent lateral force (pseudostatic linear analysis) to estimate first-mode maximum response at the height of the top of the shorter building, and application of Jeng et al.'s DDC approach.

Lopez Garcia, D (2004) provides a modified double difference combination (MDDC) approach similar to that of Jeng et al. but replacing the correlation coefficient with an empirical parameter that, he shows, provides consistent, modest conservatism and accounts for behavior of linear and nonlinear SDOF and MDOF systems.

The authors' previous research (Isteita and Porter 2017) examined the three simpler approaches to estimate safe separation distance to avoid pounding at MCE_R shaking: (1) SRSS of 5% damped elastic spectral displacement response at the top of the shorter building; (2) ASCE 7's equivalent lateral force procedure; and (3) multiple linear elastic dynamic structural analyses, with drift results multiplied by C_d/R to approximate nonlinear response. We varied seismicity (four locations whose SMS values span from 0.8g to 3.0g), combinations of seismic force-resisting systems (shearwall and steel moment frame), building heights (2 to 26 stories), and fundamental periods of vibration (0.2 sec to 2.8 sec). We estimated safe separation distance as a fraction of the height of the shorter building and as a function of SMS, system combination, and analytical method. Both the spectral displacement approach and the equivalent lateral force procedure appear to give modestly conservative estimates of safe separation distance. The former would be safe with 66% probability, the latter with 90% probability, assuming that the third approach (multiple linear elastic structural analyses with drifts factored by C_d/R to approximate nonlinear response) gives a fairly accurate estimate of the true distribution of building motion.

The present work extends the previous work by considering multiple nonlinear dynamic analysis, treating these new analyses as providing a better estimate of true safe separation distance compared with the other three approaches. That is, we compare four analytical approaches:

1. Elastic spectral displacement
2. Equivalent lateral force
3. Multiple linear elastic dynamic structural analyses, and
4. Multiple nonlinear dynamic structural analyses.

We examine 3 combinations of special reinforced concrete moment frame buildings—SMF—and ordinary reinforced concrete moment frame buildings, OMF (i.e. ductile and non-ductile reinforced concrete frame structures); 5 building heights between 2 and 20 stories for SMF; 4 building heights between 2 and 12 stories for OMF; two risk-targeted shaking levels (i.e. shaking of 2/3 MCE_R and MCE_R).

Ultimately, we aim to estimate:

1. The degree to which one can be confident that pounding will not actually occur, if one calculates the safe separation distance between the buildings by any of the three relatively simple approaches in MCE_R and 2/3 MCE_R shaking;

2. A set of conversion factors to relate the separation distances calculated by any of the simpler methods 1-3 above to method 4, which we deem to most closely approximate what happens in the real world.

3.2 Research Methodology

The procedure for this study works as follows:

3.2.1 Step 1: asset definition

We aim to investigate both the effect of buildings' seismic force-resisting systems and buildings' fundamental periods of vibration on the minimum permissible distance between two adjacent buildings. One selects a few particular buildings of various heights and one or more combinations of seismic force-resisting systems.

3.2.2 Step 2: hazard analysis and ground motions selection

We limit our study to the examination of two shaking levels beyond the elastic: 2/3 MCE_R, the level at which ASCE 7 tests safe separation distance, and MCE_R, because our initial motivation was to inform FEMA P-154, which screens buildings for collapse hazard at MCE_R. Examining two levels also informs how safe separation distance might vary with the shaking level.

One deaggregates hazard to find the modal (most likely) controlling source characteristics (modal magnitude M, distance R, and epsilon ε_0) associated with the site and each of two levels of shaking. Lastly, one selects a suite of at least 11 ground motions with approximately the same source characteristics and scales each ground motion to match the shaking level of interest. We limit our suite of ground motions to those than can be scaled to the desired shaking by multiplying all acceleration amplitudes by a factor between 0.5 to 2.0, so as to keep the time histories as realistic as possible.

For each suite of ground motions, one finds at least 11 ground motions that do not cause the nonlinear model to appear to collapse, regardless of interaction with the other building. (In a ground motion that would cause a model to collapse in isolation, safe separation distance is meaningless.) This can mean starting with a larger suite of ground motions so as to have ground motions to ignore in case they produce an estimate of collapse.

3.2.3 Step 3: first approach, spectral displacement estimate of proximity

The minimum required safe separation distance according to this approach is estimated as the square root of the sum of the squares (SRSS) of the spectral displacement response of each pair of buildings, based solely on their estimated periods, heights, and the idealized spectrum at the shaking level of interest. In addition, the spectral displacement is translated to the roof of each building, a triangular mode shape is assumed and the height of the shorter building for each building of the pair is considered, as shown in Figure 3.1 and in accordance with Equation (3.1). The approach requires very modest effort, with the disadvantage that it does not account for any building characteristics other than height and estimated period. SRSS represents almost the simplest deflection combination possible (absolute sum having been shown to be overly conservative and DDC or MDDC requiring somewhat more effort and complexity). Mathematically,

$$d^{(SD)} = \sqrt{\left(S_{d1}.\frac{h_2}{h_1}\right)^2 + (S_{d2})^2} \tag{3.1}$$

where $d^{(SD)}$ denotes the spectral displacement estimate of safe separation distance, S_{d1} and S_{d2}denote the spectral displacement response for the taller and shorter buildings, respectively, using the idealized design spectrum, and h_1 and h_2 are the heights of the taller and shorter buildings, respectively.

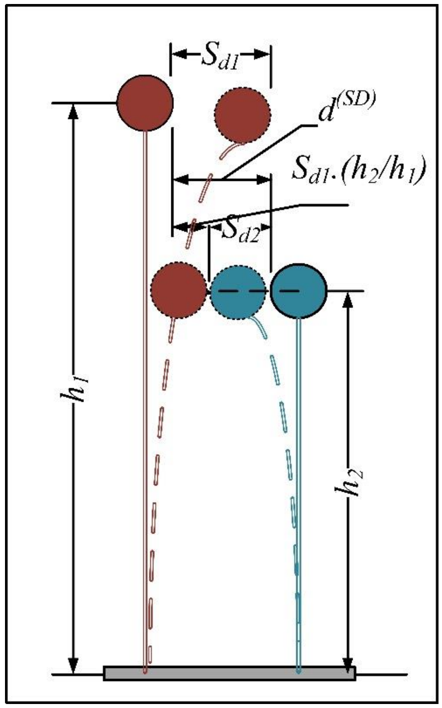

Figure 3.1 – Approach 1, the spectral estimate of proximity model

3.2.4 Step 4: second approach, equivalent lateral force

The second approach is to follow the equivalent lateral force procedure (ELF) specified in section 12.8 of ASCE 7-16, with and without the 2/3 factor of ASCE 7-16 equations 11.4-3 and 11.4-4. One estimates the required separation according to Equation (3.2), which calculates the SRSS the estimated maximum inelastic deformation of the two buildings at the top of the shorter building. Figure 3.2 illustrates the model. The second approach requires structural analysis of both buildings.

$$d^{(ELF)} = \sqrt{(\delta_{M1}^2 + \delta_{M2}^2)} \tag{3.2}$$

$$\delta_M = \frac{\delta_{Max}.C_d}{I_e} \tag{3.3}$$

where,

$d^{(ELF)}$ = equivalent lateral force estimate of safe separation distance

δ_{Max} = maximum elastic displacement at the critical location (the top of the shorter building) under loading $S_{MT}.I_e/R$

S_{MT} = soil-amplified spectral acceleration response in the idealized design spectrum and the appropriate period under risk-targeted maximum considered earthquake shaking,

R = response modification factor in ASCE 7 table 12.2-1

C_d = deflection amplification factor from ASCE 7 table 12.2-1

I_e = importance factor from ASCE 7 section 11.5-1

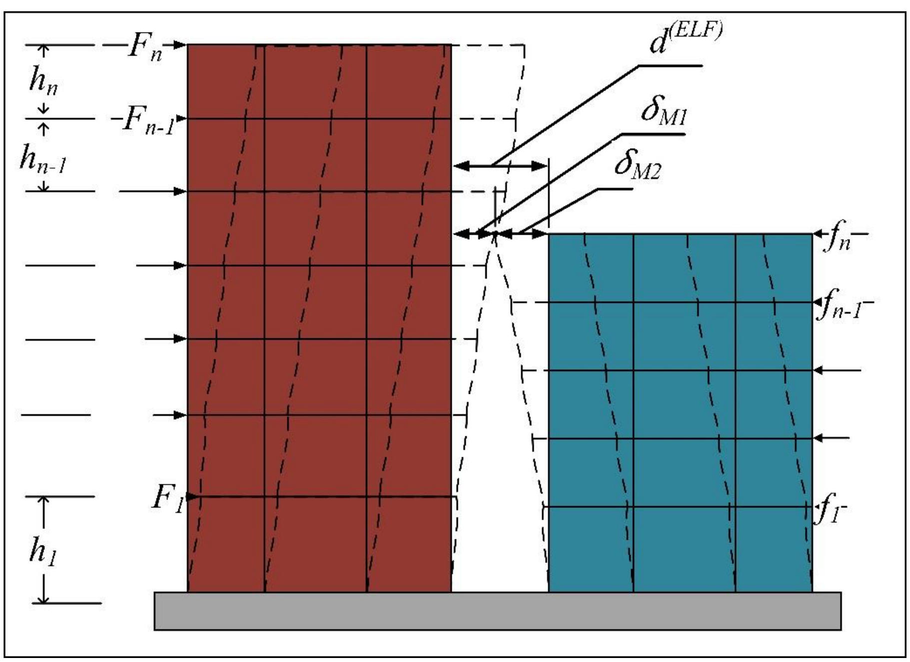

Figure 3.2– Approach 2, equivalent lateral force estimate of proximity

3.2.5 Step 5: third approach, multiple linear dynamic analyses

In this approach, one estimates the minimum safe distance at the critical location by linear dynamic analysis of each building using any convenient software such as OpenSees (PEER 2017). One subjects each building to the selected ground motions as described in step 2, records the displacement time-history of all edge nodes, and determines the separation distance time-history of each building pair as the difference between the displacement time-histories of the two buildings at the top of the shorter building. Then, one determines the minimum safe separation distance as the maximum of the absolute of the separation distance time-history according to Equation (3.4). Next, one calculates the cumulative distribution function of the minimum safe distance conditioned on building pair and shaking level (i.e., 2/3 MCE_R and MCE_R). To comply with the requirements of ASCE 7 Section 16.1, one multiplies drift by C_d/R. For example, the ratio takes on a value of 0.69 for special reinforced concrete moment frames and 0.83 for ordinary reinforced concrete moment frames. Figure 3.3 illustrates the model assembly.

$$d^{(LD)} = max\left|\left(\delta_1(t) - \delta_2(t)\right)\right| \tag{3.4}$$

where,

$d^{(LD)}$ = Linear dynamic estimate of proximity

$\delta_1(t)\ and\ \delta_2(t)$ = displacement in the positive *x*-direction (e.g., rightward in Figure 3.3 at time *t* at the critical location (the top of the shorter building) for buildings 1 and 2, respectively.

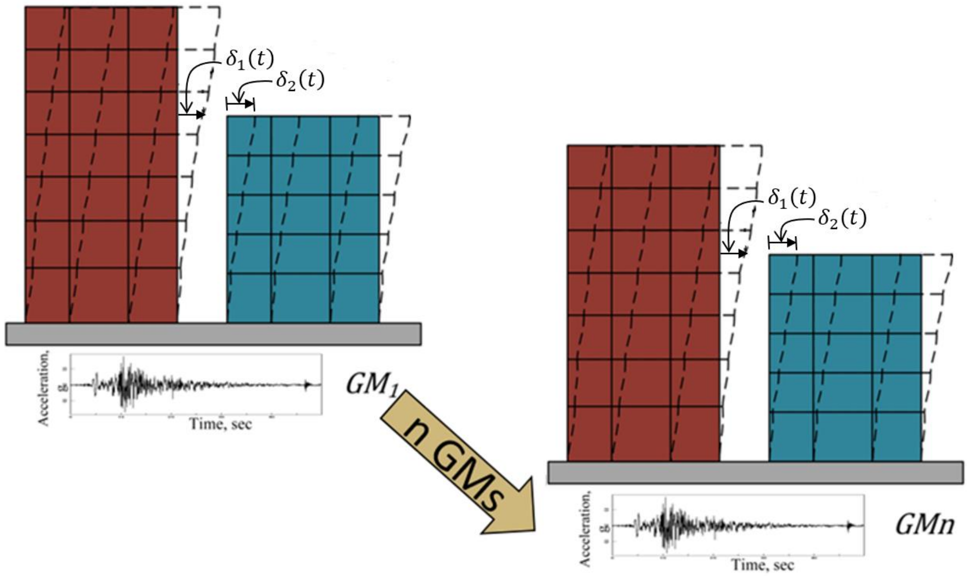

Figure 3.3 – The Linear Dynamic Estimate of Proximity

3.2.6 Step 6: fourth approach, multiple nonlinear dynamic analyses

In this approach, one estimates the minimum safe separation distance at the critical location by steps that similar to the third approach, except with nonlinear dynamic analyses instead of linear, using any convenient software such as OpenSees (PEER 2017). In this approach, the minimum safe separation distance at the critical location is determined according to Equation (3.5), and its cumulative distribution function is calculated and conditioned on building pair and shaking level. Again, one evaluates both 2/3 MCE_R for use with ASCE 7, and MCE_R for use with FEMA P-154. Figure 3.4 illustrates an example pair of building models, displacement time histories, and the time series of separation distance.

$$d^{(NLD)} = max\left|\left(\delta_1(t) - \delta_2(t)\right)\right| \tag{3.5}$$

where

$d^{(NLD)}$ = nonlinear dynamic estimate of proximity

$\delta_1(t)$ and $\delta_2(t)$ = *x*-direction displacement at time *t* at the critical location (the top of the shorter building) for buildings 1 and 2, respectively.

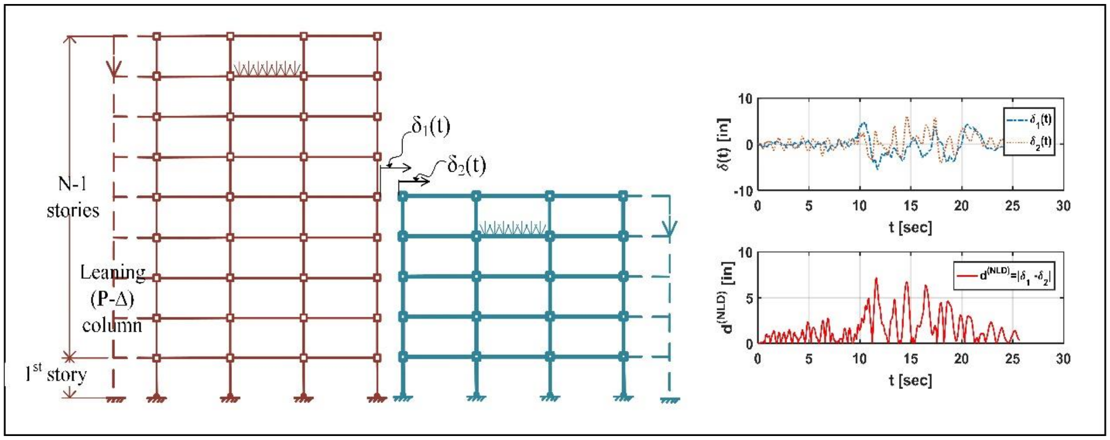

Figure 3.4 – The Nonlinear Dynamic Estimate of Proximity

3.2.7 Step 7: iterate to characterize probabilistic structural response

One iterates steps 2 through 6 for each of many combinations of lateral force resisting systems, building heights, and the two shaking levels.

3.2.8 Step 8: comparisons

One examines how safe are approaches 1, 2, and 3 versus 4, assuming approach 4 most accurately estimates what actually happens in the real world. Idealizing the reduction in proximity under the 4th approach with a lognormal cumulative distribution function, one can use Equation (3.6) to estimate the probability that a pair of buildings would NOT pound together if separated by a distance d, i.e., if approach 1, 2, or 3 estimated the safe separation distance as d:

$$p = \Phi\left(\frac{ln(d/\theta)}{\beta}\right) \tag{3.6}$$

In Equation (3.6), Φ denotes the standard normal cumulative distribution function, d is either $d^{(SD)}$, $d^{(ELF)}$, or $d^{(LD)}$, i.e., the safe separation distance calculated by approach 1, 2, or 3, θ is the median safe separation distance calculated using approach 4 (i.e., the median closest reduction in distance between the two buildings), and β is the standard deviation of the natural logarithm of safe separation distance. One can calculate p for each combination of building pair and shaking level, and do so for approaches 1, 2 and 3.

Then, one estimates a conversion factor for each of the three simpler approaches. We estimate three such factors for each simpler approach:

1. The ratio of the true mean safe separation distance (i.e., that of method 4) to the simpler estimate. In the case of method 3, one estimates the percentile of the method-3 estimate that corresponds to the mean of method 4, because method-3 produces a probability distribution of safe separation distance.
2. The ratio of the median (50th percentile) of the true safe separation distance to the simpler estimate. In the case of method 3, again one maps from a percentile of the method-3 distribution to the median of the method-4 distribution.
3. The ratio of the 84th percentile of the true safe separation distance to the simpler estimate. In the case of method 3, again one maps from a percentile of the method-3 distribution to the 84th percentile of the method-4 distribution.

3.3 Case studies

3.3.1 Asset definition

We investigated pounding within and between two seismic force-resisting systems: special RC moment frames, which are modern structures of ductile reinforced concrete frames, and ordinary RC moment frames, which are 1967 era structures of non-ductile reinforced concrete frames. The SRC models are designed to comply with ASCE 7-02. Both SRC and ORC buildings could stand at a location of high seismicity south of downtown Los Angeles, CA.

To sample special reinforced concrete moment frames, we used the 2-story, 4-story, 8-story, 12-story, and 20-story models provided by (Haselton 2006). Additional details on the structural design can be found in Haselton 2006. To sample ordinary reinforced concrete moment frames, we used the 2-story, 4-story, 8-story, and 12-story models provided by (Liel 2008). Additional details on the structural design are given in Liel 2008.

Table 3.1 summarizes our 9 sample buildings: their fundamental period of vibration T, height H, stories, and resisting system.

Table 3.1 – Sample buildings

Building ID	Ref. ID	T, sec	H, ft	Stories	Seismic Force-Resisting System
$SRC-20$	1020	2.63	262	20	SRC
$SRC-12$	1013	2.01	158	12	SRC
$SRC-08$	1011	1.71	106	8	SRC
$SRC-04$	1003	1.12	54	4	SRC
$SRC-02$	2064	0.66	28	2	SRC
$ORC-12$	3022	2.75	158	12	ORC
$ORC-08$	3015	2.36	106	8	ORC
$ORC-04$	3003	1.96	54	4	ORC
$ORC-02$	3002	1.04	28	2	ORC
	SRC: Special reinforced concrete moment frames ORC: Ordinary reinforced concrete moment frames				

Table 3.2 presents the combinations we examined: SS denotes adjacent special reinforced concrete moment frame buildings; OO denotes adjacent ordinary reinforced concrete moment frame buildings, and SO denotes a special next to an ordinary reinforced concrete moment frame building.

Table 3.2 – Reinforced concrete building combinations

Special – special RCMF		
Case #	Left	Right
SS-1	$SRC-20$	$SRC-12$
SS-2	$SRC-20$	$SRC-08$
SS-3	$SRC-20$	$SRC-04$
SS-4	$SRC-20$	$SRC-02$
SS-5	$SRC-12$	$SRC-08$
SS-6	$SRC-12$	$SRC-04$
SS-7	$SRC-12$	$SRC-02$
SS-8	$SRC-08$	$SRC-04$
SS-9	$SRC-08$	$SRC-02$
SS-10	$SRC-04$	$SRC-02$

Ordinary – ordinary RCMF		
Case #	Left	Right
OO-1	$ORC-12$	$ORC-08$
OO-2	$ORC-12$	$ORC-04$
OO-3	$ORC-12$	$ORC-02$
OO-4	$ORC-08$	$ORC-04$
OO-5	$ORC-08$	$ORC-02$
OO-6	$ORC-04$	$ORC-02$

Special – ordinary RCMF		
Case #	Left	Right
SO-1	$SRC-20$	$ORC-12$
SO-2	$SRC-20$	$ORC-08$
SO-3	$SRC-20$	$ORC-04$
SO-4	$SRC-20$	$ORC-02$
SO-5	$SRC-08$	$ORC-12$
SO-6	$SRC-08$	$ORC-04$
SO-7	$SRC-08$	$ORC-02$
SO-8	$SRC-02$	$ORC-12$
SO-9	$SRC-02$	$ORC-08$
SO-10	$SRC-02$	$ORC-04$

3.3.2 Hazard analysis and ground motion selection

We performed the analysis at the two shaking levels of interest for a location in south of downtown Los Angeles, CA, which is the approximate location for which the buildings were designed. We estimated V_{S30} using Wills and Clahan's (2006) map. We used the USGS's probabilistic seismic hazard deaggregation tool [http://geohazards.usgs.gov/deaggint/2008/] to estimate source characteristics (modal magnitude M, distance R, and epsilon ε_0) associated with

S_{DS} and S_{MS} at the target location. At this location, S_{DS} =1.445g (i.e., 2/3 MCE_R) and S_{MS} = 2.167g (MCE_R motion). We selected one suite of ground motions corresponding to the modal source characteristics and scaled them to match S_{DS} and another suite to match S_{MS}. We selected records whose scaling factors were closest to 1.0 (and always between 0.5 and 2.0) using the tools of the Pacific Earthquake Engineering Research (PEER) Center at http://ngawest2.berkeley.edu.

For simplicity, we do not comply with the requirements of ASCE 7-16 Sec 16.2.3.2, which requires scaling motions so that "the average of the maximum-direction spectra from all ground motions generally matches or exceeds the target response spectrum" and "The average of the maximum-direction spectra from all the ground motions shall not fall below 90% of the target response spectrum for any period within the same period range."

3.3.3 Results

Table 3.3 summarizes the statistics of safe distances under the four approaches. The column labeled "case group" indicates the building combinations: SS denotes all the cases with two adjacent special RC moment frame buildings, SO denotes all the cases with a special RC moment frame buildings adjacent to an ordinary RC moment frame building, and OO denotes all the cases with two adjacent ordinary RC moment frame buildings. The column labeled "shaking level" indicates the hazard level in terms of risk-targeted maximum considered earthquake shaking level: 2/3 of MCE_R or MCE_R

The columns to the right give statistics of safe separation distance as a fraction of the height of the shorter building, averaging over all particular building combinations in the given case and hazard level: μ denotes average and δ denotes coefficient of variation, averaging over all the building combinations in the group. In the cases of the 3rd or 4th approaches, we averaged over all the ground motion time histories as well. The column labeled $\hat{\beta}_{RTR}$ measures record-to-record variability. To be precise, one calculates the natural logarithm of separation distance in each pair of buildings and ground motion time history.

There are 11 such distances per combination of building pair, one per ground motion time history. The standard deviation of those natural logarithms measures the record-to-record variability in separation distance. For each case group of SS, SO, and OO, there are 10, 6 and 10 such standard deviations respectively, one for each of building pair.

The record-to-record variability varies among the cases; the value shown in the table is the average of those cases. The columns labeled $p^{(1)}$, $p^{(2)}$ and $p^{(3)}$ in Table 3.3 give the probability (averaging over all cases in the group) that an actual earthquake with risk targeted shaking will produce a smaller safe separation distance than the value of d calculated by approach 1, 2, or 3, respectively, assuming that approach 4 accurately estimates true building response. That is, they represent the probabilities that methods 1, 2, and 3 would not underestimate safe separation distance.

One can view the contents of these last three columns as indicating how safe would be the simplified approach. A probability of less than 0.50 means that the simpler approach more likely than not underestimates safe separation distance and could be called unconservative. One could call a probability of between 0.5 and 0.9 “reasonably safe,” meaning more likely than not to estimate a safe separation distance that exceeds the true safe separation distance, but not by too much (90% representing our arbitrarily chosen upper limit to “not too much”). One could interpret a probability in excess of 0.9 as suggesting an overly conservative estimate of safe separation distance.

Table 3.3 – Summary statistics

Case group	Shaking Level	1ST approach		2nd approach		3rd approach			4th approach			$p^{(1)}$	$p^{(2)}$	$p^{(3)}$
		μ	δ	μ	δ	μ	δ	$\hat{\beta}_{RTR}$	μ	δ	$\hat{\beta}_{RTR}$			
SS	$\frac{2}{3}MCE_R$	0.015	0.190	0.013	0.078	0.009	0.409	0.365	0.012	0.763	0.464	0.78	0.67	0.51
SO	$\frac{2}{3}MCE_R$	0.020	0.247	0.012	0.132	0.010	0.459	0.342	0.010	0.662	0.515	0.96	0.75	0.64
OO	$\frac{2}{3}MCE_R$	0.025	0.185	0.013	0.135	0.011	0.437	0.324	0.014	0.594	0.491	0.94	0.58	0.51
SS	MCE_R	0.022	0.190	0.019	0.078	0.015	0.413	0.352	0.018	0.741	0.451	0.76	0.64	0.53
SO	MCE_R	0.030	0.247	0.019	0.132	0.015	0.502	0.329	0.017	0.602	0.482	0.87	0.57	0.48
OO	MCE_R	0.038	0.185	0.019	0.135	0.016	0.479	0.309	0.023	0.462	0.444	0.88	0.39	0.33

Some general observations of the results in Table 3.3:

1. Approach 1, spectral displacement as expressed in FEMA P-154, appears to be overly conservative at 2/3 MCE_R, producing safe separation distance with 78% to 96% probability. The FEMA P-154 authors intended it for use at MCE_R, at which level of ground motion it is reasonably safe (76% to 88% probability), as defined here.
2. Approaches 2 and 3 (equivalent lateral force method of ASCE 7 and multiple linear dynamic analyses factored by C_d/R) are reasonably safe at 2/3 MCE_R (51% to 75% probability) and unconservative for OO cases at MCE_R shaking (33% to 39% probability).
3. Average safe distances of all four approaches, including multiple nonlinear dynamic analyses, tend to be linearly proportional to the shaking level. The observation supports the equal-displacement rule for buildings like those modeled here.
4. In general, special reinforced concrete moment frame buildings combinations have the smallest safe separation distances; however, the differences in the safe separation distances

between different building combinations are trivial in the 2nd and 3rd approaches. Since the 3rd approach probably requires more effort, the trivial difference argues for using the 2nd approach instead. ASCE 7's C_d/R values seem pretty good for these two building types, or else it is a remarkable accident that particular choices of sample buildings used here agree so well with ASCE 7's C_d/R values.

Table 3.4 summarizes the conversion factors. Set 1 converts from the simpler approaches to the μ of the 4th approach. Set 2 converts from the simpler approaches to the 50th percentile (the median) of the 4th approach. Set 3 converts from the simpler approaches to the 84th percentile of the 4th approach. The first column of each set contain factors by which the spectral estimate of safe separation distance can be multiplied to get the statistic of safe separation distance using nonlinear dynamic analyses. The second column of each set contains factors by which the equivalent lateral force estimate can be multiplied to get the statistic of safe separation distance using nonlinear dynamic analyses. The third column of each set is the percentile of the third approach corresponding to the statistic of safe separation distance using nonlinear dynamic analyses.

Table 3.4 – Conversion factors

Case group	Shaking Level	Set 1: to the μ of the 4th approach			Set 2: to 50th percentile of the 4th approach			Set 3: to 84th percentile of the 4th approach		
		1ST approach	2nd approach	3rd approach	1ST approach	2nd approach	3rd approach	1ST approach	2nd approach	3rd approach
SS	$\frac{2}{3}MCE_R$	0.77	0.95	78th	0.62	0.74	54th	1.20	1.51	97th
SO	$\frac{2}{3}MCE_R$	0.51	0.87	64th	0.40	0.65	33rd	0.77	1.40	96th
OO	$\frac{2}{3}MCE_R$	0.55	1.15	81st	0.43	0.89	54th	0.80	1.69	98th
SS	MCE_R	0.78	0.97	76th	0.62	0.73	49th	1.17	1.52	98th

SO	MCE_R	0.58	0.96	73^{rd}	0.53	0.86	60^{th}	0.87	1.66	98^{th}
OO	MCE_R	0.55	1.2	83^{rd}	0.54	1.16	78^{th}	0.83	1.75	94^{th}

Some general observations of results in Table 3.4:

1. Approach 1 overestimates safe separation distance: one must multiply the estimate by by 0.8 (for SS cases) or 0.6 (for OO) to get the mean of approach 4, but they approximate the 84th percentile reasonably well (1.2 times for SS and 0.8 for OO).
2. Approach 2, the equivalent lateral force method from ASCE 7-16, provides a very good estimate of the mean for approach 4, with conversion factors ranging between 0.9 to 1.2 and an equally weighted average of 1.0.
3. Approach 3 does a good job of estimating the median of approach 4: the 33rd to 78th percentiles of approach 3 map to the median of the 4th approach. With a relatively small record-to-record variability, that range is relatively small.
4. Variability in the 1st and 2nd approaches is much smaller than that of the 3rd and 4th as measured by the coefficients of variation (δ). That observation should surprise nobody because the 3rd and 4th approaches reflect record-to-record variability.
5. Approach 3 underestimates uncertainty: because its record-to-record variability is smaller, its 94th to 98th percentiles map to the 84th percentile of approach 4. It takes almost 2 standard deviations of the linear elastic approach to equal 1 standard deviation of the nonlinear approach. Nonlinear response increases uncertainty. And since the method-3 median estimate is liable to be reasonably accurate (at least for these case studies), the analyst who tries a dynamic linear model, does not like the answer, and goes looking for a smaller safe separation distance with a nonlinear model, is likely to be disappointed.

6. All three simpler approaches are less safe at MCE_R than at 2/3 MCE_R wherever ordinary moment frames are involved (SO or OO). We do not know why for sure but it could be because the ordinary frames experience greater drift that is close to collapse at MCE_R shaking level.
7. This study supports the finding in FEMA P-154 (Applied Technology Council 2015) that ASCE 41-13 (ASCE 2014) is overly conservative. In no case, even at MCE_R motion and the OO building combination, does method 4 suggest safe separation distance approaches 3%, let alone 4%.

3.4 Conclusions

We examine three linear approaches to estimate safe separation distance to avoid seismic pounding between adjacent buildings: (1) the square root of the sum of the squares of 5% damped elastic spectral displacement response at the top of the shorter building; (2) ASCE 7-16's equivalent lateral force procedure; and (3) multiple linear elastic dynamic structural analyses, with drift results multiplied by ASCE 7-16's C_d/R to approximate nonlinear response. We compared these with the safe separation distance produced by a fourth method, multiple nonlinear time-history structural analyses, to explore how safe it would be to use the simpler approaches.

We consider shaking at 2/3 MCE_R and MCE_R, to evaluate pounding criteria for ASCE 7 and FEMA P-154, respectively. We examined three combinations of seismic force-resisting systems (special reinforced moment frames and ordinary reinforced moment frames), building heights (2 to 20 stories), and fundamental periods of vibration (0.66 sec to 2.63 sec). We estimated safe separation distance as a fraction of the height of the shorter building and as a function of shaking level, system combination, and analytical method.

The spectral displacement approach (FEMA P-154) appears to give reasonably safe estimates of safe separation distance at MCE_R, and arguably overly conservative estimates at 2/3 MCE_R.

The approaches of using equivalent lateral force (ASCE 7) and multiple linear elastic analyses factored by C_d/R appear to give reasonably safe estimates of safe separation distance for most cases at 2/3 MCE_R and MCE_R, and unconservative estimates in a few cases at MCE_R.

Our findings seem sufficient only to make tentative conclusions about safe separation distance. We hope to perform similar analyses with reinforced concrete shearwall buildings, steel-frame buildings, hybrid systems with concrete corewalls and steel-frame outriggers, and buildings in other geographic locations. They do however seem to support using spectral displacement as a reasonable and easy initial estimate of safe separation distance.

Chapter 4

4 Effect of pounding on the collapse safety of reinforced concrete moment frame buildings

This chapter is based on:

Isteita, M., and Porter, K. (2019?). "Effect of pounding on the collapse safety of reinforced concrete moment frame buildings"

Abstract

We present incremental dynamic analyses of 140 pairs of adjacent post-2000 reinforced concrete moment frame buildings with aligned floors and various separation gaps, studying how pounding affects collapse capacity, defined here as the level of ground motion at which collapse occurs. In a few cases, pounding was estimated to reduce median collapse capacity slightly; the decrease in median capacity was always less than 11% and averaged less than 2.5%. In some cases, pounding slightly increases collapse capacity, but the equally weighted overall effect was less than 1%, within the noise level of structural analysis. The findings of this study suggest the effect of pounding on the collapse capacity seems small enough to ignore, at least for the conditions we studied, especially where floor align. A photo survey of collapsed California concrete buildings revealed no evidence that pounding caused or aggravated actual collapses. The lack of obvious pounding-induced collapses of California concrete buildings and within our analytical case study

hardly proves that pounding does not cause collapse. But it weakens the hypothesis that pounding between buildings with aligned floors significantly contributes to collapse, and strengthens the inference that pounding may matter little if at all in cases where floors align.

Keywords: seismic pounding risk; buildings collapse safety; safe Structural Separation; buildings collapse safety; reinforced concrete moment frame buildings

4.1 Introduction

Earthquake pounding occurs where strongly shaken buildings of dissimilar dynamic characteristics have too little separation between them. Pounding causes architectural and structural damage, and is believed to have contributed to collapse, e.g., in the 1985 Mexico City earthquake (Rosenblueth and Meli 1986). Seismic design standards such as ASCE 7-16 (ASCE 2016) attempt to prevent pounding in new buildings by requiring a minimum separation distance with nearby buildings. Some risk-management tools such as FEMA P-154 (ATC 2015) attempt to estimate the increase in collapse risk when two buildings are close together. The authors of FEMA P-154 estimated safe separation distance based on damped elastic spectral displacement response. They also estimated the increase in collapse probability if buildings are closer than the safe separation distance. That increase is largely guesswork by the authors of FEMA P-154. Can we do better than guesswork?

We present and exercise a simple method to estimate the degree to which pounding aggravates collapse probability. We use nonlinear dynamic structural analysis with many ground motion time histories at many levels of excitation. We estimate the collapse probability using many pairs of structural models, each model representing a modern code-compliant reinforced concrete moment frame building. We limit our inquiry to reinforced concrete moment frame buildings whose floors align, whose heights vary between 2 and 20 stories, and whose separation distances vary between essentially zero and 17 feet (effectively infinity).

4.2 Literature review

4.2.1 Pounding damage in three earthquakes

Several authors present evidence of pounding causing or aggravating collapse. Rosenblueth and Meli (1986) report on a survey of damage after the 1985 Mexico City earthquake performed by teams of engineering students led by one or two experienced structural engineers. After conducting mostly external (visual) inspections of 330 buildings that experienced severe damage or collapse, the teams found damage associated with pounding in 40% of the cases. They asserted that “in 15 percent of all cases [pounding] led to collapse.” Although perfectly plausible, the authors do not offer a basis for that 15% judgment. Nor do they offer a detailed discussion of evidence nor any validation such as blind prediction.

Kasai and Maison (1997) inspected about 500 buildings shaken by the 1989 Loma Prieta earthquake, observing approximately 200 instances of pounding. Pounding occurred mostly in older multistory masonry buildings and predominantly involved minor architectural or structural damage. Although most cases show damage of a minor nature, the authors still assert that damage would be more serious in more severe earthquakes.

Cole et al. (2012) surveyed building damage in Christchurch’s central business district after the 2011 Christchurch earthquake. Out of 376 buildings surveyed, 119 showed evidence of pounding. Damage ranged from none to complete building collapse. Two collapsed buildings showed evidence of pounding, but the authors expressed low confidence that pounding caused or substantially contributed to the collapse. Further, the researchers identified 18 buildings as having partially collapsed (15% of the 119), where they define partial collapse as loss of a facade or similar sized component. They assigned high confidence that pounding was a main contributor to the observed damage to only 4 of these 18 buildings. Their evidence of the contribution of the pounding on buildings collapse capacity was by observing the damage patterns. They assigned high confidence when the damage patterns follow the load paths of pounding forces or they are similar to recognized pounding damages in prior earthquakes. The authors concluded that pounding affects damage, but only as a secondary contributor. They do not attempt to quantify the degree to which pounding affects collapse. It appears as if none of these cases shows strong evidence that pounding significantly affected collapse. The authors' inference seems like post-hoc-ergo-propter-hoc fallacy.

4.2.2 Modeling efforts

Other authors studied the effect of pounding using structural analysis. Anagnostopoulos (1988) modeled a series of adjacent buildings subjected to strong ground motion using single-degree-of-freedom (SDOF) lollipop models connected by impact elements that simulate pounding. He found that buildings at the ends of blocks—i.e., not supported on one side—experienced quite substantial amplifications of structural response while mid-block buildings experienced generally less amplification of structural response. Pounding changed the structural response of mid-block buildings relatively modestly compared with its effect on end-block buildings, and the effects in mid-block buildings were sometimes positive and other times negative. The response increased if the adjacent buildings were more flexible, and decreased if the adjacent buildings were stiffer.

Maison and Kazuhiko (1990) performed structural analysis of a structural pounding case with a multiple-degree-of-freedom model. They modeled a building pounding at a single floor level into a rigid adjacent building. They used a single linear spring to idealize the local flexibility of the buildings at the location of contact. They considered the pounding problem as having two linear states: (1) no contact and (2) in contact. They studied a 15-story steel moment-resistant frame structure with cases of pounding at a variety of elevations, i.e., heights at which the pounding occurs. They found that, in general, the peak lateral deflections throughout the height of the building decrease when a building experiences pounding. Increasing the pounding elevation decreases the building's peak roof deflection. In stories above the pounding elevation, pounding significantly increases the peak story drifts, story shears, and overturning moments. In the stories below the pounding elevation, pounding generally decreases drift, shear, and overturning moment. They concluded that the effects of pounding decrease as separation distance increases.

Athanassiadou et al. (1994) modeled a series of buildings with SDOF structural analysis. This study was similar to (Anagnostopoulos 1988), except that they considered both the excitation phase difference due to traveling seismic waves from one structure to the adjacent structure and the change of the seismic response due to pounding. They found that pounding aggravated the response of corner buildings and of tall rigid buildings. Pounding also increased with increasing phase difference, particularly for corner buildings and building pairs with very different natural periods of vibration.

Mouzakis and Papadrakakis (2004) explored pounding with three-dimensional structural analysis. Their formulation parameterizes the coefficient of restitution and the ratio of tangential to normal impulse. They observed that pounding negatively affected the structural response of the more flexible building of the pounded buildings. They also found that a larger but inadequate separation distance had a more deleterious effect on building response than a smaller separation distance. They observe that pounding increases flexural members' rotation ductility demand (the ratio of the maximum rotation at the member end to its yield rotation) in the stiffer building and decreases it in the more-flexible one.

Cole et al. (2011) investigated the effects of mass distribution on pounding structures as opposed to lumped mass. They found that the distributed mass collisions reduced the change in post collision velocity contrasted with lumped mass models. They derived what they called “an equivalent lumped mass model” to simulate the distributed mass collisions for predicting the post-collision velocity. They presented and numerically verified a formula for collision force. Finally, they offered a framework to include inelastic distributed mass collisions in the equivalent lumped mass model to allow model plasticity in distributed mass collisions using lumped mass models.

4.2.3 Assessing building collapse by IDA

Before discussing how we will estimate building collapse probability, let us first distinguish between collapse in a real building and collapse as estimated by structural analysis. Building collapse in reality can be defined as the status of a structural system when it loses the ability to resist gravity loads. When performing structural analysis, engineers commonly use any of three conditions to indicate that collapse would occur in a real building: (1) the analysis fails to converge; (2) a calculated peak transient interstory drift ratio exceeds some value that the analyst equates with collapse (such as 5% in a moment frame); or (3) a small increase in the ground motion intensity measure level causes a large or unbounded increase of some demand parameter such as a peak transient drift ratio. If the failure to converge is caused by an infinite increase in peak transient drift ratio, it may represent story collapse or global collapse. If the failure to converge is caused by some unbounded increase in a structural response parameter that is not associated with a global collapse mechanism, then the failure to converge could represent a local collapse, which one might also call a partial collapse. In any case, let us use the phrase “median collapse capacity” to mean the intensity measure level at which half of a suite of ground motion time histories that all have that intensity measure level cause collapse as inferred from the results of structural analysis.

Many people model building collapse with incremental dynamic analysis (IDA), per Vamvatsikos and Cornell (2002). One selects and scales suites of ground motion time histories to each of many desired intensity measure levels, estimating structural response to each ground motion time history using nonlinear dynamic analysis. But which ground motion time histories? Researchers have used several suites of ground motions. Options include, among others, those of ATC-63 (ATC 2009), PEER far-field (Haselton and Deierlein 2008), PEER transportation research program (Nirmal and Baker 2010), Vamvatsikos' suite of twenty records (Vamvatsikos and Cornell 2004), Vamvatsikos' suite of thirty records (Vamvatsikos and Fragiadakis 2010), and a suite of stochastic ground motions (Yamamoto and Baker 2013). Each suite meets differing, and at times conflicting, objectives such as code consistency, ground motion intensity, and structure independency. Researchers have also proposed different methods of scaling ground motion amplitude up to collapse level. PEER adopted a method of scaling each acceleration amplitude of value in a pair of orthogonal horizontal ground motion time histories so that the geometric mean of the two motions' 5% damped elastic spectral acceleration response equals a target value.

4.3 Methodology

4.3.1 Step 1: asset definition

Like other researchers, we will use structural analyses to model collapse. We begin by defining pairs of buildings to be analyzed. This pairs of buildings are connected at every floor level with a contact element to transfer the pounding forces between them. Figure 4.1 illustrates a building pair, idealized as independent structural models on a rigid base subjected to the same ground acceleration, i.e., without phase difference between foundation elements within or between buildings. We denote the left-hand building as the investigated building and the right-hand building as the next-door building, focusing our attention on the investigated building. For vertically propagating S waves, one can reasonably expect little if any phase difference between adjacent buildings of a common footprint size. We consider pairs of buildings of various heights, designed for several levels of risk-targeted maximum considered earthquakes shaking, and restricting our initial study to modern reinforced concrete moment-frame structures whose floors align.

We characterize each building solely with a structural model because we are only concerned here with collapse. Nonstructural damage, property repair cost, human casualties, and loss of function do not enter into the analysis, so the asset definition need not include nonstructural attributes or human occupancy patterns.

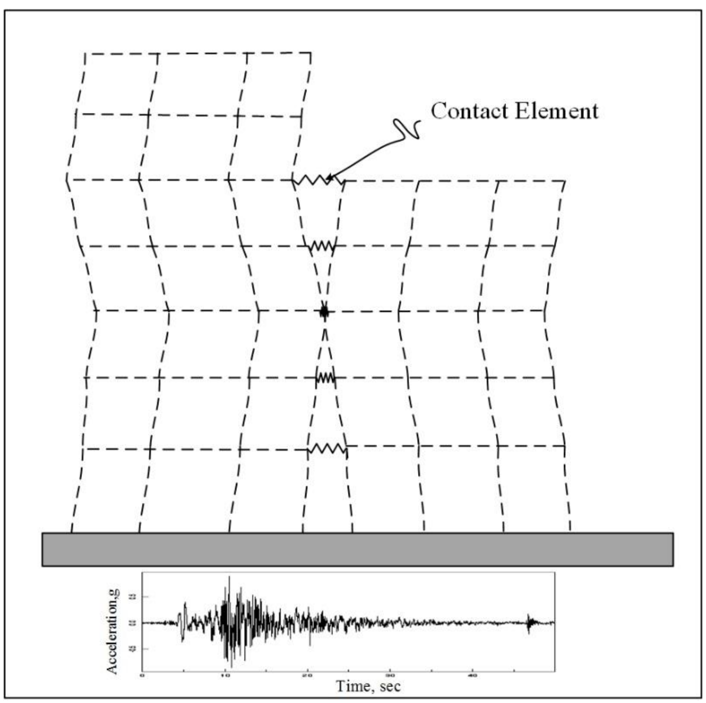

Figure 4.1 – Building assembly

4.3.2 Step 2: hazard analysis

A standard engineered design requires one to estimate the NEHRP site class and ASCE 7 MCE_R parametersS_S,S_1,S_{MS}, and S_{M1} at the building site. Here, the analyst assesses the effect of pounding on collapse probability by estimating collapse probability for various combinations of buildings and separation gaps. We use the PEER ground motion set (Haselton and Deierlein 2008), which consists of 40 pairs of ground motions, scaled as suggested by Haselton and Deierlein (2008). One scales each pair of ground motion records such that the geometric mean of the spectral acceleration of the pair at the fundamental period of the building of interest equals the targeted spectral acceleration response. We start with a spectral acceleration response of 0.11g and increase it in 0.2-g intervals until the first collapse is detected, and increment it in 0.03-g intervals for greater resolution. We scale the ground motion records based on the spectral acceleration at the fundamental period of the investigated building.

4.3.3 Step 3: structural analysis

One uses any convenient software such as OpenSees (PEER 2017) to implement incremental dynamic analysis (IDA) and models the structures using lumped plasticity technique as suggested by (Ibarra et al. 2005). The plastic hinge model is chosen because its ability to capture the deterioration of the strength and stiffness and collapse behavior. As is common, one identifies the value of $S_a(T_1)$ at which at least one story's inter-story drift increases unbounded, where T_1 denotes the estimated small-amplitude fundamental period of vibration of the building in question. The $S_a(T_1)$ value of interest is the value of the controlling component out of the two components in each pair of recorded ground motions.

4.3.4 Step 4 uncertainty propagation

The only independent variables considered are buildings heights (and their related fundamental periods of vibration), separation distance, and intensity measure level. The only uncertainties the analysis considers are record-to-record variability and the resulting uncertainty in collapse capacity. The analysis does not consider uncertainty in structural characteristics, such as uncertain force-deformation behavior, viscous damping ratio, or other attributes of the structural model. Nor does it examine the effects of selecting a different suite of ground motions or a different scaling method. To ignore these uncertainties seems more the rule than the exception. One performs the foregoing analyses for each combination of building height and separation distance.

For each pair of buildings, each separation distance, and each value of $S_a(T_1)$, one calculates the fraction of ground motion pairs that cause sidesway collapse. One then derives collapse fragility functions from pairs of ($S_a(T_1)$, Pc), where $S_a(T_1)$ denotes the 5% damped spectral acceleration response of the controlling component of the ground motion pair and P_c denotes the fraction of pairs at each Sa level in which the OpenSees analysis indicates collapse occurs in the investigated building. It is common to idealize collapse capacity with a lognormal cumulative distribution function (CDF). We use the FEMA P-58 Method A to fit the fragility functions (Porter et al. 2007). The CDF has two parameters: a median value (referred to here as the median collapse capacity) and the standard deviation of the natural logarithm of collapse capacity, which many authors call the dispersion. We are particularly interested in the median collapse capacity and how it changes in the presence of pounding.

4.4 Implementation

4.4.1 Building pairs and analysis

For this initial exercise, we consider only pairs of modern (post-2000) reinforced concrete special moment seismic force-resisting systems. We chose frames of at least three bays. Relevant parameters include building heights, number of stories, and fundamental period of vibration.

For our assets, we used various combinations of five perimeter reinforced concrete special moment resisting frames buildings: Haselton's (2006) OpenSees structural models of a 2-story, 4-story, 8-story, 12-story, and 20-story building. The buildings were designed to comply with ASCE 7-02 (ASCE 2002) and ACI 318-02 (ACI 2002) for a location in northern Los Angeles, CA on NEHRP site class D and maximum-considered earthquake shaking parameter values S_{MS} = 1.5 g and S_{M1} = 0.9 g. Each building has a 15-ft first story and 13-ft upper stories. Hence, floors align and no floor can impact a column of the adjacent building. Table 4.1 summarizes the sample buildings' fundamental period of vibration (T), height (H), and number of stories (N). Building IDs are Haselton's.

Table 4.1 – Sample buildings

Building ID	Period T, sec	Height H, ft	Stories N
1020	2.63	262	20
1013	2.01	158	12
1011	1.71	106	8
1003	1.12	54	4
2064	0.66	28	2

Haselton's models are of solitary buildings; we placed pairs of them adjacent to each other, connected at every floor level with a contact gap element. The element has zero tensile stiffness (no force required to extend the element as the buildings separate) and compressional stiffness proportional to the axial stiffness of the colliding structure (EA/L) when the gap between the two buildings diminishes to zero with maximum transfer forces equal to the force associated with crushing stress. This linear spring contact model is the most conservative model in maximum force transfer for a given impact velocity according to comparative study of a variety of impact models conducted by Muthukumar and DesRoches (2006). Figure 4.2 depicts drawing of RC frame structural analysis model.

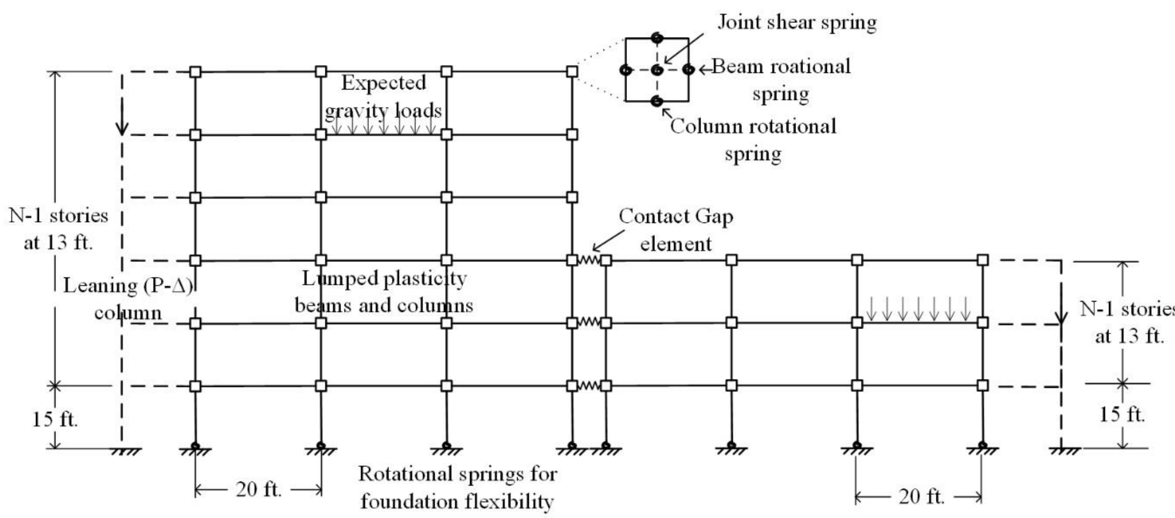

Figure 4.2 – Drawing of RC frame structural analysis model (modified from Haselton et al. 2011)

The structural elements were modeled by using nonlinear hinges. The material for the plastic hinges was as modeled by (Ibarra et al. 2005) and as implemented in OpenSees by Altoontash (2004). This material is capable of capturing the modes of monotonic and cyclic deterioration.

We performed the IDA in OpenSees using the building pairs listed in Table 4.2 and each gap distance shown in the headers of the seven right-most columns of the table, from 0.01 inches to 75 inches, plus one more: 200 inches, which represents the no-pounding case. We derived collapse fragility functions for the investigated building for each pair and each separation gap distance. We record the median collapse capacity in each case, and calculate the percent difference between the median collapse capacity for that case and that of the corresponding 200-inch separation case, as a fraction of the collapse capacity in the 200-inch (no-pounding) case. If the difference is negative, the estimated collapse capacity with pounding is lower than the collapse capacity without pounding. That is, negative values indicate that pounding seems to aggravate collapse. Positive values mean that pounding seems to hinder collapse.

4.4.2 Results

Table 4.2 summarizes the results of the effect of pounding on building safety. The left-hand column identifies the investigated building. The second column, labeled $S_a(T_1, MCE)$, denotes the design spectral acceleration at the fundamental period of the building at MCE ground motion. The third column (median collapse capacity, θ, g) denotes the median value of $S_a(T_1)$ at which the IDA estimates the building will collapse in the absence of pounding. The fourth column identifies the next-door building. Remaining columns give the relative difference in median collapse capacity of the investigated building due to pounding with the next-door building, normalized by the investigated building's median capacity without pounding, as in Equation (4.1). Figure 4.3 illustrates the results.

$$\begin{aligned}&\%\ change\ in\ \theta\ with\ pounding\\&= \frac{\theta\ with\ pounding - \theta\ without\ pounding}{\theta\ without\ pounding} \times 100\end{aligned} \tag{4.1}$$

Table 4.2 – Summary statistics

Investigated Building	$S_a(T_1, MCE)$	Median collapse capacity θ [g]	Next-door Building	% change in θ with pounding, for separation gap of						
				0.01"	1.0"	2.0"	5.0"	10.0"	35.0"	75.0"
20 Story	0.34	0.4707	2 Story	-7.6%	-11.2%	-6.8%	-7.9%	-7.1%	-0.9%	0.0%
			4 Story	-1.4%	-1.5%	-1.6%	-2.9%	-2.5%	-1.8%	-0.1%
			8 Story	-3.1%	-3.7%	-3.3%	-4.6%	-5.9%	-0.2%	-0.1%
			12 Story	-2.8%	-2.5%	-2.9%	-4.6%	-4.7%	-1.4%	-0.2%
12 Story	0.45	0.5479	2 Story	2.2%	2.7%	2.2%	1.1%	-1.0%	-0.1%	-0.1%
			4 Story	0.1%	-0.6%	0.1%	0.5%	1.9%	1.0%	-0.2%
			8 Story	-2.2%	-2.0%	-1.9%	-2.4%	-2.9%	-0.6%	-0.3%
			20 Story	7.1%	6.0%	4.3%	4.4%	4.0%	0.3%	0.0%
8 Story	0.53	0.6392	2 Story	-0.1%	0.9%	3.5%	3.6%	3.1%	0.1%	0.1%
			4 Story	-1.5%	-1.3%	-0.3%	2.3%	2.5%	-0.4%	-0.4%
			12 Story	0.5%	0.9%	1.0%	2.6%	2.1%	-0.1%	0.0%
			20 Story	-1.6%	-0.5%	1.1%	4.6%	8.4%	1.3%	-0.3%
4 Story	0.80	1.1601	2 Story	0.0%	0.7%	0.9%	0.3%	0.1%	0.1%	0.0%
			8 Story	-0.2%	-1.1%	-0.8%	-2.0%	-3.1%	-0.5%	0.2%
			12 Story	-1.1%	-0.6%	-0.9%	-0.2%	-0.8%	-1.1%	-0.1%
			20 Story	-3.5%	-3.5%	-2.6%	-0.5%	1.1%	-2.6%	-1.5%
2 Story	1.36	2.0956	4 Story	1.9%	1.4%	2.0%	2.1%	0.7%	-0.5%	0.2%
			8 Story	1.6%	0.2%	-0.3%	-1.7%	-3.9%	-3.1%	0.1%
			12 Story	-0.3%	-0.8%	-0.6%	-2.6%	-2.8%	-4.0%	0.0%
			20 Story	-9.5%	-11.2%	-9.4%	-9.7%	-2.8%	-2.7%	0.2%

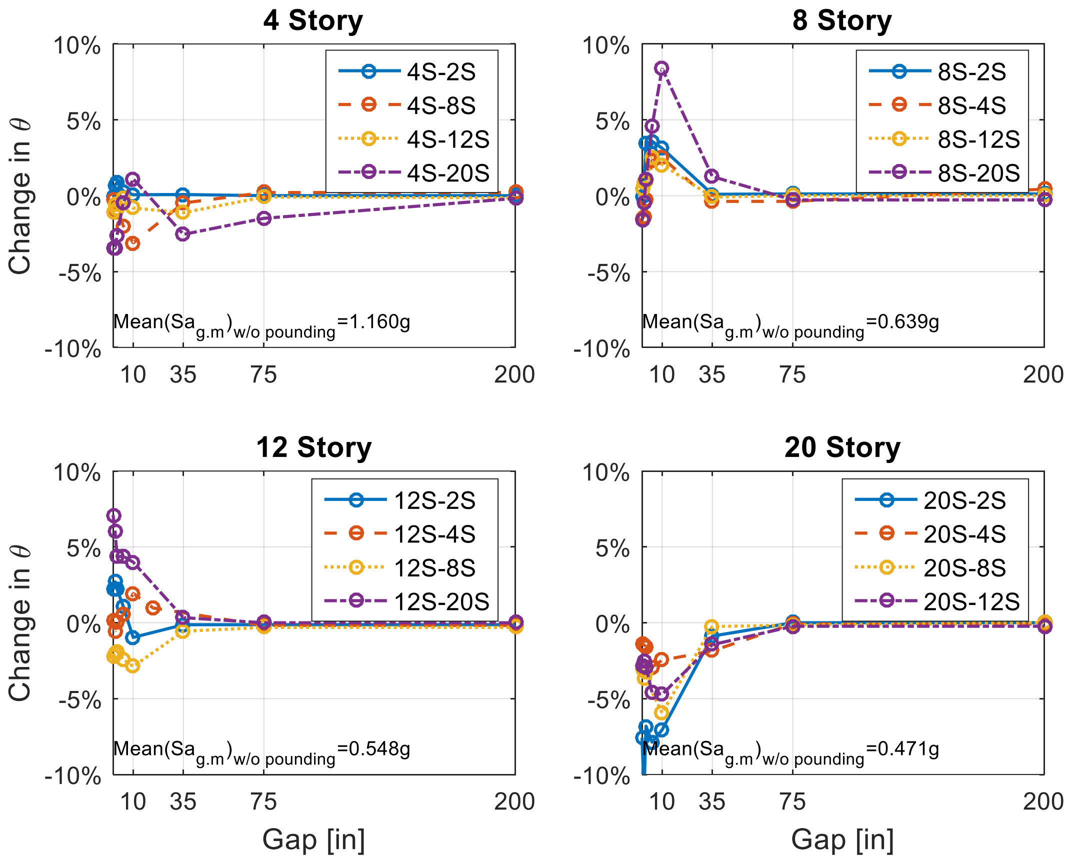

Figure 4.3 – The % change of the median collapse capacity vs. separation gap.

Another way to examine the effect of pounding on collapse fragility is to compare the fragility functions graphically.

Figure 4.4A shows fragility functions for the 4-story building without pounding and when subjected to pounding from four other buildings separated by 0.01 inches.

Figure 4.4B illustrates the 20-story building separated from each of the other buildings by 2 inches. The plots show little effect of pounding on collapse capacity, at least for these particular building models, when the buildings are very close and their floors align.

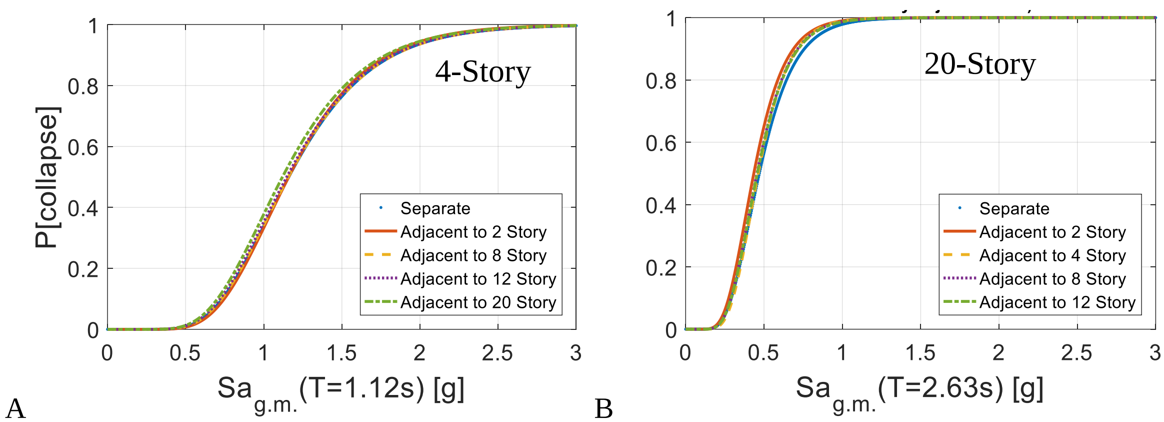

Figure 4.4 – Fragility functions for 4-story building and 20-story investigated buildings with gap of 0.01" and 2", respectively.

Figure 4.5A illustrates how the fragility function for the 2-story investigated building changes with varying separation distance from the 20-story next-door building. There is a small difference when the gap is 1 inch or less. Beyond that, separation distance does not seem to matter. Figure 4.5B illustrates the fragility functions for the 12-story investigated building with a 4-story building next door: pounding has almost no noticeable effect.

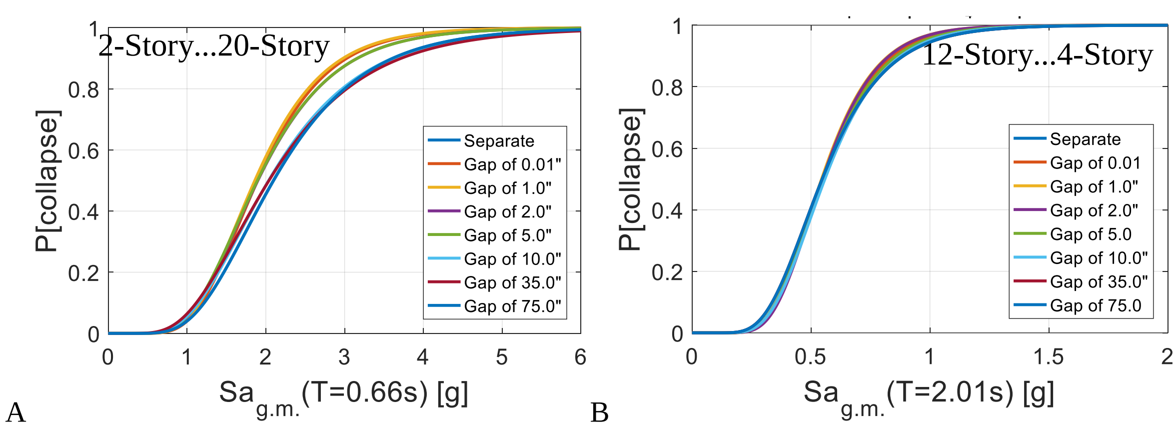

Figure 4.5 – Fragility functions for (a) 2-story adjacent to 20-Story and (b) 12-Story adjacent to 4-Story with variety of separation distances between the adjacent buildings.

Pounding does not always decrease collapse capacity. Figure 4.6 shows that the fragility function of the 8-story investigated building shifts slightly to the right (meaning that its capacity increases by a small amount) in some cases when pounding against the 20-story building.

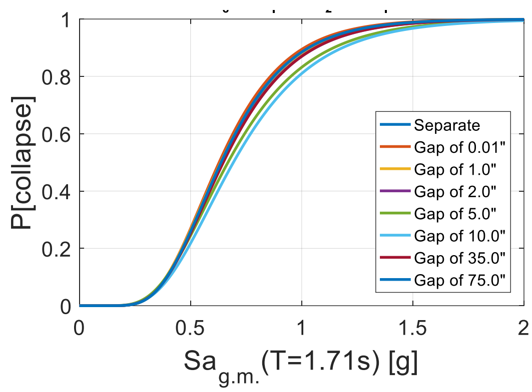

Figure 4.6 – Fragility functions of 8-story investigated buildings with a 20-story building next door, with a variety of separation distances.

Let us look more closely at the collapse mechanism of one of the buildings in the presence of pounding. Figure 4.7 shows the collapse mechanisms of an 8-story building with a gap of 1 inch between it and a variety of next-door building heights when subjected to the recording from Gilroy Array #3 in the 1989 Loma Prieta earthquake (PEER-NGA record 767). Figure 4.8 shows the collapse mechanisms of the 8-story and 2-story buildings adjacent to each other with a variety of gaps, when subjected to the same ground motion time history. Pounding does not seem to change the collapse mechanism. Regardless of adjacency—gap distance or height of the adjacent building, collapse in the 8-story building occurs because a sidesway mechanism forms in the 1st story, suggesting that characteristics of the building in isolation may govern the mechanism. We examined the collapse mechanisms of several other case studies in a similar way and found that adjacency generally does not change the collapse mechanism. We hesitate to generalize beyond our few sample buildings, but this limited evidence suggests a hypothesis that may be worthy of further study: pounding between buildings whose floors align does not affect the form of the collapse mechanism, even if it does change the value of collapse capacity.

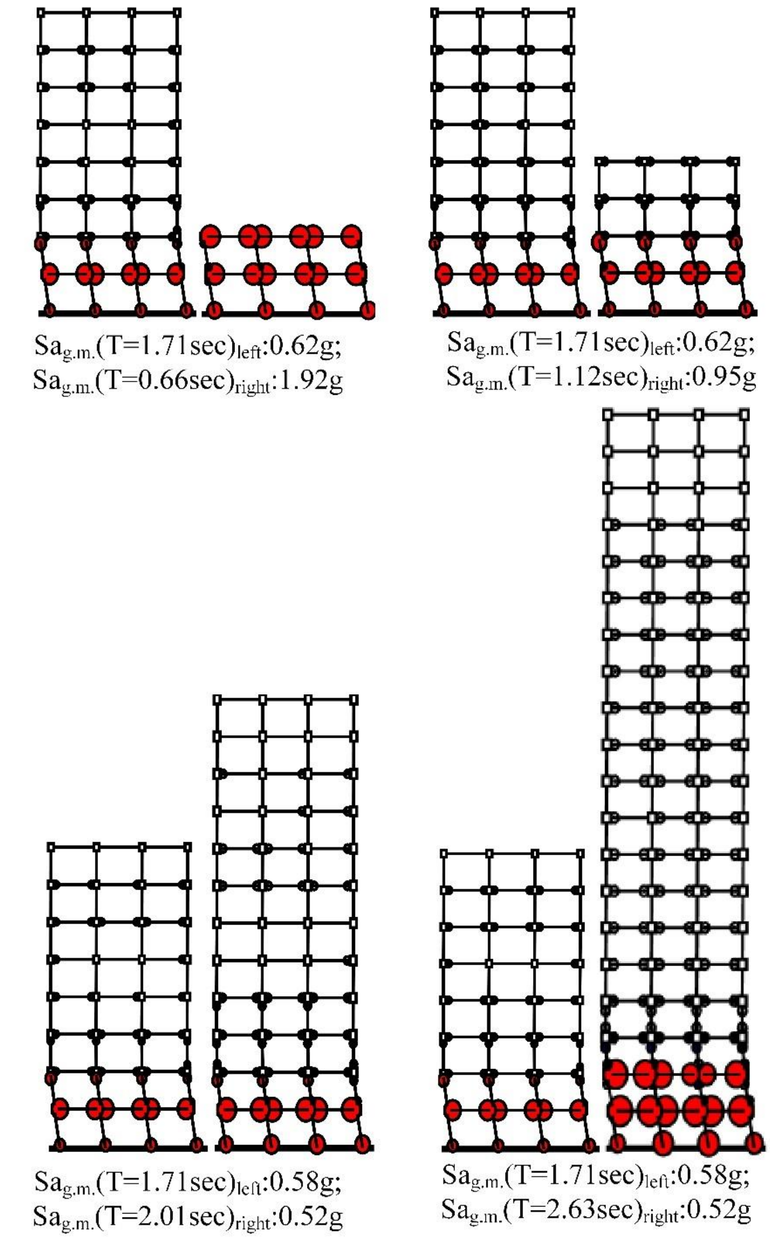

Figure 4.7 – Collapse mechanisms for 8-story building next to a variety of building heights under a moderate ground motion

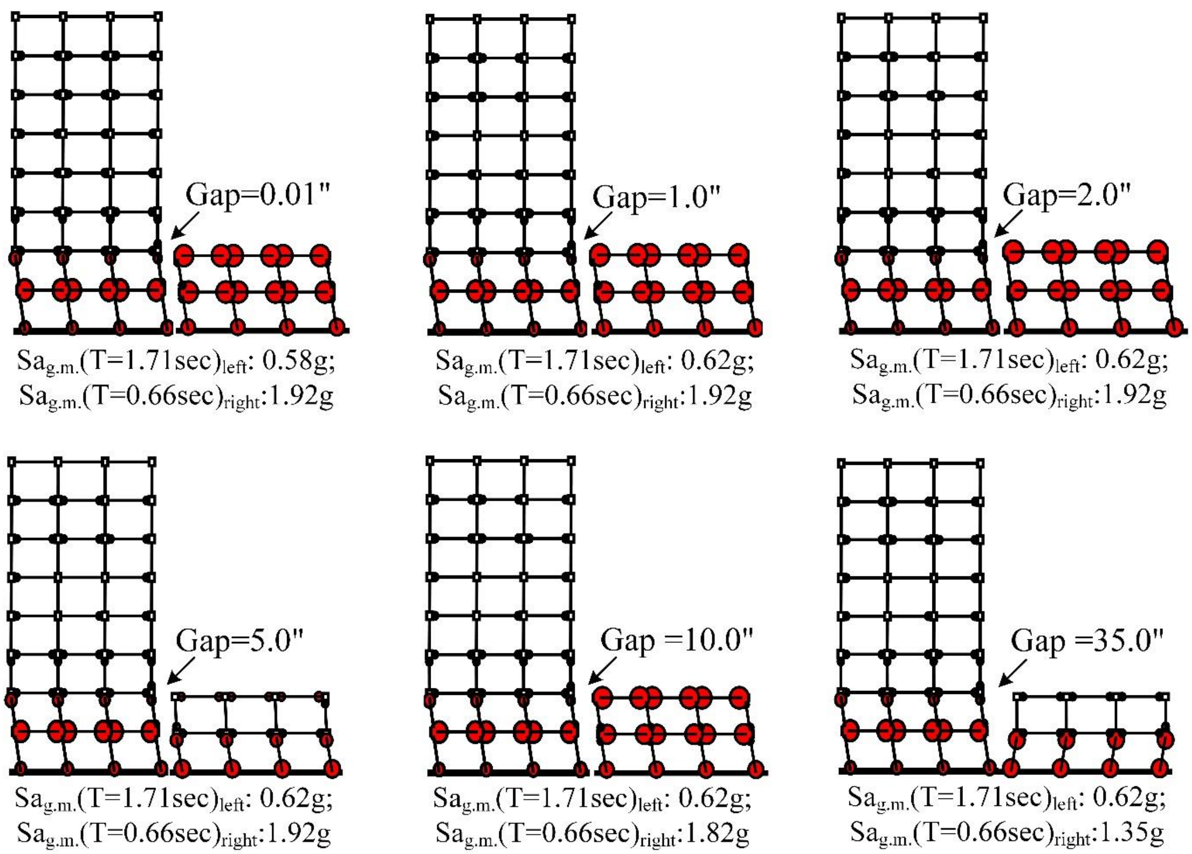

Figure 4.8 – Collapse mechanisms for 8 story and 2 story buildings adjacent to each other with a variety of gaps between them under a moderate ground motion

Some general observations of the summary results in Table 4.2 and Figure 4.3 through Figure 4.7:

- Pounding has little effect on the collapse capacity of adjacent post-2000 reinforced concrete moment-frame buildings whose floors align.
- At most, pounding reduced the median collapse capacity of the buildings examined here by 11%. The average decrease is 2.4%. The coefficient of variation among the buildings examined here whose collapse capacity decreases was 2.6%. A 2.4% decrease in collapse capacity lies well within the noise level of the accuracy of nonlinear dynamic structural analysis.

- Equally weighting the 140 combinations of building pairs and gap widths, and considering both increases and decreases in median capacity in the presence of pounding, the average effect is 0.8% decrease when pounding occurs. The standard deviation is 3.1%, meaning that the 0.8% is within the level of noise. Stated another way, we found no strong indicator that pounding either increases or reduces collapse capacity much in post-2000 reinforced concrete moment frames whose floors align.
- Pounding can modestly increase collapse capacity of some cases. The increase reaches 8.4%, but the average increase (when it does increase) is 1.8% and the standard deviation is 1.9%.
- We see no strong effect of height of the adjacent building on collapse capacity.
- As one would expect, collapse capacity changes less and less as separation distance increases.
- Collapse mechanisms do not appear to change in the presence of pounding. Again, we limit this and all other conclusions to adjacent post-2000 reinforced concrete moment frame buildings whose floor align.

4.4.3 Validation

Are these analytical findings supported by earthquake experience? Recall that three research teams reported their judgment of the effect of pounding on collapse in the 1985 Mexico City earthquake, 1989 Loma Prieta earthquake, and 2011 Christchurch earthquake. While they assert an effect, they offer little evidence that pounding caused or significantly aggravated collapse. We examined photographs of California building collapses in the last 5 decades that one of us (Porter 2016) performed for other research. The photos depict California buildings that collapsed or experienced some form of partial collapse in earthquakes between 1964 and 2014, as recorded in NISEE's Earthquake Engineering Online Archive. Of 73 instances of collapse, nine were of reinforced concrete buildings.

We searched for evidence to indicate which if any of these collapsed buildings experienced pounding, attempting to answer the question of whether collapsed concrete buildings with pounding are overrepresented in California's recent earthquake history? That is, is there a higher fraction of collapsed concrete buildings where pounding was in evidence than the fraction of California concrete buildings that are very close to adjacent buildings? Such over-representation would support the hypothesis that pounding aggravates collapse probability. We first summarize the evidence of collapse mechanism in each of the nine cases, and then attempt to answer our own question. See Table 4.3. Its columns list the earthquake, NISEE's image identifier number, NISEE's photo description, and what caused the collapse.

Table 4.3 – Database of reinforced concrete buildings that collapsed in California earthquakes between 1964 and 2014

Earthquake	ID	Damage description	Cause of collapse
San Fernando 1971	S4065	Collapsed tower at southeast corner. Olive View Hospital. Rear [east] elevation of Medical Treatment Building.	The Olive View Hospital Center, Sylmar, damaged in the 1971 San Fernando, California, earthquake, includes cases of collapse due to columns' shear failure in addition to cases of severe damage due to building pounding during ground shaking. Figure 9 shows the collapsed and leaning stair towers. The towers were structurally separated from the main hospital building by 4 inches. According to (Bertero and Collins 1973), towers A, B and D collapsed completely while tower C tilted 5 degrees but remained standing, as depicted in Figure 9. The four towers were identical except that the tower C was stronger. See Bertero and Collins Collins (1973) for more details. Those authors suggest the collapse of towers A, B and D occurred because of inadequate column reinforcement. In addition, pounding induced damage and tilted the tower C as depicted in Figure 10. (Jankowski (2009), who conducted detailed three-dimensional finite element method (FEM) analysis in order to study the pounding between the main building and tower C, concluded that the response of the stairway--the lighter structure--significantly increased. The damage intensity and range to the base of this structure may have increased due to pounding. However, the effect of pounding on the main building--the heavier structure--was insignificant. Although some portions of the main building collapsed, their collapse was mainly due to ground shaking rather than pounding.
	S4070	Ambulance garage collapsed. Olive View Hospital. Southern elevation of Medical Treatment Building. See also S4139-44.	The collapse of the ambulance garage at Olive View Hospital resulted from inadequate shear reinforcement in the columns (Bertero and Collins 1973).
	S4115, S4117	Soft-story collapse, most evident at upper right of photo. Originally a one- and two-story building, irregular in plan, the first story collapsed in the earthquake.	The main reason for the collapse of the Psychiatric Building at Olive View Hospital was the lack of shear reinforcement of the columns. Shear forces were underestimated in the designer's model and the shear capacity of light concrete was overestimated based on 1965 Los Angeles County Building Laws.

Earthquake	ID	Damage description	Cause of collapse
Northridge 1994	NR559	Parking structure on Zelzah Ave., California State University, Northridge, campus. This is a three-story precast concrete parking structure. Overall view showing collapse at east end of the structure.	The precast concrete parking structure at California State University, Northridge collapsed in the 1994 Northridge earthquake because of inadequate shear walls and inadequate steel reinforcement in columns (“Earth Science World Image Bank” 2016.)
	NR579	Collapse of parking garage floors. See NR459–461 for damage to Broadway department store. Fashion Center, Northridge, California.	The Northridge Fashion Center parking garage collapsed in the 1994 Northridge earthquake because the gravity load columns failed before the collectors in the cast-in-place topping transferred the lateral loads to the lateral-load resisting system (Corley et al. 1996).
	NR221	Northridge Fashion Island Center. Interior reinforced concrete columns remain standing following collapse of second- and third-floor concrete waffle slabs. Intact portion of waffle slab roof shows typical slab construction.	The second- and third-floor concrete waffle slabs at Bullock’s retail store collapsed in the 1994 Northridge earthquake because the two-way joist did not align with the columns, which caused punching shear failure (Somers et al. 1996).
	NR303	View of partial roof collapse. South elevation, east of front entry. View from east. Taken at 3 p.m. California State University, Northridge.	We could find no research addressing the partial roof collapse of Oviatt Library at California State University in the 1994 Northridge earthquake. Photos show no adjacency issues, so we conclude that the collapse was unrelated to pounding.
	NR542, NR543	Complete collapse of parking structure. Los Angeles, California.	The complete collapse of the Kaiser parking structure, Los Angeles, in the 1994 Northridge earthquake was probably started by column failure in the interior gravity system, which then led to pulling inward the exterior reinforced concrete shearwalls and ultimately the complete collapse of the parking structure. It is worth mentioning that the stair tower, which was separated from the garage, was undamaged either by the adjacent collapsed structure or by its own response to the earthquake(Corley et al. 1996).

Earthquake	ID	Damage description	Cause of collapse
	NR160, NR162	Overall view of Kaiser Permanente office building looking toward the northeast. The brick facades at either end of the structure have separated from the concrete frame, and the second floor of the structure has completely collapsed. The bays at the north and south ends of the building are also partially collapsed from the second to the fifth floor. Granada Hills, California.	The collapse of the second-floor and the end bays over the full height of the building at the Kaiser Permanente office building, Granada Hills, in the 1994 Northridge earthquake was because of inadequate confinement steel and inadequate connections between the frame system and the exterior wall (Osteraas et al. 1996).

Figure 4.9 – Image showing collapsed and leaning stair towers at Olive View Hospital, Sylmar, in the 1971 San Fernando, California, earthquake (Jankowski 2009, with permission from NISEE, University of California Berkeley)

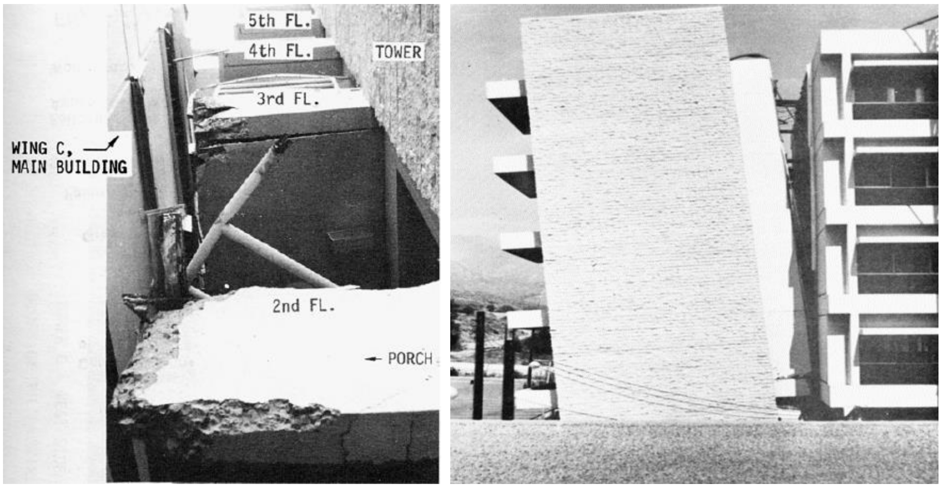

Figure 4.10 – Pounding damage and permanent tilting of a stairway tower C; San Fernando earthquake, 1971

Judging from these nine instances where concrete buildings collapsed, none appeared to have been caused by pounding, despite the occurrence of pounding in the case of Olive View Hospital Stair Towers A, B, and D. Tower C did experience pounding, but did not collapse. The stair tower at the Kaiser parking structure did not collapse despite being adjacent to the parking structure, which did collapse. Given the relative size of the two structures, it seems unlikely that the Kaiser parking structure collapsed because of pounding with the stair tower. That evidence of just nine collapsed buildings says little on its own. It merely tends to reinforce the analytical findings presented earlier, and weaken the hypothesis that pounding aggravates collapse probability.

4.5 Conclusions

We performed incremental dynamic analyses of 140 combinations of pairs of five adjacent post-2000 reinforced concrete moment frame buildings with aligned floors (20 permutations) and 7 separation gaps. Our goal was to assess the effect of pounding on median collapse capacity. The buildings included 2-, 4-, 8-, 12-, and 20-story models. Gap widths varied from near zero to effectively infinite (0.01 in, 1.0 in, 2.0 in, 5.0 in, 10.0 in, 35.0 in, 75.0 in, and 200 in). We found little effect of pounding on collapse capacity relative to the separated case (i.e., the 200-in, no-pounding case). The effect was always less than an 11% decrease in median collapse capacity, was on average a 2.4% decrease (where it decreased at all) and considering cases where pounding seemed to increase collapse capacity, the average overall effect (weighting each case equally) was less than 1%. The effect seems small enough to ignore; it is certainly not large. The conclusion is limited to post-2000 reinforced concrete moment frame buildings whose floors align.

We compared our findings with the evidence of building collapse in reinforced concrete buildings in California in the last 50 years. Pounding does not appear to have contributed to any of the few collapses of reinforced concrete buildings documented in NISEE's photo database, even where collision occurred between buildings. The lack of obvious pounding-induced collapses in California between 1964 and 2014 is hardly evidence that pounding does not cause collapse. But the negative evidence weakens the hypothesis that pounding significantly contributes to collapse, and does strengthen the inference from our study that pounding may matter little to collapse.

Chapter 5

5 Is above-code design cost effective?

This chapter is based on:
Isteita, M., and Porter, K. (2019?). “Is above-code design cost effective

---

Abstract

This work implements benefit-cost analysis for designing buildings to exceed minimum requirements code by a strength and stiffness factor $I_e \in \{1.0, 1.5, 2.0, 2.5, 3.0, 4.0\}$ at four locations of varying seismicity, $S_{MS} = \{0.8g, 1.5g, 2.3g, 3.0g\}$. The study is limited to 1-story reinforced masonry shear wall (RMSW) buildings with flexible diaphragms. The diversity of buildings within this class is modeled based on a GEM analytical methodology. The GEM methodology produces a suite of values of key seismic design attributes that a wide variety of prior authors deemed to most strongly affect the seismic performance of buildings. The individual buildings in the suite are then analyzed using performance-based earthquake engineering as encoded in FEMA P-58. The analyses test the hypothesis that above-code design can be cost effective in many, though perhaps not all, U.S. locations, at least from a benefit-cost-analysis perspective. The building class is modeled using 10 particular buildings whose distributions of plan area, degree of irregularity, and construction quality approximate those of the building class.

Then the findings of this study are tested against the findings of *Natural Hazard Mitigation Saves* to observe whether a PBEE-based methodology and a Hazus-like methodology would yield similar or different results. Designing the buildings to their incrementally efficient maximum (IEMax) level of strength and stiffness costs approximately $20,000, above that of code minimum. The average benefit, by contrast, is approximately $142,000. Consequently, the overall average BCR is approximately 7:1. Thus, new above-code design would save approximately $7 in avoided future losses for every $1 spent on additional, up-front construction cost. These findings and the findings of *Natural Hazard Mitigation Saves* agreed on the BCR within less than a factor of 2 tended to provide cross-validation, supporting the assertion that above-code design can be cost effective. Both studies also suggested that the incrementally efficient maximum degree of above-code design can range between 1.5 and 3.0. Therefore, it would be cost effective to design new buildings to be as much as 3 times as strong and stiff as the code requires. This study supports the finding that code minimum can be inefficient, producing buildings that cost society more in the long run, when one adds future losses to up-front construction cost.

Keywords: benefit-cost analysis; earthquake hazard mitigation; Global Earthquake Model's; Natural Hazard Mitigation Saves; reinforced masonry shear wall.

5.1 Introduction

Earthquakes kill, injure, and traumatize people; damage property; cause homes and businesses to lose functionality; affect the businesses that buy or sell from the people whose homes or businesses are impaired; cost cities tax revenue and emergency response expenses; ignite costly fires; and cause numerous less-tangible losses to people, society, and the environment. These impacts are inevitable. We pay for them eventually. If we pay sooner rather than later, by making new buildings more resilient in the first place or by retrofitting existing buildings before an earthquake, does the investment pay for itself? How much extra resilience makes economic sense?

Recent work suggests that the answer is, quite a lot. A report entitled *Natural Hazard Mitigation Saves* (MMC 2017) makes the case that a simple approach to above-code design, using a factor to increase required strength and stiffness, results in lower long-term societal costs of ownership than life safety alone demands. But that study, which required inventory and loss estimation at a national level, demanded a catastrophe risk model that operates at the level of the entire building stock. It could not practically employ the building-specific, and more deeply defensible, performance-based earthquake engineering methods of FEMA P-58 (ATC 2012a). (The present authors designed and performed the analyses in MMC 2017 addressed here).

This work partly remedies the deficiency of the earlier work. It tests the hypothesis that it is cost effective to design a narrow category of common-looking commercial buildings to exceed IBC strength and stiffness requirements in many US locations, at least from a societal benefit-cost-analysis perspective. It measures benefit-cost ratio, *BCR*, of a simple strength-and-stiffness approach to above-code design, counting as many of the benefits listed in the opening sentence as possible: life safety, building repair cost, direct and indirect business interruption.

This work differs from Natural Hazard Mitigation Saves (MMC 2017) in how it estimates relationships between ground motion and loss (called vulnerability functions). It creates them using the Global Earthquake Model's (GEM) analytical methodology for building categories (Porter et al. 2014), which essentially analyzes a small number of carefully selected specimens of the class using FEMA P-58 (ATC 2012a). *Natural Hazard Mitigation Saves* (MMC 2017) by contrast uses a method very similar to Hazus (FEMA 2012a) to produce its vulnerability functions.

One can integrate the seismic vulnerability function with site hazard to estimate the expected value of loss during a single year, called expected annualized loss (EAL). The difference between EAL under a base case (code-level design) and above-code design resembles an annuity that applies over the building's useful economic life. The present value of that annuity represents the benefit of the above-code design. The ratio of that benefit to the cost of above-code design is the benefit-cost ratio. The present work probably represents a first in several ways:

(1) First use of the GEM analytical methodology for benefit-cost analysis of above-code design;

(2) First to characterize the behavior of the particular building class examined here;

(3) First to characterize the behavior of a building class at several different levels of design (in the sense of varying design base shear requirements); and

(4) First cross-validation of a societal risk analysis that uses a different approach to estimating seismic vulnerability.

5.2 Literature Review

Let us briefly review some of the analytical methods to estimate the seismic vulnerability of a building: particularly Hazus, FEMA P-58, and the Global Earthquake Model. Let us ignore expert-opinion approaches, which would tend to be circular in nature: experts expect better performance from stronger buildings, so their vulnerability functions are lower, so they produce lower EAL, and voila, cost-effective above-code design! Let us also ignore empirical approaches. They require observational loss data that generally do not exist.

5.2.1 HAZUS earthquake model

Hazus is widely used to estimate damage and loss to large portfolios of buildings and essential facilities in earthquake scenarios. What distinguish this model are that: (1) it addresses regional impacts of earthquakes such as service outages, fire spread, hazardous materials release, and indirect economic impacts; and (2) it operates on a geographic information systems (GIS) platform. The methodology is built on six modules. Outputs of each module are inputs of another module. The first module (the potential earth science hazards, PESH) estimates the hazard scenario. The second module (inventory) describes the physical infrastructure and demographics of the studied region. The third module (direct damage) estimates damage in terms of probabilities of exceeding distinct states of damage for a given ground motion. The fourth module (induced damage) evaluates induced damage such as fire following earthquake, hazardous materials release, etc. The fifth module (direct loss) calculates (1) direct economic losses including repair and replacement costs of damaged buildings and lifeline components and income related costs; and (2) direct social losses in terms of causalities, displaced households, and short-term shelter needs. The sixth module (indirect loss) assesses the impacts of direct business interruption on undamaged businesses. It is worth mentioning that, while most people use the Hazus software that implements the loss-estimation methodology, some use elements of the methodology in calculations outside of Hazus, by referring to the Technical Manual.

Results from Hazus tend to be more accurate when aggregated to county or regional levels (FEMA 2018). The model reflects a range of uncertainties, because of imperfect knowledge of earthquakes; modeling approximations and simplifications; and the insufficiency or inaccuracy of the inventories of the built environment, demographics and economic parameters. The result is that earthquake loss estimates tend to be accurate at the societal level only within a factor of two or so (FEMA 2012a).

5.2.2 FEMA P-58

FEMA P-58 (ATC 2012a) employs a single deterministic structural model of a building to represent its structural behavior. It represents all the damageable building elements—structural architectural, mechanical, electrical, and plumbing—at a level of resolution similar to RSMeans assemblies, again, with a single deterministic inventory of potentially thousands or more components. It subjects the structural model to multiple nonlinear dynamic analyses at each of many values of ground motion (measured by an intensity measure, IM, such as damped elastic spectral acceleration response averaged over a range of periods). The result is an estimate of the joint probability distribution of a vector of member forces and deformations (called demand parameters, DP) conditioned on the ground motion intensity measure (IM). One then employs Monte Carlo simulation to simulate potentially tens of thousands of earthquakes to estimate damage, repair cost, repair duration, and the potential to cause human casualties by each component using a suite of previously encoded fragility functions to estimate damage measures (DM) and consequence functions to estimate decision variables (DV).

Some important features distinguish FEMA P-58 from Hazus: (1) FEMA P-58 offers high fidelity of the model to the building, versus Hazus' 3-component model. Hazus simplifies any building into a single structural drift-sensitive component that represents all the entire structural system, a single nonstructural drift-sensitive component that represents all such components such as wallboard partitions, and a single nonstructural acceleration-sensitive component to represent, for example, most mechanical, electrical, and plumbing equipment. (2) FEMA P-58 uses nonlinear dynamic structural analysis, versus Hazus' nonlinear pseudostatic approach. (3) FEMA P-58 can resolve the contribution that each individual component makes to the system-level seismic loss. (4) Hazus is intended to represent building classes, and can estimate losses at the societal level, whereas FEMA P-58 is building-specific. This is important: FEMA P-58 does not do societal loss, any more than a medical examination of a single person tells us much about public health.

5.2.3 Global Earthquake Model (GEM)

GEM Vulnerability Consortium offers a procedure to derive analytically the seismic vulnerability of building classes using FEMA-58, or a simplified version of it (Porter et al. 2014). The analyst represents the building class with a small suite of index buildings drawn from the class. The index buildings differ from each other in three or so variables that cause the greatest variability in vulnerability. The values of those variables for each index building are selected using a generalized quadrature method call moment matching (Porter and Cho 2013). The seismic vulnerability of each index building is then estimated using same FEMA P-58 methodology, or by a simplification involving only a few structural and non-structural components that contribute most to construction cost. In the simplified approach, one scales up losses to account for the components that were not simulated in the first place. The seismic vulnerability functions for the index buildings are then combined probabilistically using moment matching to characterize the vulnerability function of the class. What distinguish the GEM methodology from FEMA P-58 is that its asset definition is probabilistic rather than deterministic: the probability distribution of the asset's important characteristics makes the resulting vulnerability function represent the seismic performance of the building class rather than of single buildings. One can then use the vulnerability functions for catastrophe risk modeling.

5.2.4 Natural Hazard Mitigation Saves

The National Institute of Building Sciences in recent study entitled *Natural Hazard Mitigation Saves* (MMC 2017) performed benefit-cost analysis of design of new buildings to exceed ASCE 7 minimum safety requirements for seismic and wind loading, and ASCE 24 flood elevation requirements. The study found that design to exceed code requirements can save society \$4 per additional \$1 construction cost to achieve an optimal design. Here, optimal design means the best level of investment in a benefit-cost analysis in which neither the inputs nor outputs are fixed. See Newnan et al. (2004) for details of such a standard benefit-cost analysis. The work required the project team to estimate the vulnerability of every building type in the U.S. in every U.S. census tract of the conterminous 48 states. For practicality, the project team used a Hazus-style methodology to estimate seismic vulnerability, as described in (FEMA 2012a).

The analysis accounted for ASCE 7 site class and mapped MCE_R spectral response acceleration parameters in each census tract, as well as geographically varying preferences for building types and heights. The analysis examined the expected present value of future losses under several design alternatives. Alternatives varied only by factoring design strength (parameterized via ASCE 7's seismic response coefficient C_s) with an additional factor denoted here by I_e to increase strength and stiffness. Stiffness was varied in proportion to strength by holding ASCE 7's allowable interstory drift Δ_a constant while C_s was factored by several test values of I_e (1.0, 1.25, 1.5, 2.0, 3.0, ... 8.0). Benefit was calculated as the present value of avoided future loss using an I_e value greater than 1.0, relative to I_e = 1.0. Added construction cost was estimated to vary linearly with I_e, where an I_e value of 1.5 requires 1% additional construction cost relative to I_e = 1.0. The added cost was estimated based on construction cost estimates for a variety of real and hypothetical buildings in several different studies, and validated based on judgment from several experts, as detailed in Porter (2016).

The project team opted not to use performance-based analytical methods such as FEMA P-58 for practical reasons. Vulnerability functions were needed for most combinations of 36 structural systems, 3 height categories, 33 occupancy classes, enough C_s values to span the range of U.S. seismicity, and 10 values of I_e: about 1.3 million seismic vulnerability functions in total, which were practical using a Hazus-like methodology, not using a PBEE methodology. But the study's project team nonetheless wondered whether a PBEE-based method would yield similar or different results; hence the present study.

5.3 Research scope and methodology

This work duplicates the NIBS (2017) experiment, except using state-of-the-art, second-generation performance-based earthquake engineering as encoded in FEMA P-58, and only for a single structural system, height category, and occupancy class, and only a few C_s values. The present study thereby aims in a sense for depth over breadth: a deeper, more defensible model of seismic vulnerability, at the cost of breadth of structural systems, height categories, etc.

As with NIBS (2017), the goal of the present study is to test whether designing new buildings to exceed current requirements of ASCE 7 (in particular, ASCE 7-16) and the International Building Code (ICC 2018) saves more than it costs for various locations in the U.S. The difference is that NIBS (2017) used simplified loss-estimation tools to estimate BCR on a nationwide basis for virtually every building type. We offer an obvious methodology for repeating that experiment on a single-building, detailed basis, and exercise it for a common building type. To do so, we estimate the cost and expected present value of future losses of various kinds for each of several levels of a particular seismic design criterion, in particular, by increasing the ASCE 7-

16 seismic response coefficient C_s, while holding the ASCE 7-16 allowable story drift limit Δ_a constant.

All else being equal, buildings with higher strength and stiffness should experience less risk of structural damage, drift-sensitive nonstructural damage, collapse, loss of safety, repair costs, and downtime. Many of these quantities can be expressed in monetary terms, especially repair costs, direct and indirect business interruption costs associated with the need to perform repairs before resuming work or residence in the building, and urban search and rescue cost. The monetary value of protecting human life is estimating using the U.S. Department of Transportation's acceptable costs to avoid future statistical deaths and nonfatal injuries ("Economic Values Used in Analyses" 2016). The difference between the expected present value of future losses under code-level and above-code design is used here to measure the benefit of above-code design. The difference between construction cost of above-code versus code-level design is used here as the sole measure of the cost of above-code design.

We estimate benefit-cost ratio for above-code design of a single building type, height class, and occupancy: a special reinforced masonry shearwall (in ASCE 7-16 terms), 1 story, with flexible roof diaphragm, with a professional, technical, and business services occupancy. It is practical to perform the test for several seismic regions and for several I_e values. We use the framework of the Global Earthquake Model's (GEM) analytical methodology (Porter et al. 2014) to parameterize and vary building configuration consistent with an observed joint probability distribution of size and shape.

We use FEMA P-58 (ATC 2012a) to estimate the seismic vulnerability for each of 30 sample buildings (10 geometric configurations and three levels of construction quality), at each of four sample locations whose C_s values jointly span U.S. seismicity (at least where seismic design requirements govern lateral strength), and each of six values of I_e. We estimate BCR for each location and for the one building type, height, and occupancy, and compare the results with Natural Hazard Mitigation Saves. The procedure for this study works as follows.

5.3.1 Step 1: Define the asset class

We use moment-matching approach (Ching et al. 2009) to select a set of index buildings with the proper joint distribution of three seismic attributes that most strongly affect seismic performance after seismic hazard. In the moment-matching approach, one replaces a continuous (potentially joint) probability density function of one or more random variables with an equivalent probability mass function, determined such that its first moments (e.g., mean, covariance, and higher joint moments) match those observed in the original probability density function of the random variable. The attributes recommended in that work (ignoring hazard level, which is treated separately) are height range, plan area, and the plan irregularity ratios in two orthogonal directions. Plan irregularity is parameterized as in ASCE 7-16 (ASCE 2016) as the ratio of the plan projection beyond a reentrant corner to the plan dimension of the structure in each of two orthogonal directions.

Construction quality is typically not an observed attribute in building inventories, but as in Porter et al. (2006), it is believed to affect seismic performance. To propagate that uncertainty, we select strength attributes and nonstructural inventory for three variants: a poor-quality case, a typical case, and a superior case. These selected variants are with relatively fragile, median and strong components.

5.3.2 Step 2: Estimate seismic hazard

To explore the effect of degree of seismicity on the benefit-cost ratio, one selects several geographic locations that span U.S. seismicity levels, at least the subset of levels where seismic design governs lateral strength. Seismic hazard is parameterized in two ways: seismic response coefficient C_s as per ASCE 7, and the hazard curve for each location, by which we mean the site-specific relationship between 5% damped spectral acceleration response near the building's small-amplitude fundamental period of vibration and the mean annual exceedance frequency (*not* probability, which is different), using an authoritative source such as Petersen et al. (2014).

5.3.3 Step 3: Design the buildings

Design each index building to comply with the model building code, such as by using ASCE 7 and the International Building Code. Iterate the design for each index building with variety of I_e values at each selected location. Quality level is parameterized by a ratio of actual component strength and stiffness to nominal strength and stiffness, as well as anchorage conditions of nonstructural components. As with Porter et al. (2006), absent empirical observations of the probability distribution of actual, installed component strengths, one can use judgment to assign attributes for high, medium, and low quality. For simplicity, the GEM analytical procedure requires the component inventory to include only eight or so top components, that is, approximately eight components that contribute most to construction cost.

One estimates each building's component inventory in terms of standard component types from FEMA P-58 (ATC 2012a) and estimates construction costs using a standard cost-estimation reference such as RSMeans Square Foot Cost Manual (RSMeans 2017). It is important to estimate the differences in construction costs between buildings in the same location, same configuration, but different I_e values. Doing so by paying special attention to the added structural materials involved in making the building stronger, whether by heavier or more numerous steel reinforcing bars, higher grade concrete, more numerous or heavier connections, etc.

5.3.4 Step 4: Perform structural analysis

One uses the simplified structural analysis procedures developed for the Global Earthquake Model's (GEM) analytical methodology (Porter et al. 2014), evaluating the building seismic responses: peak horizontal acceleration and peak transient drift ratio, at each of several levels of 5% damped short-period spectral acceleration response, denoted here by $Sa(0.2\,sec, 5\%)$. We evaluate structural response at many levels of ground motion $Sa(0.2\,sec, 5\%) \in \{0.1, 0.2, \ldots 3.5g\}$. The simplified structural analysis procedure estimates demand parameters (floor and roof accelerations and peak transient interstory drift ratios at each story level) as a deterministic function of ground motion, using one of three assumed mode shapes reflecting frames, shearwall systems, and combined systems. One estimates the peak roof horizontal acceleration and peak transient interstory drift ratio at each story level for each level of ground motion $Sa(0.2\,sec, 5\%)$, using simplified structural analysis in Equations (5.1) and (5.2), respectively.

$$S_{ha} = PGA + \varphi(h) \times (\Gamma \times Sa(0.2\,sec, 5\%) - PGA \leq S_{max}) \tag{5.1}$$

$$S_{hd} = \Gamma \frac{Sa(0.2\,sec, 5\%) \times {T_1}^2}{4\pi^2} \times \frac{\varphi(h+1) - \varphi(h)}{Z_{h+1} - Z_h} \tag{5.2}$$

where,

PGA =peak ground acceleration, for simplicity, $\approx S_a(1\,sec, 5\%)$ for $T_1 \geq 0.5\,sec$ or $\approx 0.4 \times S_a(0.3\,sec, 5\%)$ for $T_1 < 0.5\,sec$;

$\varphi(h)$ = response at floor h, normalized by response at the roof given $Sa(0.2\,sec, 5\%)$. For simplicity, $\varphi(h)$ can be evaluated for all values of $Sa(0.2\,sec, 5\%)$ as shown in Equation (5.3), (5.4), and (5.5) for shearwall, frame, and dual-system buildings, respectively. These default mode shapes are derived from first principles using the deflected shape of a cantilever beam subjected to linearly increasing distributed load with infinite shear modulus and finite bending stiffness for a shearwall building, finite shear modulus and infinite bending stiffness for a frame building, and linear for a dual system;

$$\varphi(h) = \frac{z^2}{Z^5} \times \frac{70Z^3 - 40Z^2 z + 5Zz^2 + 2z^3}{27} \quad \text{shearwall building} \tag{5.3}$$

$$\varphi(h) = \frac{z}{Z^3} \times \frac{12Z^2 - 3Zz - 2z^2}{7} \quad \text{frame building} \tag{5.4}$$

$$\varphi(h) = \frac{z}{Z} \quad \text{dual system building} \tag{5.5}$$

$\Gamma =$ roof acceleration as a factor of modal acceleration, ≈ 1.3;

$z =$ height of story h above the ground; and

$Z =$ roof height above the ground;

$T_1 =$ the fundamental period of vibration of the building, can be estimated, for example, from ASCE 7-16 section 12.8.2.1 (ASCE 2016) as shown in Equation (5.6).

$$T_1 = C_t h_n^x \tag{5.6}$$

In Equation (5.6), h_n denotes structural height, and the coefficients C_t and x are determined from Table 12.8-2 of ASCE 7-16.

5.3.5 Step 5: Determine damage and loss parameters

Damage and loss analyses generally follow the procedures of FEMA P-58, with fragility functions and consequence functions (repair cost and repair time distributions) taken from the FEMA P-58-3, Performance Assessment Calculation Tool (PACT) (ATC 2012b). Because the building inventories are defined in terms of FEMA P-58 component types, their fragility functions and consequence functions can be taken from the same source. Damage analysis means the simulation by Monte Carlo methods of damage on a component-by-component basis, in which each simulation produces a vector damage state of each damageable structural and nonstructural component in the building. Loss analysis means the simulation by Monte Carlo of repair costs and repair durations on a component-by-component basis.

The parameters of the analysis include: the names and descriptions of the damage states for each building component; the demand parameter to which each component is most sensitive; the median and logarithmic standard deviation of the value of the demand parameter that causes the component to reach or exceed each specified damage state; and the median and logarithmic standard deviation of repair cost and repair duration for each component and damage state.

5.3.6 Step 6: Calculate the vulnerability functions: repair cost, repair time, and fatality

For each combination of geographic location, index building, quality level, and I_e value, one estimates vulnerability functions for repair cost, repair time, and number of fatalities, using the GEM procedures. Here, vulnerability function means a probabilistic relationship between the loss measure (repair cost, etc.) and ground motion in terms of $Sa(0.2sec, 5\%)$. In more detail, one estimates whether collapse occurs, and if not, the repair cost, repair duration, deaths, and nonfatal injuries for a given index building, quality level, I_e value, and geographic location. Using Monte Carlo simulation, one does so many times (say, at least 20) at each level of ground motion. The simulations are used to estimate the collapse probability and probability distribution of repair cost, repair duration, and number of deaths and nonfatal injuries, conditioned on index building, quality level, I_e value, and geographic location. Detailed steps follow.

5.3.6.1 Step 6-1: Determine the repair cost and the repair time

One evaluates the probabilistic damage, repair cost, and repair duration at each level of ground motion, as follows. For each component, one determines component damage state probabilities using the fragility functions in step 5 as shown in Equation (5.7).

$$P[Ds \geq d|SA02 = x] = \Phi\left(\frac{ln(S_h/\theta}{\beta}\right) \tag{5.7}$$

In Equation (5.7), S_h denotes the demand parameter to which each component is sensitive: peak floor acceleration (in the case of acceleration-sensitive components) or peak transient drift ration (in the case of drift-sensitive components). The parameters θ and β denote the median and logarithmic standard deviation of capacity of component original fragility.

Then based on the component damage state probability, we calculate its median repair cost and repair time as shown in Equations (5.8) and (5.9).

$$y_{r\_cost} = Q \times \theta_{r\_cost} * exp\left(-\beta_{r\_cost} \times \Phi^{-1}(u_{r\_cost})\right) \tag{5.8}$$

In Equation (5.8), Q denotes the component quantity in the building inventory; θ_{r_cost} and β_{r_cost} denote the median and logarithmic standard deviation of repair cost of the component at damage state d; the u_{r_cost} is a sample of a uniformly distributed random variable between 0 and 1; and the operation $\Phi^{-1}(u_{r\_cost})$ returns the inverse of the standard normal cumulative distribution function, evaluated at the probability values in u_{r_cost} .

$$y_{r\_time} = \theta_{r\_time} * exp\left(-\beta_{r\_time} \times \Phi^{-1}(u_{r\_time})\right) \tag{5.9}$$

In Equation (5.9), θ_{r_time} and β_{r_time} denote the median and logarithmic standard deviation of repair time of the component at damage state d; the u_{r_time} is a sample of a uniformly distributed random variable between 0 and 1; and the operation Φ^{-1} is as defined previously.

We convert the repair cost and time from median to mean and repeat for all components. Then, we sum repair cost of all components to get the repair cost for this simulation. We upgrade the determined repair cost of each simulation to the index building level by multiplying it by $1/f_1$ to account for the fact that only the top structural and non-structural component categories are inventoried where f_1 is the construction cost of those components as fraction of the building's full replacement cost new, RCN. It is worth mention that if the repair cost exceeds about 60% of RCN, it is common to demolish and replace the building, meaning that in such a case one uses the RCN as the repair cost. We pick the maximum of the repair times of all components to get the repair time of the simulation based on the principle of fault tree procedure (Porter and Ramer 2012).

5.3.6.2 Step 6-2: Calculate the building collapse probability

In each simulation, the analyst must identify cases of collapse. Collapse mechanisms will vary by asset class. For example, in reinforced masonry shearwall buildings with wood roofs, collapse mechanisms might include in-plane shear failure of a wall, or failure of the roof-to-wall connection. One can estimate the former mode using the simplified approach of FEMA P-695 (ATC 2009), as in Equation (5.10).

$$P_c(x) = \Phi\left(\frac{ln\left(x/\hat{S}_{CT}\right)}{\beta_{TOT}}\right) \tag{5.10}$$

where,

β_{TOT}= the total logarithmic standard deviation of the collapse capacity= 0.8 based on FEMA P-695;

$\hat{S}_{CT}$= building median collapse capacity; $\hat{S}_{CT} = C_s \times 1.5 \times R \times CMR \times SSF$

where,

C_s= seismic response coefficient; $C_S = S_{DS}/(R/I_e\ )$

R= Response modification factor;

CMR = Collapse margin ratio;

SSF= Spectral shape factor.

One can estimate component-based collapse mechanisms such as the failure of roof-to-wall connections by an analytically derived fragility function following the guidelines of FEMA P-58 (ATC 2012a).

5.3.6.3 Step 6-3: Estimate the fatalities rate

Fatality rate is defined here as the fraction of indoor occupants who die because of earthquake damage to the building. Most U.S. earthquake fatalities in buildings occur because of structural collapse. For each simulation in which collapse occurs, the fatality rate is taken as the average of the GEM analytical methodology's lower and upper recommended fatality rate for the given building category, as shown in Equation (5.11).

$$f_r = \frac{f_L + f_H}{2} \tag{5.11}$$

For simulations in which collapse does not occur, one can neglect fatalities, and assume zero fatalities occur.

5.3.6.4 Step 6-4: Apply the collapse probability on the functions: repair cost, repair time, and fatality

In each simulation, the analyst has determined whether the building collapsed. In case of collapse, adjust the repair cost and repair time of step 6-1 be equal to the replacement cost new of the building, RCN, and the replacement time new of the building, RTN, respectively. The RCN is determined previously in step 1. RTN can be taken as any reasonably defensible value; we use 240 days according to Table 15.9 of the Hazus-MH 2.1 Technical Manual (FEMA 2012a).

5.3.6.5 Step 6-5: Repeat to define the vulnerability function

For each index building, I_e value, quality level, geographic location, and level of ground motion, iterate the steps 6-1 to 6-4 for many simulations. For each loss measure—repair cost, repair duration, and fatality rate—calculate the average. Repeat for all levels of ground motion (e.g., $Sa(0.2\ sec, 5\%) \in \{0.1, 0.2, \ldots 3.5g\}$. We define the mean vulnerability function for a combination of index building, I_e value, quality level, and geographic location as the relationship between the mean of the loss measure and the level of ground motion. Each combination of index building, I_e value, quality level, and geographic location has three mean seismic vulnerability functions: one for repair cost, one for repair duration, and one for fatality rate, denoted by $Y_c\ (x)$, $Y_t\ (x)$, $Y_f\ (x)$ respectively. Compile these vulnerability functions for each combination of index building, I_e value, quality level, and geographic location.

5.3.7 Step 7: Estimate expected annualized losses

One next calculates the expected annualized value of each loss measure (referred to here as the expected annualized loss, EAL) for each combination of index building i, I_e value, quality level q, and geographic location. The expected annualized building repair cost, $EAL_{c,i,q}$ can be determined by Equation (5.12). In this equation, $Y_c(x)$ denotes the repair cost vulnerability function of the index building and $G(x)$ denotes the mean annual rate of exceeding ground motion level x from step 2.

$$EAL_{c,i,q} = \int_{x=0}^{\infty} Y_c(x) \left| \frac{dG(x)}{dx} \right| dx \tag{5.12}$$

The expected annualized building repair time cost, $EAL_{t,i,q}$ can be determined by Equation (5.13). In this equation, $Y_t(x)$ denotes the repair time vulnerability function of the index building, $\mathrm{N_{occ2PM}}$ denotes the average number of indoor occupants per square foot at 2PM (taken for example from the Hazus Earthquake Technical Manual), and A_i denotes the index building floor area in square feet. In the equation, in the case of a commercial building, V_{BI} denotes the direct business interruption loss per person per day of downtime. Q denotes the ratio of indirect to direct business interruption, which can be derived from input-output economic analysis as described in MMC (2017).

$$EAL_{t,i,q} = V_{BI} \times (1 + Q) \times \mathrm{N_{occ2PM}} \times \mathrm{A_i} \times \int_{x=0}^{\infty} Y_t(x) \left|\frac{dG(x)}{dx}\right| dx \qquad (5.13)$$

Estimate the expected annualized value of avoiding statistical fatalities, $EAL_{f,i,q}$ as shown in Equation (5.14). In this equation, N_{occ} denotes the time-average number of indoor occupants per square foot, taken for example from the Hazus Earthquake Technical Manual. The term V_f denotes the acceptable cost to avoid a statistical fatality.

$$EAL_{f,i,q} = N_{occ} \times A_i \times V_f \times \int_{x=0}^{\infty} Y_f(x) \left|\frac{dG(x)}{dx}\right| dx \qquad (5.14)$$

The calculated expected annualized value of each loss in Equations (5.12), (5.13), and (5.14) is constant for every year of the building life and accounts for both the possibility that any whole number of earthquakes occur in the given year and the uncertain intensity of each earthquake.

5.3.8 Step 8: Aggregate expected annualized losses and added costs by location and I_e value

Iterate step 7 for each combination of index building, quality level, and I_e value. Let q denote an index to quality levels (q =1, 2, and 3 denotes low, typical, and high quality), n denotes the number of index buildings, and i denotes an index to those buildings. Let $EAL_{c,i,q}$ $EAL_{t,i,q}$, and $EAL_{f,i,q}$ denote the expected annualized losses for repair cost, business interruption, and fatalities, respectively, for index building i, quality level q. For each combination of location and I_e value, calculate the weighted average values of EAL_c, EAL_t, and EAL_f results as follows.

$$EAL_c = \sum_{q=1}^{3}\sum_{i=1}^{n} w_i w_q EAL_{c,i,q} \tag{5.15}$$

$$EAL_t = \sum_{q=1}^{3}\sum_{i=1}^{n} w_i w_q EAL_{t,i,q} \tag{5.16}$$

$$EAL_f = \sum_{q=1}^{3}\sum_{i=1}^{n} w_i w_q EAL_{f,i,q} \tag{5.17}$$

In the equations, w_i is the moment-matching weight assigned to index building i, and w_q is the weight assigned to quality level q. One also calculates the weighted average construction cost for each combination of location and I_e value, by similar means. Let $RCN_{i,q,Ie}$ denote the replacement cost new from step 6-1 for index building i and quality level q, for a given value of I_e and geographic location. The weighted average replacement cost new for a given location and I_e value is estimated as:

$$RCN_{I_e} = \sum_{q=1}^{3}\sum_{i=1}^{n} w_i w_q RCN_{i,q,I_e} \tag{5.18}$$

5.3.9 Step 9: Estimate benefits, costs, and benefit-cost ratios by I_e and location

The benefit of above-code design for a particular geographic location and value of $I_e > 1.0$ is taken here as the reduction in the present value of future losses achieved by a design with $I_e >$ 1.0, relative to a building with $I_e = 1.0$. It is denoted by B_{I_e} and is calculated in Equations (5.19) and (5.20). In the equations, r denotes the real (after inflation) annual discount rate, which measures the time value of money and t denotes the number of years that the mitigation strategy is effective. We do not discount human life, consistent with MMC (2017). In the equations, PV_{Ie} denotes the expected present value of future losses to a building designed with a particular value of I_e.

$$PV_{I_e} = (EAL_c + EAL_t) \times \frac{(1 - exp(-r \times t))}{r} + EAL_f \times t \qquad (5.19)$$

$$B_{\ I_e > 1.0} = PV_{\ I_e = 1.0} - PV_{I_e > 1.0} \qquad (5.20)$$

It is worth mentioning that Equation (5.19) assumes: 1) Earthquakes occur randomly in time but at a constant long-term average rate (events per year), with each later earthquake occurring independently of the last one; 2) The intensity of each earthquake is uncertain and its probability distribution is constant over the building life; 3) The estimated vulnerability functions do not change as the building ages, and the building is restored to its initial condition after any event of earthquake; and 4) The value of the building is constant (Porter 2019).

For each geographic location, one calculate the average marginal cost to exceed $I_e = 1.0$ as the increasing of the average replacement cost new as shown in Equation (5.21).

$$C_{\ I_e > 1.0} = RCN_{I_e > 1.0} - RCN_{I_e = 1.0} \qquad (5.21)$$

Then, for each geographic location, one calculates the benefit-cost ratio (BCR_{Ie}) for designing buildings to exceed I-code minima as shown in Equation (5.22).

$$BCR_{Ie} = B_{\ I_e} / C_{\ I_e} \qquad (5.22)$$

5.3.10 Step 10: Identify the incrementally efficient maximum I_e value by location

In an investment situation without fixed inputs or outputs, the optimal investment is the largest one (here, the maximum I_e value) in which $\Delta B > \Delta C$, defined as follows. That value of I_e is referred to here (as in MMC 2017) as the incrementally efficient maximum, IEMax. Let i now denote an index to I_e values and let n here denote the number of above-code options considered, that is, the number of I_e values greater than 1.0. For example, in a study with six values of $I_e \in \{1.0, 1.5, 2.0, 2.5, 3.0, 4.0\}$, $n = 5$, $i = 0$ refers to the baseline case $I_e = 1.0$, $i = 1$ refers to $I_e = 1.5$,

i = 2 refers to I_e = 2.0, etc., through i = 5 referring to I_e = 4.0. The IEMax case is the one satisfying the inequality

$$IEMax = \max(i) : \frac{\Delta B_i}{\Delta C_i} > 1.0,\ i \in \{1, 2, \ldots n\} \tag{5.23}$$

where

$$\begin{aligned} \Delta B_i &= B_i - B_{i-1} \\ \Delta C_i &= C_i - C_{i-1} \end{aligned} \tag{5.24}$$

For each location, one identifies the IEMax value of I_e, and calculates the benefit-cost ratio of the IEMax design:

$$BCR_{IEMax} = B_{IEMax} / C_{IEMax} \tag{5.25}$$

Again, IEMax refers to the particular value of i that represents the incrementally efficient maximum level of above-code design at the given geographic location.

5.3.11 Step 11: Repeat for each geographic location

Step 10 identifies the incrementally efficient maximum value of I_e for a given geographic location, and gives the benefit-cost ratio for that level of design and location. One repeats step 9 for each geographic location.

5.4 Implementation and Results

5.4.1 Define the asset class

The case study presented here examines a special reinforced masonry shearwall (in ASCE 7-16 terms), one story, with flexible roof diaphragm, with a professional, technical, and business services occupancy. Table 5.1 shows an example of index building definition of one of the index buildings.

Table 5.1 – Index building definition

Asset class	1-story (RMSW) buildings with flexible diaphragm
Structural material (if used, from GEM building taxonomy)	Masonry
Lateral load resisting system (if used, from GEM building taxonomy)	Shearwall
Broad category (choose one)	Shearwall
Height category (if used, from GEM building taxonomy)	1-story
Occupancy (if used, from GEM building taxonomy)	COM4
Other attribute 1	Commercial
Other attribute 2	I_e = 1.0
Other attribute 3	S_{MS}= 1.5g
Index building quality (if using 3 index buildings; choose one)	Typical
Index building name (if a particular real building is selected)	i8 (as an example)
Index building model (if using local per-square-meter cost manual)	M.455 Office,1 Story
Stories	1
Story height (ft)	17
Building height (ft)	18
Design year	2016
Construction year	2017
Labor cost as a fraction of total labor + material in construction cost	0.5
Local labor cost as a fraction of US labor cost	1
Gamma (default = 1.3)	1.3
Logarithmic standard deviation of collapse capacity (default 0.8)	0.8
Design base shear as fraction of building weight CS	0.2
Cost manual reference (if used)	RSMeans (2017)

Total building cost (currency per ft^2)	\$179.07
Total building floor area (ft^2)	7200
Total building construction cost (currency, RCN)	\$1,289,306.88
Fraction f_1, construction cost as fraction of RCN	0.417

We applied the moment-matching approach (Ching et al. 2009) to select a sample of index buildings that represent the observable attributes that most strongly affect seismic performance after seismic hazard matter. The attributes believed to most strongly affect seismic performance for the defined asset were the design base shear, the plan irregularity ratios, and the plan area. The height range was excluded because the definition of the asset was 1-story height. The design base shear (which relates to local hazard level) was treated by repeating the analysis at several locations. Thus, the building class was characterized using a suite of building designs that comply with recent code at various locations and that vary only by plan irregularity ratios and building area.

We considered irregularity as two attributes, one for each direction. For a roughly L-shaped plan, we parameterized irregularity in the x-direction as X_p/X_{max}, and in the y-direction as Y_p/Y_{max} where X_p and Y_p were the plan projection beyond a reentrant corner in the X and Y directions, respectively, and X_{max} and Y_{max} were largest plan dimensions in x-direction and y-direction, respectively. To determine the joint probability distribution of the key seismic attributes, we split the buildings in the database (an unpublished database of 116 actual reinforced masonry electric substation control buildings in California) into two groups. The first group contains seven index buildings that span three key dimensions: X-irregularity, Y-irregularity, and floor area, where the first several moments of the joint distribution match those observed in a subset of irregular (generally L-shaped) buildings within a large, reasonably representative sample of buildings of the class of interest. The second group contains three regularly shaped (rectangular) index buildings that span floor area, again where the first several moments of the probability distribution of plan area match those observed in a subset of regularly-shaped (rectangular) buildings among the substation control buildings. Table 5.2 shows the number and weight of the irregular and regular masonry buildings in the database.

Table 5.2 – Masonry buildings of the database

	Buildings with irregularity	Buildings without irregularity
Number	42	78
Weight	35%	65%

Figure 5.1 shows the dimensions and weight of index buildings matching the substation control building database. Dimensions are rounded to the nearest 20ft to be consistent with common bays widths.

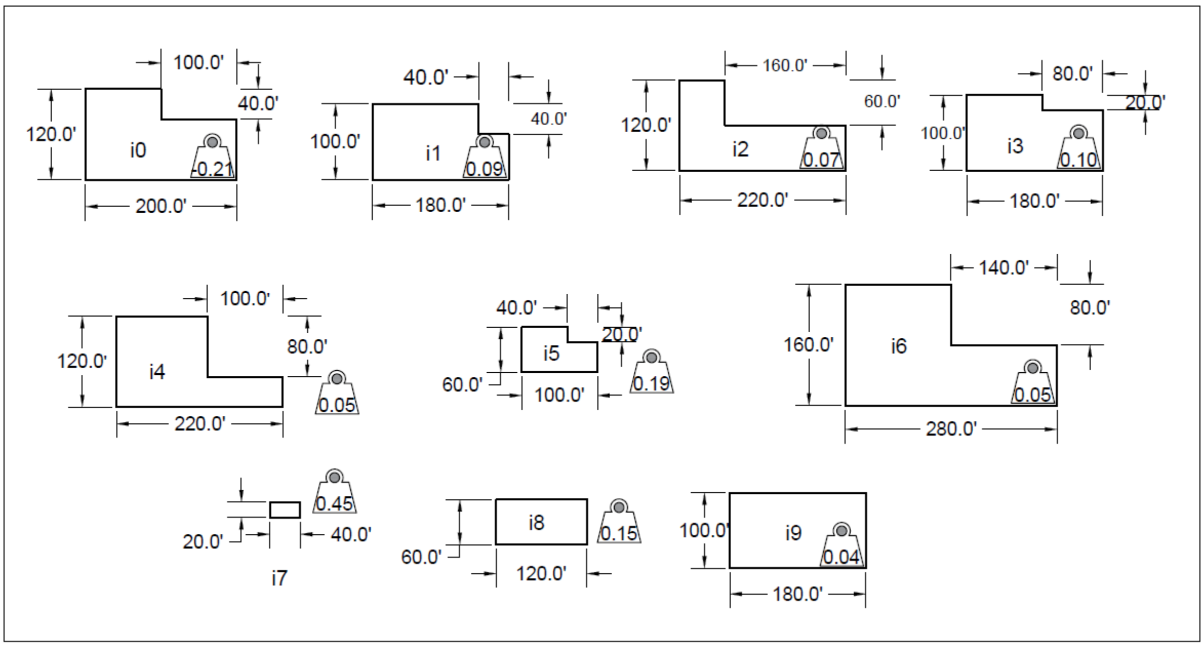

Figure 5.1 – Dimensions and weight of index buildings

For each index building, we designed three quality variants of FEMA P-58 component types: a poor case (relatively fragile components), a typical case (moderately fragile), and a superior case (strong components) to explicitly propagated uncertainty within-specimen variability.

We used the RSMeans M.455 office model (RSMeans 2017) to pick the eight assemblies that contribute the most to the construction cost. See Table 5.3 for an example index building, labeled i8. The total cost of RSMeans M.455 office model is $207.65 per square foot. The cost is adjusted to account for the combination of I_e and S_{MS}, and to account for a wood roof rather than the standard concrete roof of RSMeans' M.455 office model.

Table 5.3 – Ranking of components in decreasing order of contribution to construction cost for index building i8

	Nonstructural components						Structural	
Rank[1]	1	2	3	4	5	6	1	2
Description[2]	Terminal & Package Units	Lighting & Branch Wiring	Communication & Security	Ceiling Finishes	Floor Finishes	Electrical Service/ Distribution	Exterior Walls-Masonry	Roof construction-Wood
NISTIR 6389 class ID[3]	D3050	D5020	D5030	C3030	C3020	D5010	B2010-111	B1020-102
FEMA P-58 class ID[4]	D3052.013k	C3034.002	(rugged)	C3032.003d	C3027.002	D5012.023h	B1052.002	(rugged)
Demand Parameter (PFA or PTD)[5]	PFA	PFA	--	PFA	PFA	PFA	PTD	--
Cost per (ft^2)	$22.55	$13.22	$7.43	$5.89	$5.14	$5.09	$8.7	$6.65
Total cost/ft^2 these items	$74.67							

[1] Component in decreasing order of construction cost.
[2] Component description.
[3] The 5-character component category from NISTIR 6389 (NIST 1999)
[4] The code for the component type per FEMA P-58 (ATC 2012a).
[5] Fragility input parameter: PFA = peak floor acceleration, PTD = peak transient drift ratio

Total cost/ft^{2}[6]	\$179.07
f1 (frac RCN in inventory)	0.417

5.4.2 Estimate seismic hazard

We selected four locations with degrees of seismicity in roughly equal increments corresponding to short-period mapped spectral acceleration response S_{MS} from 0.8 to 3.0g: Sacramento CA (38.57705°N, 121.4953°W), eastern San Francisco (37.779°N, 122.418°W), western San Francisco (37.74162°N, 122.50534°W) , and northwestern Tennessee (36.216°N, 89.477°W, which is near the highest value of S_{MS} in the United States). Table 5.4 shows the maximum considered earthquake risk-targeted, MCE_R , ground motion spectral response accelerations of 0.2-second and 1.0-second (5% of critical damping) and $Vs30$ from the USGS's 2014 National Seismic Hazard Maps (Petersen et al. 2014) and USGS's OpenSHA site data app (Field et al. 2003), respectively, for the four locations.

Table 5.4 – MCE_R - Spectral response accelerations and $Vs30$ for the selected locations

location	Site Coordinates	MCE_R - Spectral response accelerations		$Vs30$, m/s
		S_{MS},g	S_{M1}, g	
Sacramento CA	38.57705°N, 121.4953°W	0.853	0.533	280
Eastern San Francisco	37.779°N, 122.418°W	1.500	0.941	302
Western San Francisco	37.74162°N, 122.50534°W	2.306	1.657	302
Northwestern Tennessee	36.216°N, 89.477°W	2.996	1.821	254

[6] Total cost from RSMeans 2017 of M.455 model after subtracting the wall and roof cost and adding the wood roof cost B1020.

Site hazard is spatially interpolated from the gridded seismic hazard data of the 2014 National Seismic Hazard Maps of the US Geological Survey (Petersen et al. 2014). The hazard is converted from 1 year exceedance probability to mean annual exceedance frequency G, in units of events per year, assuming Poisson arrivals. Figure 5.2 shows the resulting site hazard curves.

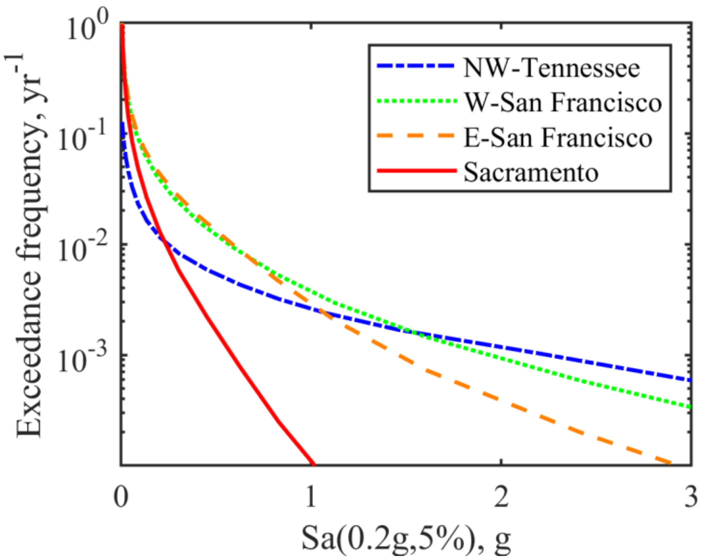

Figure 5.2 – Amplified sites hazard curves

5.4.3 Design the buildings

We designed the selected index buildings to meet or exceed requirements of ASCE 7-16 for strength and stiffness by a factor I_e = {1.0, 1.5, 2.0, 2.5, 3.0, 4.0}, for each location. For simplicity, we designed the exterior masonry walls and roof connections to the walls of only one index building for each combination of I_e and S_{MS} , i.e., one index building for each seismic response coefficient (C_s) , and then assumed the nine other index buildings would have the same design. The justification for this assumption is that our buildings are only 1-story high and increasing the building area would not increase the self-weight of the walls per wall length. The only weight increase is the wood roof dead load, which is small compared to the masonry walls. We verified our assumption by designing some random buildings for each group. This assumption decreased the effort of designing the buildings from designing 10 x 6 x 4 = 240 buildings to designing only 1 x 6 x 4 = 24 buildings. The buildings designed to satisfy the requirements of TMS 402/602-16: Building Code Requirements and Specification for Masonry Structures (TMS 2016). Table 5.5 summarizes the 24 buildings design of each combination of I_e and S_{MS} for both the side wall and the end wall of each building: wall thickness, vertical grout spacing, rebar, horizontal bond beam, cost, and roof connections.

Table 5.5 – Buildings design

I_e	Side wall: $\boldsymbol{S_{MS} = 0.8g}$					End wall: $\boldsymbol{S_{MS} = 0.8g}$					roof connections	
	Wall Thickness	Grout Spacing	Rebar	Bond Beam	Cost	Wall Thickness	Grout Spacing.	Rebar	Bond Beam	Cost	Connection Separation	Tension Capacity
	in	in		Rebar @ in	\$/sf	in	in	# @ in	Rebar@ in	\$/sf	ft	kips
1.0	6	48	1#4	#5@48	14.12	8	@40	1#4	2#4@48	15.56	4	1.355
1.5	6	48	1#4	#6@48	14.27	8	@40	1#4	2#4@48	15.56	4	1.355
2.0	6	48	1#5	#6@48	14.39	8	@40	1#4	2#4@48	15.56	3.875	1.355
2.5	6	48	1#6	#6@48	14.54	8	@40	1#5	2#4@48	15.68	3	1.355
3.0	6	48	1#6	#6@48	14.54	8	@40	1#5	2#4@48	15.68	2.5	1.355
4.0	6	48	1#7	#6@48	14.71	8	@40	1#6	2#5@48	16.08	1.875	1.355
	Side wall: $\boldsymbol{S_{MS} = 1.5g}$					End wall: $\boldsymbol{S_{MS} = 1.5g}$						
1.0	6	24	1#4	#5@48	15.29	8	@32	2#4	2#3@48	15.98	3.000	1.500
1.5	6	24	1#5	#6@48	15.56	8	@32	2#4	2#4@48	16.10	2.875	1.500
2.0	6	24	1#5	#6@48	15.56	8	@32	2#5	2#4@32	17.59	2.125	1.500
2.5	6	24	1#6	#6@48	15.71	8	Full	2#5@32	2#4@48	18.18	1.750	1.500

3.0	6	24	1#7	#6@48	15.88	8	Full	2#6@32	2#5@48	20.54	1.375	1.500
4.0	6	24	1#8	#6@48	16.09	8	Full	2#7@32	2#5@24	21.19	1.000	1.500
	Side wall: $\boldsymbol{S_{MS} = 2.3g}$					End wall: $\boldsymbol{S_{MS} = 2.3g}$						
1.0	8	24	1#4	5@48	17.17	10	@24	2#4	2#5@48	20.34	4	3
1.5	10	24	1#5	6@48	20.48	10	@24	2#5	2#6@48	20.88	3	4.065
2.0	10	24	1#6	6@48	20.63	10	@24	2#6	2#6@24	25.67	2.25	4.065
2.5	10	24	1#6	6@48	20.63	10	@24	2#6	2#6@24	25.67	1.8	4.065
3.0	10	24	1#7	6@48	20.80	10	Full	2#7@24	2#6@24	25.60	1.5	4.065
4.0	12	24	1#8	6@48	24.04	12	Full	2#9@24	2#7@16	31.55	1	4.83
	Side wall: $\boldsymbol{S_{MS} = 3.0g}$					End wall: $\boldsymbol{S_{MS} = 3.0g}$						
1.0	8	24	1#5	5@48	17.30	10	@24	2#4	2#4@48	20.34	3.5	3.000
1.5	10	24	1#6	6@48	20.48	10	@24	2#5	2#4@40	22.34	2.25	3.000
2.0	10	24	1#7	6@48	20.80	10	Full	2#6@24	2#5@24	25.92	1.75	3.000
2.5	10	24	1#8	6@48	21.01	10	Full	2#7@24	2#7@24	26.63	1.375	3.000
3.0	10	24	1#8	6@48	21.01	12	Full	2#8@24	2#7@24	29.55	1	3.610
4.0	12	24	1#8	6@48	24.04	2x8	Full	2x2#8@24	3#7@16	44.04	0.875	5.090

5.4.4 Perform structural analysis

We performed, in Matlab manuscript, the simplified structural analysis of the Global Earthquake Model's (GEM) analytical methodology (Porter et al. 2014). The result of the analysis are as depicted in Figure 5.3. The linearity of the structural analysis should surprise nobody because the asset class is only one story, so $Sa\ (0.2g, 5\%)$ is linearly proportional with the peak roof horizontal acceleration and peak transient interstory drift ratio.

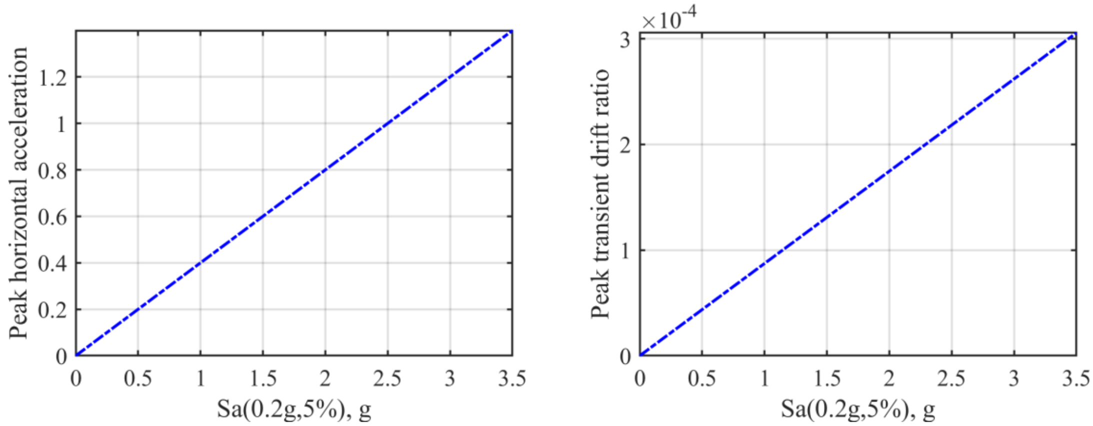

Figure 5.3 – Peak horizontal acceleration and peak transient drift ratio vs Sa(0.2, 5%)

5.4.5 Determine damage and loss parameters

We extracted from the FEMA P-58-3, Performance Assessment Calculation Tool (PACT) (ATC 2012b) the values of the parameters of the fragility functions for each component and converted the extracted unit repair cost and repair time consequences to the median and logarithmic standard deviation as shown in Table 5.6 to Table 5.13. It is important to mention to that the repair time parameters of the PACT database are for the time to fully complete the repair, while our intent is the time only to clean up and go back to functionality, so we adjusted these parameters based on judgment. The adjusted parameters were for the components: lighting and branch wiring, ceiling finishes, and floor finishes.

Table 5.6 – Fragility functions, unit repair cost, and repair time
Nonstructural component rank #1

NISTIR Class: D3050	Component name: Terminal & Package Units
FEMA P-58 Class: D3052.013k, D3052.013k, D3052.011d	Unit: Each
Demand parameter: PFA	Reference: Pact 2.9.65

	Damage state	Fragility function		Repair cost by damage state		Repair Time Consequence	
Quality variant		$\theta_{capacity}$	$\beta_{capacity}$	θ_{cost}	β_{cost}	$\theta_{repair\ time}$	$\beta_{repair\ time}$
Typical	1	1.54	0.6	36300	1.05	37.54	1
Superior	1	1.54	0.6	36300	1.05	37.54	1
Poor	1	0.25	0.4	36300	1.05	37.54	1

Table 5.7 – Fragility functions unit repair cost, and repair time
Nonstructural component rank #2

NISTIR Class: D5020					Component name: Lighting &Branch Wiring		
FEMA P-58 Class: C3034.002, C3034.002, C3034.001					Unit: Each		
Demand parameter: PFA					Reference: Pact 2.9.65		
	Damage state	Fragility function		Repair cost by damage state		Repair Time Consequence	
Quality variant		$\theta_{capacity}$	$\beta_{capacity}$	θ_{cost}	β_{cost}	$\theta_{repair\ time}$	$\beta_{repair\ time}$
Typical	1	1.5	0.4	425	0.637	0	0
Superior	1	1.5	0.4	425	0.637	0	0
Poor	1	0.6	0.4	425	0.637	1.33	0.637

Table 5.8 – Fragility functions unit repair cost, and repair time
Nonstructural component rank #3

NISTIR Class: D5030					Component name: Communication& Security		
FEMA P-58 Class: N/A – rugged					Unit: N/A – rugged		
Demand parameter: PFA					Reference: Pact 2.9.65		
	Damage state	Fragility function		Repair cost by damage state		Repair Time Consequence	
Quality variant		$\theta_{capacity}$	$\beta_{capacity}$	θ_{cost}	β_{cost}	$\theta_{repair\ time}$	$\beta_{repair\ time}$
Typical	1	rugged	rugged	rugged	rugged	rugged	rugged

Superior	1	rugged	rugged	rugged	rugged	rugged	rugged
Poor	1	rugged	rugged	rugged	rugged	rugged	rugged

Table 5.9 – Fragility functions unit repair cost, and repair time
Nonstructural component rank #4

NISTIR Class: C3030				Component name: Ceiling Finishes			
FEMA P-58 Class: C3032.003d, C3032.004d, C3032.001d				Unit: each 2500 SF			
Demand parameter: PFA				Reference: Pact 2.9.65			
	Damage state	Fragility function		Repair cost by damage state		Repair Time Consequence	
Quality variant		$\theta_{capacity}$	$\beta_{capacity}$	θ_{cost}	β_{cost}	$\theta_{repair\ time}$	$\beta_{repair\ time}$
Typical	1	0.35	0.4	3400	0.551	1	0.6
	2	0.55	0.4	29300	0.504	3	0.6
	3	0.8	0.4	58400	0.205	183	0.208
Superior	1	0.4	0.4	3400	0.551	1	0.6
	2	0.6	0.4	29300	0.504	3	0.6
	3	1	0.4	58400	0.205	183	0.208
Poor	1	0.25	0.4	3400	0.551	1	0.6
	2	0.4	0.4	27300	0.518	3	0.6
	3	0.6	0.4	56600	0.203	177.81	0.202

Table 5.10 – Fragility functions unit repair cost, and repair time
Nonstructural component rank #5

NISTIR Class: D3020	Component name: Floor Finishes
FEMA P-58 Class: C3027.002, C3027.002, C3027.001	Unit: S.F.
Demand parameter: PFA	Reference: Pact 2.9.65

	Damage state	Fragility function		Repair cost by damage state		Repair Time Consequence	
Quality variant		$\theta_{capacity}$	$\beta_{capacity}$	θ_{cost}	β_{cost}	$\theta_{repair\ time}$	$\beta_{repair\ time}$
Typical	1	1.5	0.4	50	1.284	0	0.5
Superior	1	1.5	0.4	50	1.284	0.5	1
Poor	1	0.5	0.5	50	1.284	0.5	1

Table 5.11 – Fragility functions unit repair cost, and repair time
Nonstructural component rank #6

NISTIR Class: D5010					Component name: Electrical Service/ Distribution		
FEMA P-58 Class: D5012.023h, D5012.023h, D5012.021c					Unit: unit		
Demand parameter: PFA					Reference: Pact 2.9.65		
	Damage state	Fragility function		Repair cost by damage state		Repair Time Consequence	
Quality variant		$\theta_{capacity}$	$\beta_{capacity}$	θ_{cost}	β_{cost}	$\theta_{repair\ time}$	$\beta_{repair\ time}$
Typical	1	2.4	0.4	29500	0.073	27.92	0.074
Superior	1	2.4	0.4	29500	0.073	27.92	0.074
Poor	1	1.28	0.4	29500	0.0728	27.92	0.074

Table 5.12 – Fragility functions unit repair cost, and repair time
Structural component rank #1

NISTIR Class: B2010-111					Component name: Exterior Walls-Masonry		
FEMA P-58 Class: B1052.002, B1052.002, B1052.004					Unit: each 225ft^2 Wall Panel		
Demand parameter: PDA					Reference: Pact 2.9.65		
	Damage state	Fragility function		Repair cost by damage state		Repair Time Consequence	

Quality variant		$\theta_{capacity}$	$\beta_{capacity}$	θ_{cost}	β_{cost}	$\theta_{repair\ time}$	$\beta_{repair\ time}$
Typical	1	0.0036	0.59	7600	0.087	20.17	0.087
	2	0.0059	0.51	16130	0.122	44.65	0.125
Superior	1	0.0036	0.59	7600	0.087	20.17	0.087
	2	0.0059	0.51	16130	0.122	44.65	0.125
Poor	1	0.0031	0.47	1250	0.358	4.17	0.390
	2	0.009	0.4	7600	0.087	20.17	0.087
	3	0.0151	0.32	16130	0.122	44.65	0.125

Table 5.13 – Fragility functions unit repair cost, and repair time
Structural component rank #2

NISTIR Class: B1020-102					Component name: Roof construction-Wood		
FEMA P-58 Class: N/A – rugged					Unit: N/A – rugged		
Demand parameter: PDA					Reference: Pact 2.9.65		
	Damage state	Fragility function		Repair cost by damage state		Repair Time Consequence	
Quality variant		$\theta_{capacity}$	$\beta_{capacity}$	θ_{cost}	β_{cost}	$\theta_{repair\ time}$	$\beta_{repair\ time}$
Typical	1	rugged	rugged	rugged	rugged	rugged	rugged
Superior	1	rugged	rugged	rugged	rugged	rugged	rugged
Poor	1	rugged	rugged	rugged	rugged	rugged	rugged

The component inventory for each index building is vary from index building to another based on the area of the index building. Table 5.14 shows the component inventory for index building i8 as an example of the component inventory for one of the index building.

Table 5.14 – Component inventory for index building i8

Rank	Nonstructural components						Structural	
	1	2	3	4	5	6	1	2
Name	Terminal & Package Units	Lighting &Branch Wiring	Communication & Security	Ceiling Finishes	Floor Finishes	Electrical Service/ Distribution	Exterior Walls-Masonry	Roof construction-Wood
Unit	Each	Each	100 units	each 2500 S.F	S.F.	unit	Each 225 S.F.	S.F.
Story	Quantity (total)							
1	4	144	1.8	2.88	7200	1	28.8	7200

5.4.6 Calculate the vulnerability functions: repair cost, repair time, and fatality

We used Monte Carlo simulation at each level of ground motion, according the GEM procedures, to estimate the collapse probability and probability distribution of repair cost, repair duration, and number of deaths, conditioned on index building, quality level, I_e value, and geographic location. We initially evaluated the probabilistic damage, repair cost, and repair duration for each component at each level of ground motion as if collapse did not occur. We upgraded the determined repair cost and repair time of each simulation to the index building level as illustrated previously in step 6.

Then, we examined whether collapse occurs or not for each simulation. We identified two cases of collapse mechanisms for our reinforced masonry shearwall buildings with wood roofs collapse mechanisms: (1) in-plane shear failure of a wall; and (2) failure of the roof-to-wall connection. We estimated the former mode using the simplified approach of FEMA P-695 (ATC 2009) as illustrated in step 6, and the later mode using analytically derived fragility function following the guidelines of FEMA P-58 (ATC 2012a). The detailed analytical derivation of the fragility function of the roof-to-wall connections as follows. In this context, connection capacity and collapse probability are two sides of the same coin. Here is an explanation: if a roof-to-wall connection fractures, the fracture immediately produces local collapse and potentially global collapse. Let us express its fragility function with the x-axis measuring tension across the connection (denoted by X_1), i.e., the force with which the wall pulls the roof across the connection. Let x_1 denote a particular value of X_1. Let the y-axis measure the probability that the connection fractures (denoted by the damage state $D_1 = 1$). Let us take the connection capacity as lognormally distributed, with median value denoted by q_1, and standard deviation of its natural logarithm denoted by b_1. Let $\Phi(\ )$ denote the standard normal cumulative distribution function evaluated at the term in parentheses. The fragility function is thus given by Equation (5.26).

$$P[D_1 > 0 \,|X_1 = x_1] = \Phi(ln(x_1/q_1)/b_1) \tag{5.26}$$

Let us denote the local collapse damage state of the building bear a given connection by the uncertain quantity D_2. D_2 can take on two values: $D_2 = 0$ means the building has not collapsed, and $D_2 = 1$ means that building has collapsed near the given connection. We take the probability of collapse given that the connection fractures as 1.0, that is, $P[D_2 = 1|D_1 = 1] = 1.0$. Thus,

$$\begin{aligned} P[D_2 = 1|X_1 = x_1] &= P[D_2 = 1|D_1 = 1] \times P[D_1 > 0|X_1 = x_1] \\ &= 1.0 \times \Phi(ln(x_1/q_1)/b_1) = \Phi(ln(x_1/q_1)/b_1) \end{aligned} \tag{5.27}$$

$x_1$can be estimated from the ASCE 7-16 (ASCE 2016), Equation 12.11-1, as,

$$x_1 = SA02 \times k_a \times W_p \tag{5.28}$$

$$K_a = 1.0 + L_f/100 \tag{5.29}$$

where,

$SA02$= spectral acceleration response at short period;

k_a= amplification factor for diaphragm flexibility;

L_f = the span of a flexible diaphragm that provides the lateral support for the wall;

W_p= the weight of the wall tributary to the anchor.

So, $x_1$is a function of uncertain ground motion say X_2, measured in terms of 5%-damped spectral acceleration response at short period ($T = 0.2\ sec$). Let x_2 denote a particular value of X_2 .We could handle the structural analysis properly, that is, acknowledging an uncertain relationship between X_2 and X_1. Let us assume that X_1 is related to X_2 as:

$$x_1 = g(x_2) \times E_2 \tag{5.30}$$

where E_2 is say lognormally distributed with unit mean and logarithmic standard deviation denoted by b_2. From (Shome et al. 1998), we can estimate $b_2 \cong 0.25$. We establish that functional relationship, $x_1 = g(x_2)$, through structural analysis. Then,

$$P[D_2 = 1|X_1 = g(x_2)] = \Phi(ln(g(x_2)/q_1)/\overline{b_1}) \tag{5.31}$$

where, $$\bar{b}_1 = \sqrt{{b_1}^2 + {b_2}^2}\ ; \tag{5.32}$$

The logarithmic standard deviation of the capacity, b_1, is taken as 0.4 as indicated in FEMA P-58, Appendix H, Method H.2.4 (Derivation) .

So, $\bar{b}_1 = \sqrt{(0.4^2 + 0.25^2)}$= 0.47, which can be rounded to 0.5 for simplicity.

The median capacity, q_1, is taken as 0.92 times the nominal capacity of the anchors, F_p based on FEMA P-58, Appendix H, Method H.2.4 (Derivation), So, $q_1 = 0.92 \times F_p$.

Now, the roof connections collapse probability can be calculated by:

$$P[D_2 = 1|X_2 = x_2] = \Phi\left(\frac{ln(g(x_2)/q_1))}{\overline{b_1}}\right) \tag{5.33}$$

In each simulation, if the building did not collapse, the repair cost was taken as calculated in Equation X and number of fatalities was taken as zero. If the building collapsed, the repair cost and repair were taken to be the replacement cost new of the building, RCN, and the replacement time new of the building, RTN, respectively, and the fatality rate was taken as as the average of the GEM analytical methodology's lower and upper recommended fatality rate for our building category: 2% and 8%, respectively.

We executed, for each index building, I_e value, quality level, geographic location, and level of ground motion a hundred simulation. We calculated all three seismic vulnerability functions: repair cost, $Y_c\ (x)$; repair duration, $Y_t\ (x)$; and fatality rate, $Y_f\ (x)$ for a combination of index building, I_e value, quality level, and geographic location.

Figure 5.4 and Figure 5.5 show the vulnerability functions for the class building at the location of $S_{MS} = 0.8g$ and $S_{MS} = 2.3g$ as an example of the results. The vulnerability functions are jagged as a result of Monte Carlo simulation; more simulations at each level of ground motion would smooth the jaggedness but would probably not change the general trend.

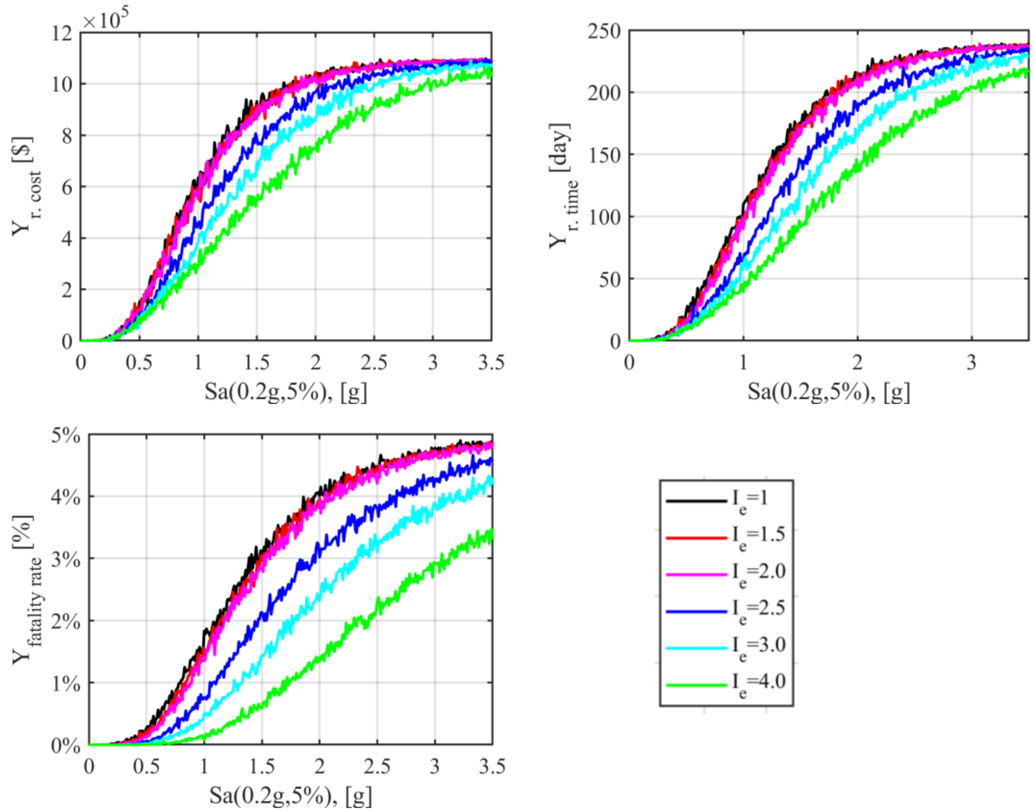

Figure 5.4 – Vulnerability functions: repair cost, repair time, and fatality rate at $S_{MS} = 0.8g$

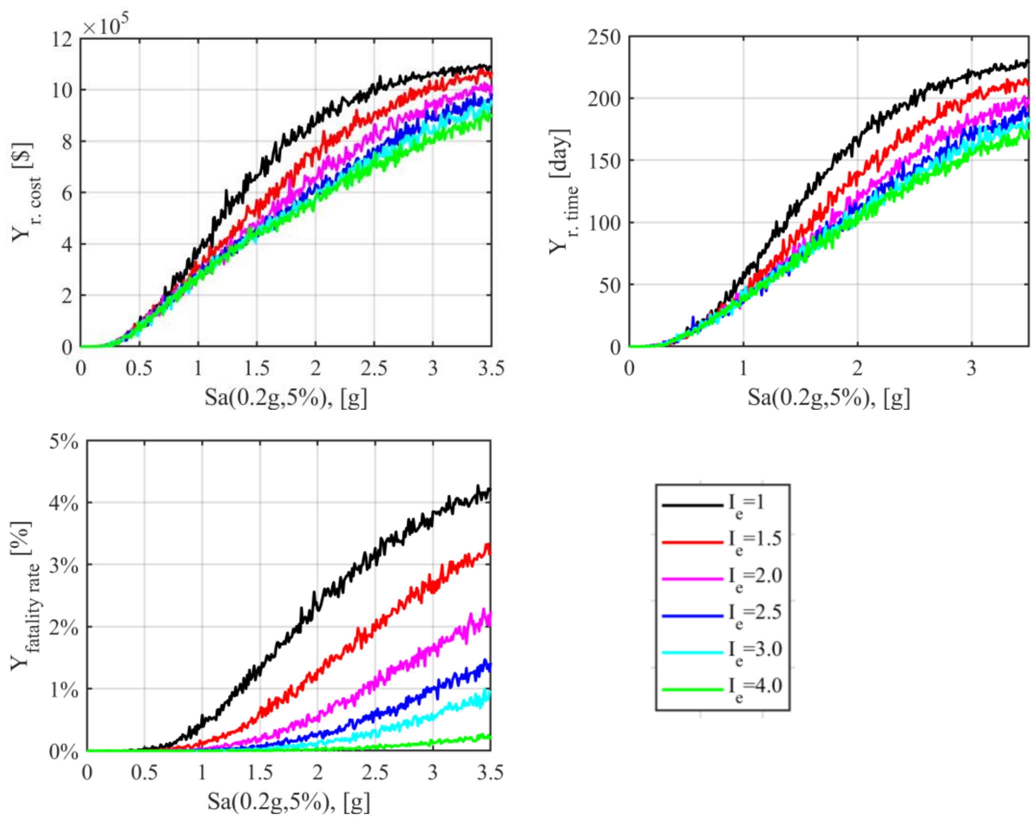

Figure 5.5 – Vulnerability functions: repair cost, repair time, and fatality rate at $S_{MS} = 2.3g$

Some general observations from comparing the vulnerability functions within and between locations of degree of seismicity in

Figure 5.4 and Figure 5.5:

- The buildings designed to exceed current seismic design criteria demonstrate reduced vulnerability at all levels of ground motion.
- Among the four geographic locations with S_{MS} values between 0.8g and 3.0g, above-code design most dramatically reduces the vulnerability functions at the geographic location with the highest degree of seismicity. The reduction is parameterized here in terms of a factor defined as the vulnerability function for above code design, divided by the vulnerability function for I_e = 1.0. For example, the vulnerability functions for the geographic location of S_{MS}= 0.8g of designing with I_e value = 2.0, Figure 5.4, appears to be undistinguishable from the vulnerability functions of designing with I_e value = 1.0. By contrast, they are very separated from each other for the geographic location of S_{MS}= 2.3g, as shown in Figure 5.5.
- Among the three vulnerability functions, above-code design most dramatically reduces the vulnerability of fatality rate, in terms of a reduction factor defined as the vulnerability function for above code design, divided by the vulnerability function for I_e = 1.0.

5.4.7 Estimate expected annualized losses and added costs

We calculated the expected annualized loss, EAL, of each loss measure for each combination of index building, Ie value, quality level, and geographic location. We used the previously mentioned Equations (5.12), (5.13), and (5.14) to calculate the expected annualized building repair cost, EAL_c, the expected annualized building repair time cost, EAL_t, and the expected annualized value of avoiding statistical fatalities, EAL_f, respectively. In Equation (5.13) and (5.14), we used a Hazus-based California inventory circa 2002 to estimate the average number of indoor occupants per square foot at 2PM, $\mathrm{N_{occ2PM}}$, and the average of the time-average number of indoor occupants per square foot, N_{occ} , for the occupancy class COM4 (Professional/Technical/Business Services).

We estimate the direct business interruption loss per day of downtime, V_{BI} equal to $414.93, and indirect business interruption, the per dollar indirect business interruption loss Q resulting from $1.00 of direct business interruption, equal to 0.016 as used and explained in detail in *Natural Hazard Mitigation Saves* (MMC 2017). We considered the acceptable cost to avoid a statistical fatality equals to $9,500,000 as it was taken in 2016 by the U.S. Department of Transportation ("Economic Values Used in Analyses" 2016). Table 5.15 summarizes the results for the expected present value of future losses to a building designed for a particular location and value of I_e, denoted by PV_{Ie}, and the weighted average replacement cost of the building class for each combination of location and I_e value, denoted by RCN_{Ie}.

Table 5.15 – Present value of future losses and replacement cost new of each building class

	S_{MS}=0.8g		S_{MS}=1.5g		S_{MS}=2.3g		S_{MS}=3.0g	
I_e	PV_{Ie} [$]	RCN_{Ie} [$]	PV_{Ie} [$]	RCN_{Ie} [$]	PV_{Ie} [$]	RCN_{Ie} [$]	PV_{Ie} [$]	RCN_{Ie} [$]
1.0	97,362	1,094,068	465,445	1,099,147	465,013	1,113,184	249,072	1,113,674
1.5	92,481	1,094,835	438,509	1,100,557	374,023	1,126,721	185,472	1,129,049
2.0	82,111	1,095,488	352,611	1,103,134	332,271	1,135,125	170,276	1,136,165
2.5	57,009	1,096,446	314,868	1,104,842	310,341	1,135,327	160,448	1,138,289
3.0	46,660	1,096,648	291,109	1,109,447	301,858	1,136,057	156,662	1,143,147
4.0	39,922	1,098,329	283,030	1,111,677	294,137	1,158,158	154,763	1,178,073

5.4.8 Estimate benefits, costs, and benefit-cost ratios by I_e and location

Figure 5.6 (a) shows the benefit (reduction in the present value of future losses achieved by a design with $I_e > 1.0$, relative to a building with $I_e = 1.0$) of above-code design for each location and value of $I_e > 1.0$. We considered in Equation (5.19) the real annual discount rate, r,equals to 0.0213 and the number of years that the mitigation strategy is effective, t, equals to 75 years as was done in MMC (2017). The real annual discount rate is obtained considering the following. In December 2016, the annual U.S. inflation rate was 2.1%, according to the Trading Economics website ("Trading Economics" n.d.). The weighted average interest rate for a mortgage through JP Morgan Chase was 4.23%, as reported in December, 2016 U.S. Securities and Exchange Commission (SEC) filing ("SEC Info", page 132). So, the real annual discount rate = 0.0423 - 0.021 = 0.0213. The duration over which benefits is recognized is considered as the average of 100 years (approximately the half-life of a new building) and 50 years (the duration that MSv1 recognized benefit for it).

Figure 5.6 (b) shows the average marginal cost (the increasing of the average replacement cost new) to exceed $I_e = 1.0$ for each geographic location and value of $I_e > 1.0$. The curve of the average marginal cost is not purely linear with I_e because both the wall thickness and rebar size have standard increments. Most often, we use wall sections that are thicker than the minimum that would be required if one could choose any thickness down to the fraction of an inch. In some cases, therefore, increasing the design requirement may not impact the design of the wall section, because it is already stronger than required. Also, among geographic locations, the increment is not linearly because increasing $I_e$at a location of small S_{MS} does not increase seismic response coefficient, C_s as much comparing to location of higher S_{MS}.

Figure 5.6 (c) shows the benefit-cost ratio (BCR_{Ie}) for designing buildings to exceed I-code minima for each geographic location. Figure 5.6 (d) shows benefit on the vertical axis and cost on the horizontal axis for designing buildings to exceed I-code minima for each geographic location.

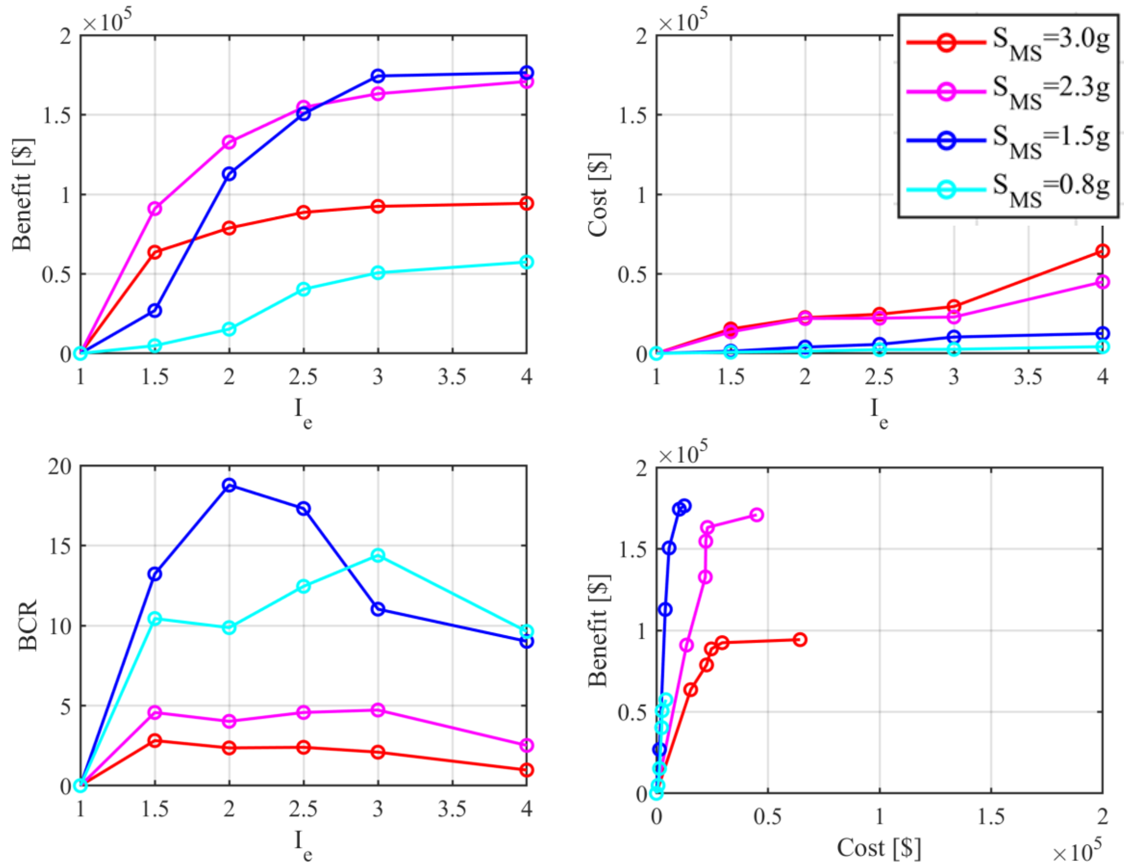

Figure 5.6 – The “Benefit”, “Cost”, and “BCR”

Some general observations of the results of “Benefit”, “Cost”, and “BCR” in Figure 5.6:

- The locations of lower levels of degree of seismicity appears to have the highest $BCRs$. That is because increasing I_e at location of small S_{MS} only weakly impacts the seismic response coefficient, C_s; consequently, it does not increase the corresponding marginal cost as much as it does for location with higher S_{MS}.

- In general, the benefit does not increase in proportion to S_{MS}, while the cost does. It is observable that the benefit of the location of $S_{MS} = 3.0g$is less than for the locations of $S_{MS} = 2.3g$ and $S_{MS} = 1.5g$ but higher than for the location of $S_{MS} = 0.8g$.
- The location of $S_{MS} = 3.0g$ has less benefit than the location of $S_{MS} = 2.3g$ can be explained because the area under the hazard curve for the location of $S_{MS} = 3.0g$ is smaller than that for the location of $S_{MS} = 2.3g$ as shown in Figure 5.2. This needs more research, and it could be a subject of future study.
- Increasing the design requirement does not increase the cost very much. The average increase in construction costs associated with increasing I_e from 1.0 to 1.5. is 0.7%, consistent with the finding that "resilient design costs about 1% more,"(Porter 2016).
- The $BCRs$, in general, decrease with increasing the level of degree of seismicity, although benefits increase. The BCR decreases because the associated cost increases. For example, the BCR for the location of $S_{MS} = 3g$ for $I_e = 2$ is 2.36 while it is 9.87 for the location of $S_{MS} = 0.8g$, but the benefit for the former is $\$78.8 \times 10^3$ and for the latter is $\$15.3 \times 10^3$. Yet, the associated costs are $\$22.5 \times 10^3$ and $\$1.4 \times 10^3$, respectively.

5.4.9 Identify the incrementally efficient maximum I_e value by location

Table 5.16 shows the incrementally efficient maximum I_e value by location, IEMax, that is, the point of diminishing returns. Designing buildings to exceed I-code minima up to 4 for geographic location of $S_{MS} = 0.8g$ does not show the point of diminishing returns.

Table 5.16 – IEMax and its associated benefit and cost

	$S_{MS} = 0.8g$	$S_{MS} = 1.5g$	$S_{MS} = 2.3g$	$S_{MS} = 3.0g$
$IEMax$	--	3.0	3.0	2.5
Benefit [$]	--	174×10^3	163×10^3	89×10^3
Cost [$]	--	10.3×10^3	22.9×10^3	24.6×10^3

This seems important: Table 5.16 shows that it can be cost effective to design new buildings to be as much as 3 times as strong and stiff as the code requires. There are well populated places in highly seismically active regions of the U.S. with this level of S_{MS}, including much of California, Oregon, Washington, Idaho, Wyoming, Nevada, near the New Madrid Seismic Zone, and near Charleston, South Carolina.

5.4.10 Comparing with *Natural Hazard Mitigation Saves* (MMC 2017)

The calculations performed here can be compared with BCRs calculated in *Natural Hazard Mitigation Saves* (MMC 2017) for the census tracts in which these sites stand and the Hazus occupancy class to which they belong: Professional/Technical/Business Services (COM4 in Hazus' notation). Figure 5.7 illustrates the comparison.

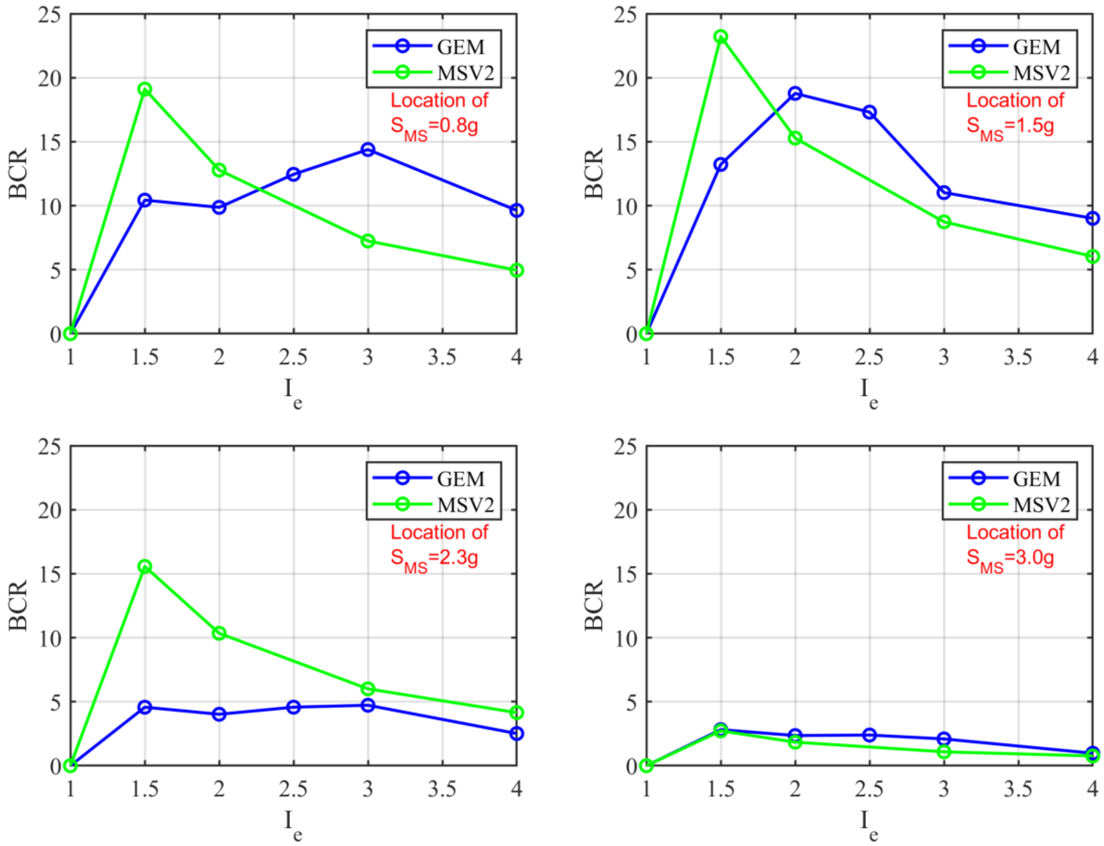

Figure 5.7 – Comparing BCR based on GEM as opposed to *Natural Hazard Mitigation Saves* (MMC 2017)

Some general observations of comparing BCR from this work as opposed to *Natural Hazard Mitigation Saves* in Figure 5.7:

- The $BCRs$ results of *Natural Hazard Mitigation Saves* cross the ones obtained in this work for the location of $S_{MS} = 0.8g$ and $S_{MS} = 1.5g$.
- The $BCRs$ results of *Natural Hazard Mitigation Saves* are higher at the locations of $S_{MS} =$ 2.3g, however the differences decrease as I_e increases.
- The $BCRs$ results at the location of $S_{MS} = 3.0g$ are almost identical.

Although this work and the *Natural Hazard Mitigation Saves* employed different methodologies, the BCRs results in this work and the *Natural Hazard Mitigation Saves* are comparable and agreed within less than a factor of 2. *Natural Hazard Mitigation Saves* (MMC 2017) aggregated its results over 28 lateral force resisting systems and 3 height ranges, weighting the relative quantities of buildings in proportion to their estimated quantity in the real world, on a census-tract-by-census-tract basis. In contrast, this work examined one lateral force resisting system (masonry shear walls) and one height range (one story high) using FEMA P-58 (ATC 2012a) and the Global Earthquake Model's (GEM) analytical methodology (Porter et al. 2014).

Table 5.16 shows that the equally weighted average benefit of designing one of these buildings to the incrementally efficient maximum is $142,000, while the average of the cost is approximately $20,000. Therefore, the overall average BCR is approximately 7:1. I.e., according to this work, new above-code design of 1-story reinforced masonry shear walls (RMSW) buildings with flexible diaphragm would save approximately $7 in avoided future losses for every $1 spent on additional, up-front construction. To compare with *Natural Hazard Mitigation Saves*, the overall average BCR of all type of buildings is 4:1. The 7:1 result of this study is for the overall average for one class of building, while the 4:1 result of *Natural Hazard Mitigation Saves* is for overall average of all types of buildings. Therefore, the result of this study tends to support, rather than weaken, that of *Natural Hazard Mitigation Saves*, while avoiding the relatively simplistic method to estimate seismic vulnerability used in *Natural Hazard Mitigation Saves*. Both studies suggest that above-code design is cost effective in many places.

5.4.11 Apples-to-apples comparison with Hazus vulnerability of a single building type

For a more apples-to-apples comparison of the FEMA P-58 and GEM calculations with Hazus, the present author repeated the BCR calculations from the *Natural Hazard Mitigation Saves*, but just for the comparable model building type, occupancy, and location: low rise reinforced masonry with flexible diaphragms (RM1L), professional/technical/business services

(COM4 in Hazus' notation), in the same census tracts. Figure 5.8 illustrates the comparison. For present purposes, the BCRs calculated using FEMA P-58 and GEM are labeled "GEM," those using a single Hazus building type and occupancy class are labeled "HAZUS," and those using a weighted average of all Hazus building types and occupancy classes are labeled "MSv2."

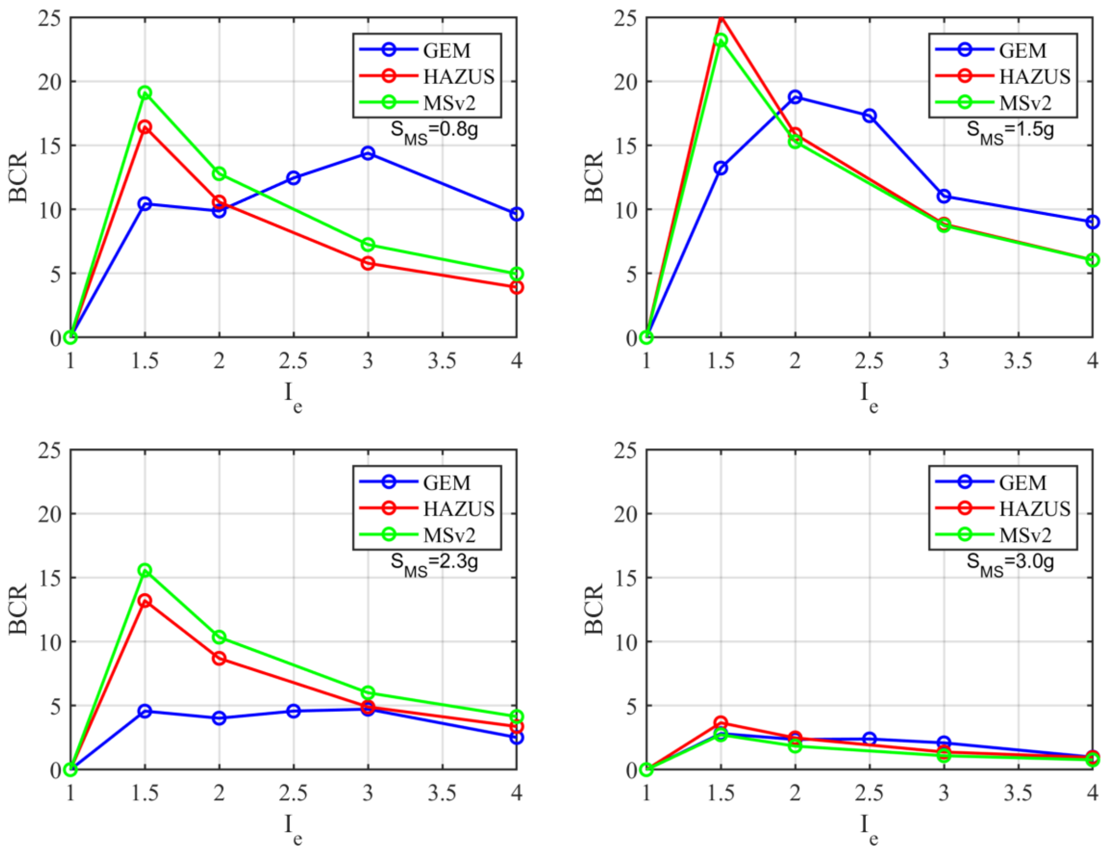

Figure 5.8 – Comparing *BCR* based on GEM and *Natural Hazard Mitigation Saves* as opposed to HAZUS earthquake model

The HAZUS *BCRs* are closer to the ones obtained in this work (GEM) than are those of *Natural Hazard Mitigation Saves*. However, the differences between the results of HAZUS earthquake model and *Natural Hazard Mitigation Saves* are within 20%.

5.5 Conclusions

This chapter presents benefit-cost analysis for designing buildings to exceed minimum requirements code by a strength and stiffness factor $I_e \in \{1.0, 1.5, 2.0, 2.5, 3.0, 4.0\}$ at four locations of varying seismicity, $S_{MS} = \{0.8g, 1.5g, 2.3g, 3.0g\}$ for 1-story reinforced masonry shear wall (RMSW) buildings with flexible diaphragms. The building class was modeled using 10 particular buildings whose distributions of plan area, degree of irregularity, and construction quality approximate those of the building class. The goal was to test the hypothesis: above-code design can be cost effective in many, though perhaps not all, U.S. locations, at least from a benefit-cost-analysis perspective. Designing the buildings to their incrementally efficient maximum (IEMax) level of strength and stiffness costs approximately $20,000 above that of code minimum. The average benefit, by contrast, is approximately $142,000. Consequently, the overall average BCR is approximately 7:1. Thus, new above-code design would save approximately $7 in avoided future losses for every $1 spent on additional, up-front construction cost.

The analysis presented here relies on a simplified version of performance-based earthquake engineering (FEMA P-58) to model the seismic vulnerability of individual buildings. It relies on a relatively new method developed for the Global Earthquake Model to design a suite of individual buildings that collectively reflect the distribution of building features believed to most strongly affect seismic performance of the building class. The analysis thus overcomes one of the weaker aspects of a similar, recent study entitled *Natural Hazard Mitigation Saves* (MMC 2017), which relies on a Hazus-like approach to modeling seismic vulnerability, and does not explicitly address variability of engineering attributes or of seismic performance within the building class. This analysis therefore serves as cross-validation of *Natural Hazard Mitigation Saves*, albeit only for one category of lateral force resisting system and occupancy, and only four locations. *Natural*

Hazard Mitigation Saves by contrast considers all building types, occupancy classes, on a nationwide basis.

The overall average BCR at IEMax is approximately 7:1 in this work while it is 4:1 in the *Natural Hazard Mitigation Saves*. The fact that the two studies agree on the BCR within a factor of 2 tends to provide cross-validation, supporting the assertion that above-code design can be cost effective. Both studies also suggest that the incrementally efficient maximum degree of above-code design can range between 1.5 and 3.0. That is, it can be cost effective to design new buildings to be as much as 3 times as strong and stiff as the code requires. This study supports the finding that code minimum can be inefficient, producing buildings that cost society more in the long run, when one adds future losses to up-front construction cost.

Some notes on novelty. This appears to be the first time the GEM analytical methodology has been used to estimate the behavior of:

- The particular building class examined here (namely, reinforced masonry shearwall buildings with flexible diaphragms);
- One building class at several locations, accounting for how seismic microzonation affects design requirements;
- One building class at any level of design above code minimum; or
- The loss-of-use costs for a commercial building.

This study may also represent the first time the GEM analytical methodology has been used either for benefit-cost analysis or to cross-validate a Hazus-based study. Of course, two analytical methodologies that produce consistent results could agree by accident while still both being wrong—inconsistent with what actually happens in real buildings. However, absent strong empirical evidence, which seems practically impossible to acquire, cross-validated analysis may be the best that one can hope for.

Chapter 6

6 Conclusions and Future Research Needs

6.1 Summary and Conclusions

This thesis addressed three questions: (1) Is US practice to determine the required separation distance to preclude pounding between neighboring buildings overly conservative? (2) Does pounding between buildings with aligned floors significantly aggravate collapse? (3) is it cost effective to design a narrow category of common-looking commercial buildings to exceed IBC strength and stiffness requirements in many US locations, at least from a societal benefit-cost-analysis perspective?

Narrower questions related to pounding include the following:

- Is the simple FEMA P-154 spectral approach any good? How well does it estimate safe separation distance?
- Is ASCE 41-13’s 3% to 4% separation distance actually overly conservative?
- Is ASCE 7-16’s elastic structural analyses of both buildings worth the effort? Is its estimate any safer, more reliable, more accurate, than a simpler approach that does not require structural analyses of both buildings?

- To what degree the one can be confident that pounding will not actually occur, if one calculated the safe separation distance between the buildings by any of the three relatively simple approaches: (1) SRSS of 5% damped elastic spectral displacement response at the top of the shorter building; (2) ASCE 7's equivalent lateral force procedure; and (3) multiple linear elastic dynamic structural analyses, with drift results multiplied by C_d/R to approximate nonlinear response, in MCE_R and $\frac{2}{3}MCE_R$ shaking?
- What are the conversion factors to relate the separation distances calculated by any of the simpler methods (elastic spectral displacement, equivalent lateral force, and multiple linear elastic dynamic structural analyses) to multiple nonlinear dynamic structural analyses method, which we deem to most closely approximate what happens in the real world?
- If the separation distance was not sufficient to preclude neighboring buildings to pound each other, does the pounding scenario increases/ decreases the probability of collapse for each building of the pounded buildings?

Two narrower questions related to the cost-effectiveness of above-code design:

- If we pay sooner rather than later, by making new buildings more resilient than is required for life safety, does the investment pay for itself? How much extra resilience makes economic sense?
- Would the two different approaches of a societal risk analysis: Hazus-based methodology and a PBEE methodology cross-validate each other?

The conclusions of this research can be summarized as follows:

Chapter 2 examined three relatively simple analytical approaches to estimate safe separation distance to avoid pounding at MCE_R shaking: (1) SRSS of 5% damped elastic spectral displacement response at the top of the shorter building; (2) ASCE 7-10's equivalent lateral force procedure; and (3) multiple linear elastic dynamic structural analyses, with drift results multiplied by C_d/R to approximate nonlinear response. This chapter considered four levels of seismicity (S_{MS} from 0.8g to 3.0g), three combinations of seismic force-resisting systems (shearwall and steel moment frame), several building heights (2 to 26 stories), and several fundamental periods of vibration (0.2 sec to 2.8 sec). Finally in this chapter, the safe separation distance was estimated as a fraction of the height of the shorter building and as a function of S_{MS}, system combination, and analytical method. It was found that:

- Both the spectral displacement approach and the equivalent lateral force procedure appear to give modestly conservative estimates of safe separation distance.
- The former would be safe with 66% probability, the latter with 90% probability, assuming that the third approach (multiple linear elastic structural analyses with drifts factored by C_d/R to approximate nonlinear response) gives a fairly accurate estimate of the true distribution of building motion.

Chapter 3 assessed how safe it would be if one uses the simpler approaches (elastic spectral displacement, equivalent lateral force, and multiple linear elastic dynamic structural analyses) to determine the safe separation distance between the buildings in MCE_R and 2/3 MCE_R shaking. This was explored by comparing the safe separation distance produced by these relatively simple approaches with the ones that produced by multiple nonlinear time-history structural analyses. This chapter considered the shaking at 2/3 MCE_R and MCE_R to evaluate pounding criteria for

ASCE 7 and FEMA P-154, respectively. Three combinations of seismic force-resisting systems (special reinforced moment frames and ordinary reinforced moment frames), building heights (2 to 20 stories), and fundamental periods of vibration (0.66 sec to 2.63 sec) were examined. Safe separation distance was calculated as a fraction of the height of the shorter building and as a function of shaking level, system combination, and analytical method. Chapter 3, also, developed a set of conversion factors to relate the separation distances calculated by any of the simpler methods (elastic spectral displacement, equivalent lateral force, and multiple linear elastic dynamic structural analyses) to multiple nonlinear dynamic structural analyses method. The findings can be summarized as follows:

- The spectral displacement approach (FEMA P-154) appears to give reasonably safe estimates of safe separation distance at MCE_R, and arguably overly conservative estimates at 2/3 MCE_R.
- The approaches of using equivalent lateral force (ASCE 7) and multiple linear elastic analyses factored by C_d/R appear to give reasonably safe estimates of safe separation distance for most cases at 2/3 MCE_R and MCE_R, and unconservative estimates in a few cases at MCE_R.
- Although the findings seem sufficient only to make tentative conclusions about safe separation distance, they do seem to support using spectral displacement as a reasonable and easy initial estimate of safe separation distance.

Chapter 4 evaluated seismic safety concerns of pounding of modern ductile reinforced concrete moment frame buildings whose floors align. Incremental dynamic analyses of 140 combinations of pairs of five adjacent post-2000 reinforced concrete moment frame buildings with aligned floors (20 permutations) and 7 separation gaps were performed. The studied buildings included 2-, 4-, 8-, 12-, and 20-story models. The considered gap widths varied from near zero to effectively infinite (0.01 in, 1.0 in, 2.0 in, 5.0 in, 10.0 in, 35.0 in, 75.0 in, and 200 in). The effect of pounding on median collapse capacity was assessed. The findings were compared with the evidence of building collapse in reinforced concrete buildings in California in the last 50 years. The results of chapter 4 revealed the follows:

- Pounding produces little effect on collapse capacity relative to the separated case (i.e., the 200-in, no-pounding case). The effect was always less than an 11% decrease in median collapse capacity, was on average a 2.4% decrease (where it decreased at all) and considering cases where pounding seemed to increase collapse capacity, the average overall effect (weighting each case equally) was less than 1%. The effect seems small enough to ignore; it is certainly not large. This conclusion is limited to post-2000 reinforced concrete moment frame buildings whose floors align.
- Pounding does not appear to have contributed to any of the few collapses of reinforced concrete buildings documented in NISEE's photo database, even where collision occurred between buildings. The lack of obvious pounding-induced collapses in California between 1964 and 2014 is hardly evidence that pounding does not cause collapse. But the negative evidence weakens the hypothesis that pounding significantly contributes to collapse, and does strengthen the inference from our study that pounding may matter little to collapse.

Chapter 5 investigated whether above-code design can be cost effective. It estimated benefit-cost ratio for above-code design of a single building type, height class, and occupancy: a special reinforced masonry shearwall (in ASCE 7-16 terms), 1 story, with flexible roof diaphragm, with a professional, technical, and business services occupancy. It tested cost-effectiveness of above-code design in several seismic regions and for several I_e values, using the framework of the

Global Earthquake Model's (GEM) analytical methodology (Porter et al. 2014) to parameterize and vary building configuration consistent with an observed joint probability distribution of size and shape. It cross-validated a PBEE approach to seismic vulnerability with the Hazus-based approach used in *Natural Hazard Mitigation Saves* (MMC 2017), as each is used in a societal risk analysis. It found:

- Designing the buildings to their incrementally efficient maximum (IEMax) level of strength and stiffness costs approximately $20,000 per square foot above that of code minimum. The average benefit, by contrast, is approximately $142,000. Consequently, the overall average BCR is approximately 7:1. Thus, new above-code design would save approximately $7 in avoided future losses for every $1 spent on additional, up-front construction cost.
- The two studies (this one and *Natural Hazard Mitigation Saves)* agree on the BCR within less than a factor of 2. This general agreement tends to provide cross-validation, supporting the assertion that above-code design can be cost effective. Both studies also suggest that the incrementally efficient maximum degree of above-code design can range between 1.5 and 3.0. That is, it can be cost effective to design new buildings to be as much as 3 times as strong and stiff as the code requires. This study supports the finding that code minimum can be inefficient, producing buildings that cost society more in the long run, when one adds future losses to up-front construction cost.

6.2 Future Research Needs

The research presented here suggests the following needs for future study:

- Safe separation distance to avoid pounding was quantified for special reinforced concrete moment frames and ordinary reinforced concrete moment frames. It would be interesting to perform similar analyses with reinforced concrete shearwall buildings, steel-frame buildings, hybrid systems with concrete core walls and steel-frame outriggers, and buildings in other geographic locations.
- The finding that pounding does not significantly change collapse capacity in this research is limited to post-2000 reinforced concrete moment frame buildings with aligned floors. It would be useful to extend the present research to quantify the reduction in collapse capacity in buildings with other seismic force-resisting systems and especially in buildings where floors do not align.
- The finding that above-code design can be cost effective is limited here to one building type, analyzed using GEM and FEMA P-58. While it tends to support a similar finding using a simpler approach to estimating seismic vulnerability, it would be valuable to repeat the test with other common building types.

Bibliography

ACI. (2002). *Building Code Requirements for Structural Concrete (ACI 318-02) and Commentary (ACI 318R-02).* American Concrete Institute, Farmington Hills MI.

Anagnostopoulos, S. A. (1988). "Pounding of Buildings in Series During Earthquakes." *Earthquake Engineering & Structural Dynamics*, 16(3), 443–456.

ASCE. (2002). *Minimum Design Loads for Buildings and Other Structures, ASCE/SEI Standard 7-02*. American Society of Civil Engineers/Structural Engineering Institute, Reston, VA.

ASCE. (2014). *Seismic Evaluation and Retrofit of Existing Buildings (41-13)*. American Society of Civil Engineers.

ASCE. (2016). *Minimum Design Loads and Associated Criteria for Buildings and Other Structures. ASCE/SEI Standard 7-16*. American Society of Civil Engineers/Structural Engineering Institute, Reston, VA.

ATC. (2009). *Quantification of Building Seismic Performance Factors, ATC-63, FEMA P695*. Federal Emergency Management Agency, Redwood City, CA.

ATC. (2012a). *Seismic Performance Assessment of Buildings, Volume 1- Methodology, FEMA P-58-1*. Federal Emergency Management Agency, Washington, D.C., 278.

ATC. (2012b). *Seismic Performance Assessment of Buildings, Volume 3—Spreadsheet Tools, FEMA P-58-3*. Federal Emergency Management Agency, Washington, D.C., 278.

ATC. (2015). *Rapid Visual Screening of Buildings for Potential Seismic Hazards: a Handbook, Third edition, FEMA P-154*. Federal Emergency Management Agency, Washington, D.C.

Athanassiadou, C. J., Penelis, G. G., and Kappos, A. J. (1994). "Seismic Response of Adjacent Buildings with Similar or Different Dynamic Characteristics." *Earthquake Spectra*, 10(2), 293–317.

Bertero, V. V., and Collins, R. G. (1973). *Investigation of the Failures of the Olive View Stairtowers During the San Fernando Earthquake and their Implications on Seismic Design*. Earthquake Engineering Research Center, University of California, Berkeley.

"Canadian Commission on Building and Fire Codes." (1990). National Building Code of Canada, Ottawa, Ontario.

Ching, J., Porter, K. A., and Beck, J. L. (2009). "Propagating Uncertainties for Loss Estimation in Performance-Based Earthquake Engineering Using Moment Matching." *Structure and Infrastructure Engineering*, 5(3), 245–262.

Cole, G., Dhakal, R., Carr, A., and Bull, D. (2011). "An Investigation of the Effects of Mass Distribution on Pounding Structures." *Earthquake Engineering & Structural Dynamics*, 40(6), 641–659.

Cole, G. L., Dhakal, R. P., and Turner, F. M. (2012). "Building Pounding Damage Observed in the 2011 Christchurch Earthquake." *Earthquake Engineering & Structural Dynamics*, 41(5), 893–913.

Corley, W. G., Cluff, L., Hilmy, S., Holmes, W., and Wight, J. (1996). "Concrete Parking Structures." *Earthquake Spectra*, 12(S1), 75–98.

CSI. (2017). *SAP2000 (Structural Software for Analysis and Design)*. Computers & Structures, INC. https://www.csiamerica.com/products/sap2000.

"Economic Values Used in Analyses." (2016). *US Department of Transportation*, <https://www.transportation.gov/regulations/economic-values-used-in-analysis> (Apr. 2, 2019).

FEMA. (2012a). *Multihazard Loss Estimation Methodology Earthquake Model Hazus®MH 2.1, Technical Manual*. Federal Emergency Management Agency, Washington, DC.

FEMA. (2012b). *2009 NEHRP Recommended Seismic Provisions: Design Examples, FEMA P-751*. Federal Emergency Management Agency.

FEMA. (2018). "Hazus Earthquake Model | FEMA.gov." Federal Emergency Management Agency, <https://www.fema.gov/hazus-mh-earthquake-model> (Dec. 14, 2018).

Field, E. H., Jordan, T. H., and Cornell, C. A. (2003). “OpenSHA: A Developing Community-Modeling Environment for Seismic Hazard Analysis.” *Seismological Research Letters*, 74(4), 406–419.

Filiatrault, A., and Cervantes, M. (1995). “Separation Between Buildings to Avoid Pounding During Earthquakes.” *Canadian Journal of Civil Engineering*, 22(1), 164–179.

Goel, R. K., and Chopra, A. K. (1998). “Period Formulas for Concrete Shear Wall Buildings.” *Journal of Structural Engineering*, 124(4), 426–433.

Gupta, A., and Krawinkler, H. (1999). “Seismic Demands for the Performance Evaluation of Steel Moment Resisting Frame Structures.” Stanford University.

Haselton, C. B. (2006). “Assessing Seismic Collapse Safety of Modern Reinforced Concrete Moment Frame Buildings.” Stanford University.

Haselton, C. B., and Deierlein, G. G. (2008). *Assessing Seismic Collapse Safety of Modern Reinforced Concrete Moment-Frame Buildings; PEER Report 2007/08*. Pacific Earthquake Engineering Research Center/University of California, Berkeley, CA.

Haselton, C. B., Liel, A. B., Deierlein, G. G., Dean, B. S., and Chou, J. H. (2011). “Seismic Collapse Safety of Reinforced Concrete Buildings. I: Assessment of Ductile Moment Frames.” *Journal of Structural Engineering*, 137(4), 481–491.

Ibarra, L. F., Medina, R. A., and Krawinkler, H. (2005). “Hysteretic Models that Incorporate Strength and Stiffness Deterioration.” *Earthquake Engineering & Structural Dynamics*, 34(12), 1489–1511.

ICC. (2018). *2018 International Building Code*. International Code Council, Falls Church, Va.

Isteita, M., and Porter, K. (2017). “Safe Distance Between Adjacent Buildings to Avoid Pounding in Earthquakes.” *16th World Conference on Earthquake*.

Jankowski, R. (2009). “Non-linear FEM Analysis of Earthquake-Induced Pounding Between the Main Building and the Stairway Tower of the Olive View Hospital.” *Engineering Structures*, 31(8), 1851–1864.

Jeng, V., Kasai, K., and Maison, B. F. (1992). “A Spectral Difference Method to Estimate Building Separations to Avoid Pounding.” *Earthquake Spectra*, 8(2), 201–223.

Kasai, K., and Maison, B. F. (1997). "Building Pounding Damage During the 1989 Loma Prieta Earthquake." *Engineering Structures,* 19(3), 195–207.

Liel, A. B. (2008). "Assessing the Collapse Risk of California's Existing Reinforced Concrete Frame Structures: Metrics for Seismic Safety Decisions." Stanford University.

Lopez Garcia, D. (2004). "Sepration Distance Necessary to Prevent Seismic Pounding Between Adjacent Structures." Ph. D. dissertation, The State University of New Yourk at Buffalo.

Maison, B. F., and Kazuhiko, K. (1990). "Analysis for a Type of Structural Pounding." *Journal of Structural Engineering,* 116(4), 957–977.

MMC, Porter, K. A., Scawthorn, C., Dash, N., Santos, J., and Schneider, P. (2017). *Natural Hazard Mitigation Saves 2017 Interim Report: An Independent Study – Summary of Findings*. Multihazard Mitigation Council/ National Institute of Building Sciences, Washington.

Mouzakis, H. P., and Papadrakakis, M. (2004). "Three Dimensional Nonlinear Building Pounding with Friction During Earthquakes." *Journal of Earthquake Engineering*, 08(01), 107–132.

Muthukumar, S., and DesRoches, R. (2006). "A Hertz Contact Model with non-linear Damping for Pounding Simulation." *Earthquake Engineering & Structural Dynamics*, 35(7), 811–828.

Newnan, D. G., Lavelle, J. P., and Eschenbach, T. G. (2004). *Engineering Economic Analysis*. Oxford University Press, New York.

Nirmal, J., and Baker, J. W. (2010). "Ground-Motion Selection for PEER Transportation Research program." *Proceedings, 7th International Conference on Urban Earthquake Engineering (7CUEE) & 5th International Conference on Earthquake Engineering (5ICEE).*

(NIST), N. I. of S. and T. (1999). *NISTIR 6389: Official NIST Guide To The UNIFORMAT II Standard; UNIFORMAT II Elemental Classification for Building Specifications, Cost Estimating, and Cost Analysis*. 195.

Osteraas, J., Somers, P., Carpenter, J., Ferner, H., Holmes, W., Krawinkler, H., Longstreth, M., Ryan, P., and Wight, J. (1996). "Reinforced Concrete Buildings." *Earthquake Spectra*, 12(S1), 49–74.

PEER. (2017). *OpenSees (Open System for Earthquake Engineering Simulation)*. University of California, Berkeley. http://opensees.berkeley.edu/.

Petersen, M. D., Moschetti, M. P., Powers, P. M., Mueller, C. S., Haller, K. M., Frankel, A. D., Zeng, Y., Rezaeian, S., Harmsen, S. C., Boyd, O. S., Field, E. H., Chen, R., Rukstales, K. S., Luco, N., Wheeler, R. L., Williams, R. A., and Olsen, A. H. (2014). *Documentation for the 2014 Update of the United States National Seismic Hazard Maps*. Open-File Report, USGS Numbered Series, U.S. Geological Survey, Reston, VA, 255.

Porter, K. (2019). “A Beginner’s Guide to Fragility, Vulnerability, and Risk.” University of Colorado Boulder, http://www.sparisk.com/pubs/Porter-beginners-guide.pdf.

Porter, K. A. (2016). “Not Safe Enough: The Case for Resilient Seismic Design.” *2016 SEAOC Convention*.

Porter, K. A., and Cho, I. H. (2013). “Characterizing a Building Class via Key Features and Index Buildings for Class-Level Vulnerability Functions.” *11th International Conference on Structural Safety and Reliability (ICOSSAR)*.

Porter, K. A., Farokhnia, K., Vamvatsikos, D., and Cho, I. H. (2014). *Guidelines for Component Based Analytical Vulnerability Assessment of Buildings and Nonstructural Elements*. GEM Foundation, Pavia, Italy.

Porter, K. A., and Ramer, K. (2012). “Estimating Earthquake Induced Failure Probability and Downtime of Critical Facilities.” *Journal of Business Continuity & Emergency Planning*, 5(4), 352–364.

Porter, K., Kennedy, R., and Bachman, R. (2006). *Developing Fragility Functions for Building Components for ATC-58*. Applied Technology Council, Redwood City, CA.

Porter, K., Kennedy, R., and Bachman, R. (2007). “Creating Fragility Functions for Performance-Based Earthquake Engineering.” *Earthquake Spectra*, 23 (2), 471–489.

Rosenblueth, E., and Meli, R. (1986). “The 1985 Earthquake: Causes and Effects in Mexico City.” *Concrete International*, 8, 23–34.

RSMeans. (2017). *Square Foot Costs with RSMeans Data 2017 38th Annual Edition*. The Gordian Group.

"SEC Info - JP Morgan Chase Commercial Mortgage Securities Corp, et al. - '424B2' on 12/22/16." (132AD). <http://www.secinfo.com/d1evd6.w48g.htm> (Feb. 23, 2019).

Shome, N., Cornell, C. A., Bazzurro, P., and Carballo, J. E. (1998). "Earthquakes, Records, and Nonlinear Responses." *Earthquake Spectra*, 14(3), 469–500.

Somers, P., Johnson, M. W., Kehoe, B. E., Lizundia, B., and Longstreth, M. (1996). "Retrofitted Buildings." *Earthquake Spectra*, 12(S1), 219–228.

"Summary of the updates to ASCE/SEI 41-17 - SEAOC." (2017). *Structural Engineers Association of California*, <https://www.seaoc.org/news/379271/Summary-of-the-updates-to-ASCESEI-41-17.htm> (Apr. 3, 2019).

TMS. (2016). *TMS 402/602, Building Code Requirements and Specification for Masonry Structures, 2016*. The Masonry Society.

"Trading Economics." (n.d.). *Trading Economics*, <https://tradingeconomics.com/> (Feb. 23, 2019).

Vamvatsikos, D., and Cornell, C. A. (2002). "Incremental Dynamic Analysis." *Earthquake Engineering & Structural Dynamics*, 31(3), 491–514.

Vamvatsikos, D., and Cornell, C. A. (2004). "Applied Incremental Dynamic Analysis." *Earthquake Spectra*, 20(2), 523–553.

Vamvatsikos, D., and Fragiadakis, M. (2010). "Incremental Dynamic Analysis for Estimating Seismic Performance Sensitivity and Uncertainty." *Earthquake Engineering & Structural Dynamics*, 39(2), 141–163.

Wald, D. J., and Allen, T. I. (2007). "Topographic Slope as a Proxy for Seismic Site Conditions and Amplification." *Bulletin of the Seismological Society of America*, 97(5), 1379–1395.

Wills, C. J., and Clahan, K. B. (2006). "Developing a Map of Geologically Defined Site-Condition Categories for California." *Bulletin of the Seismological Society of America*, 96(4A), 1483–1501.

Yamamoto, Y., and Baker, J. W. (2013). "Stochastic Model for Earthquake Ground Motion Using Wavelet Packets." *Bulletin of the Seismological Society of America*, 103(6), 3044–3056.